

— Model Geometry: There are 15 modules over the 90 degrees of meridian included in this model.

try42.GENOPT/BIGBOSOR4 model of the balloon with radial webs

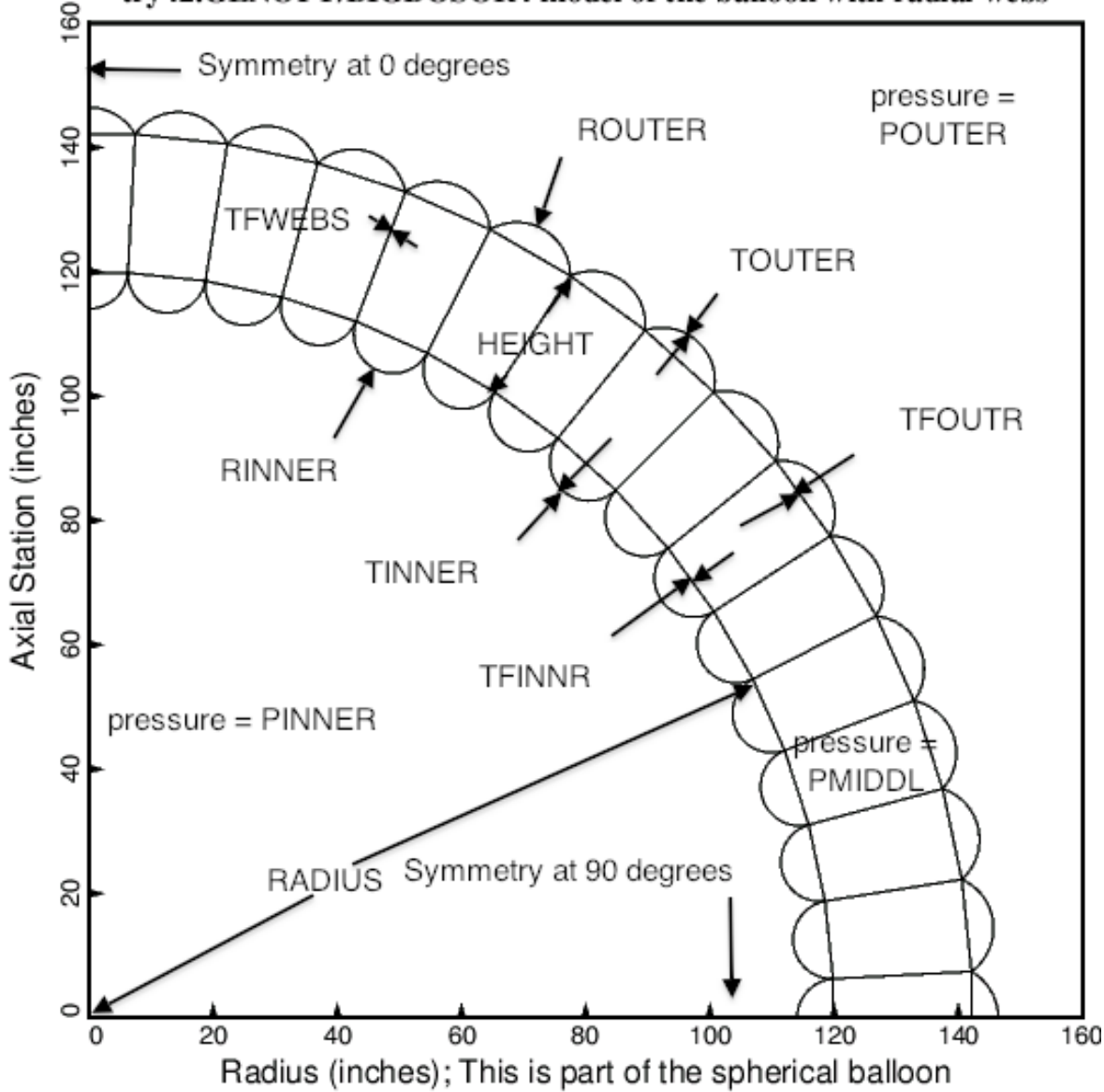


Fig. 1 Cross section of the “double” wall of the spherical vacuum chamber with **radial webs**. The radius to the inner wall is RADIUS, which is not a decision variable. The decision variable candidates are the distance between the inner and outer walls, HEIGHT, the two radii of curvature, RINNER and ROUTER, and the five thicknesses, TINNER, TOUTER, TFINNR, TFOUTR, and TFWEBS. The pressure inside the inner wall is PINNER; the pressure outside the outer wall is POUTER; the pressure between the inner and outer walls is PMIDDLE. PMIDDLE > POUTER > PINNER. The segments of the wall of thickness TFINNR and TFOUTR have little holes in them so that PMIDDLE acts on both surfaces of them (no net pressure on them). Buckling of and stress in this configuration is computed with use of the BIGBOSOR4 computer program. The wall is optimized (minimum weight) with the use of the system of computer programs called “**GENOPT/BIGBOSOR4**” [3, 6 – 9].

— Model Geometry: There are 15 modules over the 90 degrees of meridian included in this model.

try41.GENOPT/BIGBOSOR4 model of the balloon with truss-like webs

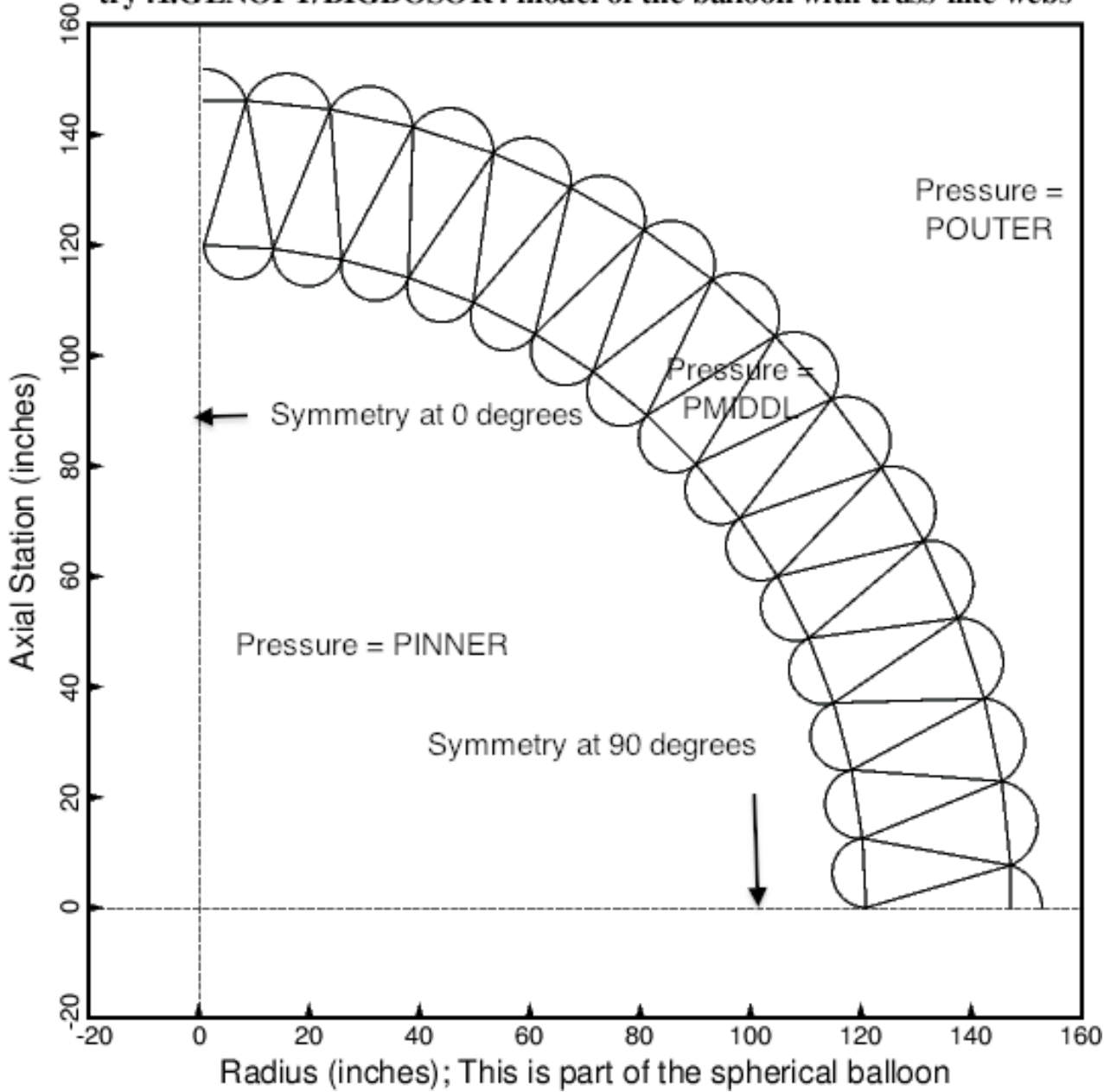


Fig. 2 Cross section of the double wall of the spherical vacuum chamber with **truss-like (slanted) webs**. The pressure inside the inner wall is PINNER; the pressure outside the outer wall is POUTER; the pressure between the inner and outer walls is PMIDDLE. PMIDDLE > POUTER > PINNER. The segments of the wall of thickness TFINNR and TFOUTR have little holes in them so that PMIDDLE acts on both surfaces of them (no net pressure on them). Buckling of and stress in this configuration is computed with use of the BIGBOSOR4 computer program. The wall is optimized (minimum weight) with the use of the system of computer programs called "**GENOPT/BIGBOSOR4**" [3, 6 – 9].

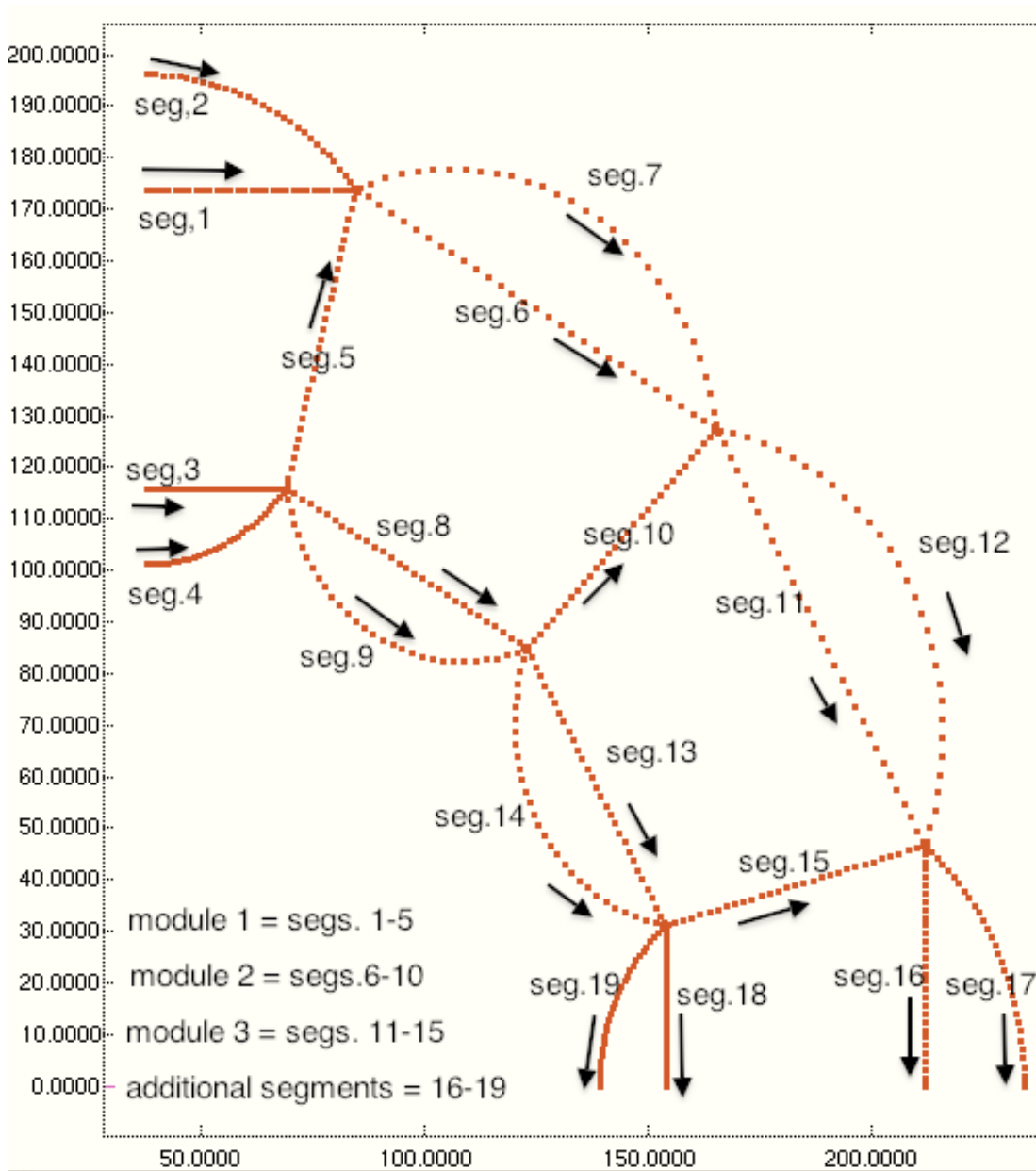


Fig. 3 (Taken from [1]). The complex wall of the cylindrical vacuum chamber (balloon) consists of a number of modules, NMODUL. NMODUL is an input quantity that the end user chooses when executing the GENOPT processor, BEGIN. In this crude model of a balloon wall **with radial webs** NMODUL = 3. The "shell" segment numbering convention and the direction of "travel" along each segment in the BIGBOSOR4 model are displayed here. Each "shell" segment is discretized in the meridional coordinate: 31 nodal points per segment. Variation of the buckling modal displacements in the direction normal to the plane of the paper is trigonometric. Although the computer program, BIGBOSOR4, was created to analyze shells with finite bending stiffness and the segments of the vacuum chamber treated in this paper act more like membranes than like shells, useful predictions are obtained. The same arrangements of modules and segments, the segment numbering scheme, and the direction of travel along each segment are used also for the spherical balloons.

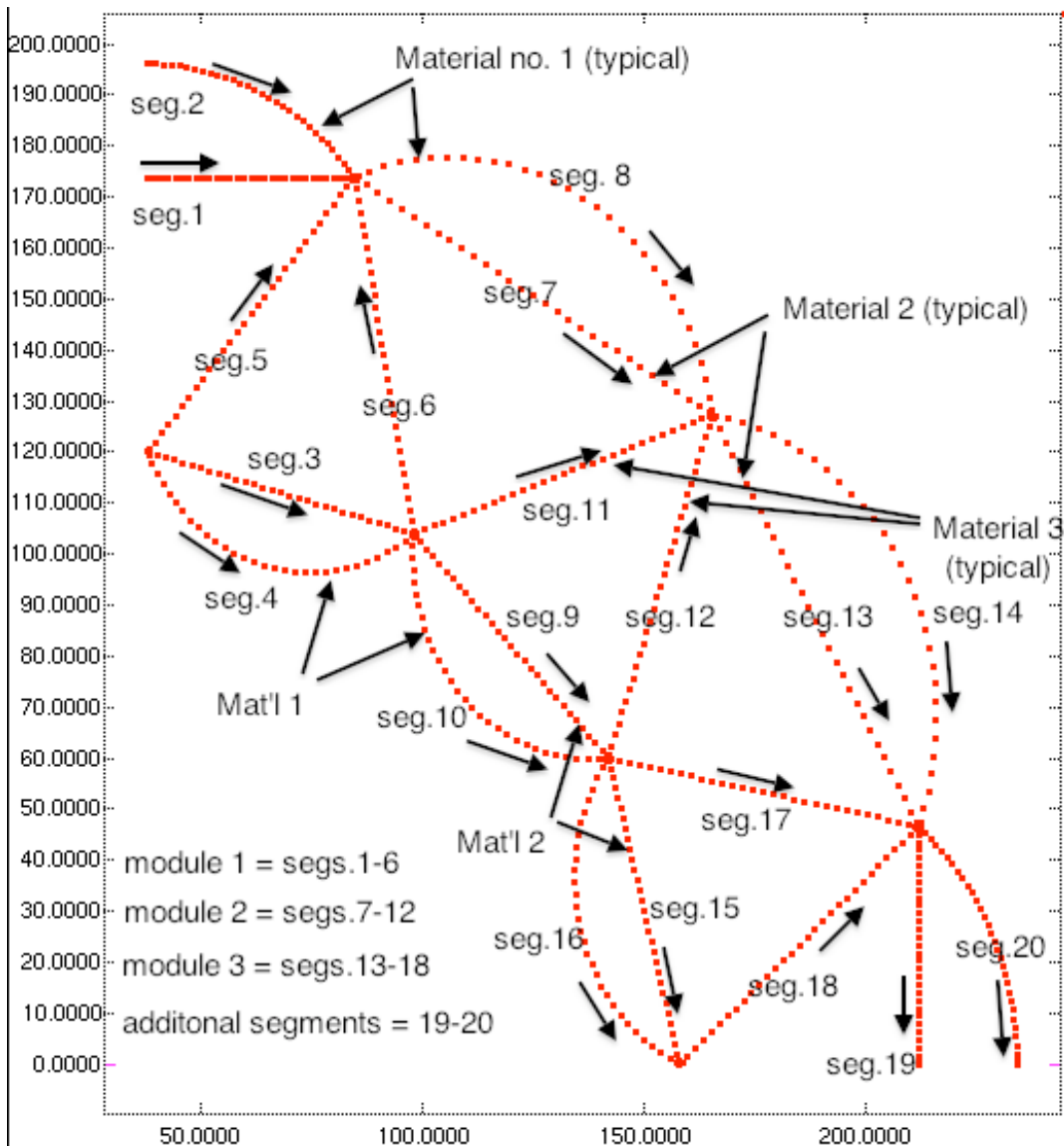


Fig. 4 (Taken from [1]). The complex wall of the cylindrical vacuum chamber (balloon) consists of a number of modules, NMODUL. NMODUL is an input quantity that the end user chooses when executing the GENOPT processor, BEGIN. In this crude model of a balloon wall **with truss-like (slanted) webs** NMODUL = 3. The “shell” segment numbering convention and the direction of “travel” along each segment in the BIGBOSOR4 model are displayed here. Each “shell” segment is discretized in the meridional coordinate: 31 nodal points per segment. Variation of the buckling modal displacements in the direction normal to the plane of the paper is trigonometric. There are 3 material types in this model and also in the model shown in the previous figure. In the studies reported in this paper all three material types have the same properties. Although the computer program, BIGBOSOR4, was created to analyze shells with finite bending stiffness and the segments of the vacuum chamber treated in this paper act more like membranes than like shells, useful predictions are obtained. The same arrangements of modules and segments, the segment numbering scheme, and the direction of travel along each segment are used also for the spherical balloons.

-- Undeformed; There are 8 modules over 90 degrees of the meridian of the spherical balloon.
— Deformed; Load set B = PINNER=0 psi, P = 0.002 x PMIDDLE=0.002 x 60 psi, POUTER=0 psi

try4 (spherical shell); LOADB, STEP 1; P = 0.002xPMIDDLE = 0.002 x 60 psi

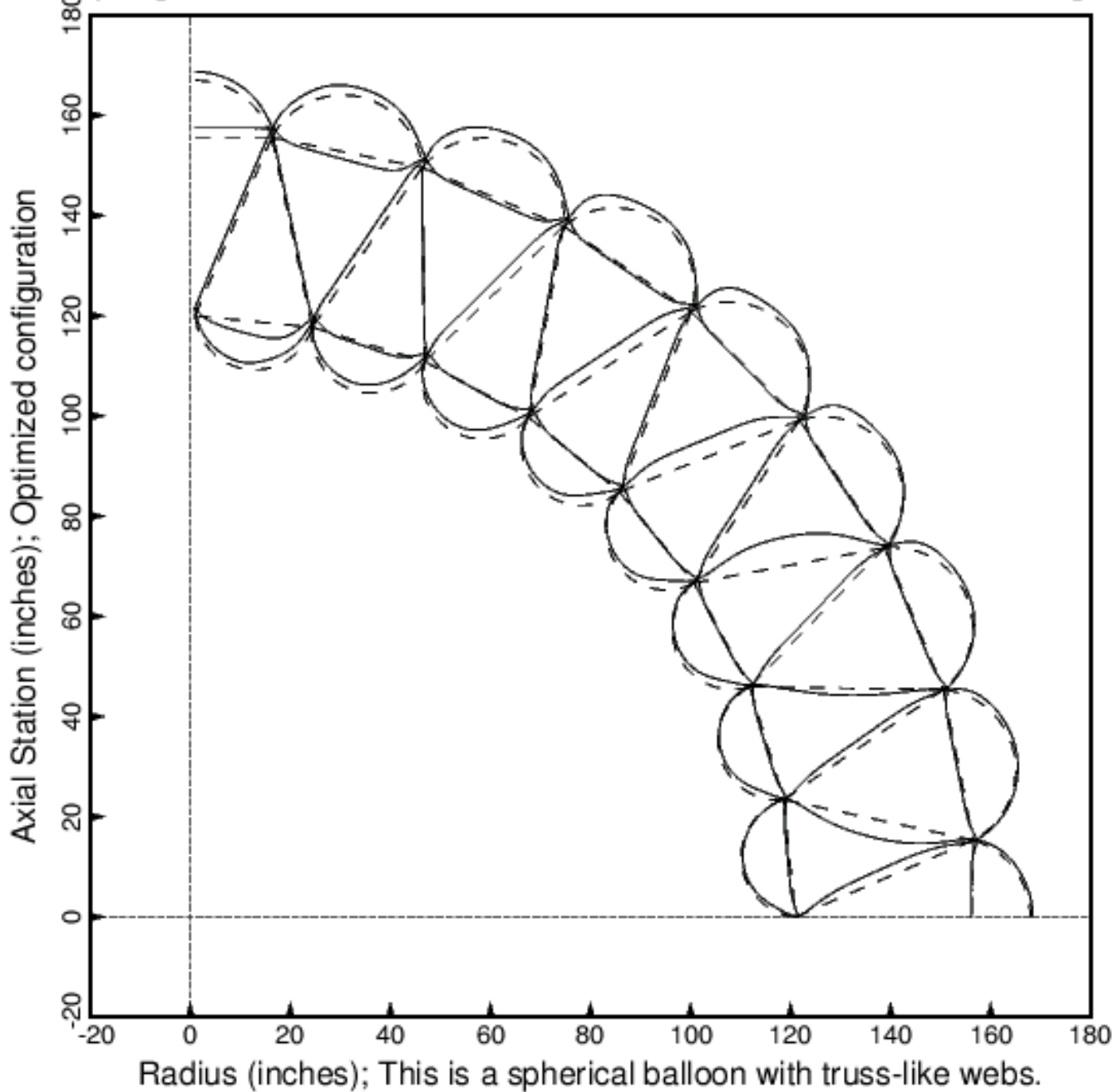


Fig. 5 Pre-buckling axisymmetric deformation of the optimized spherical balloon with 8 modules over 90 degrees of the meridian and with truss-like (slanted) webs. The loading is pressure between the innermost and outermost walls equal to $P = 0.002 \times PMIDDLE = 0.002 \times 60$ psi. See Item 6, Load Step 1 in Table 9. Compare with the next figure.

—— Undeformed; There are 8 modules over 90 degrees of the meridian of the spherical balloon.
 — Deformed; Load set B = PINNER=0 psi, P = 1.002 x PMIDDLE=1.002 x 60 psi, POUTER=0 psi

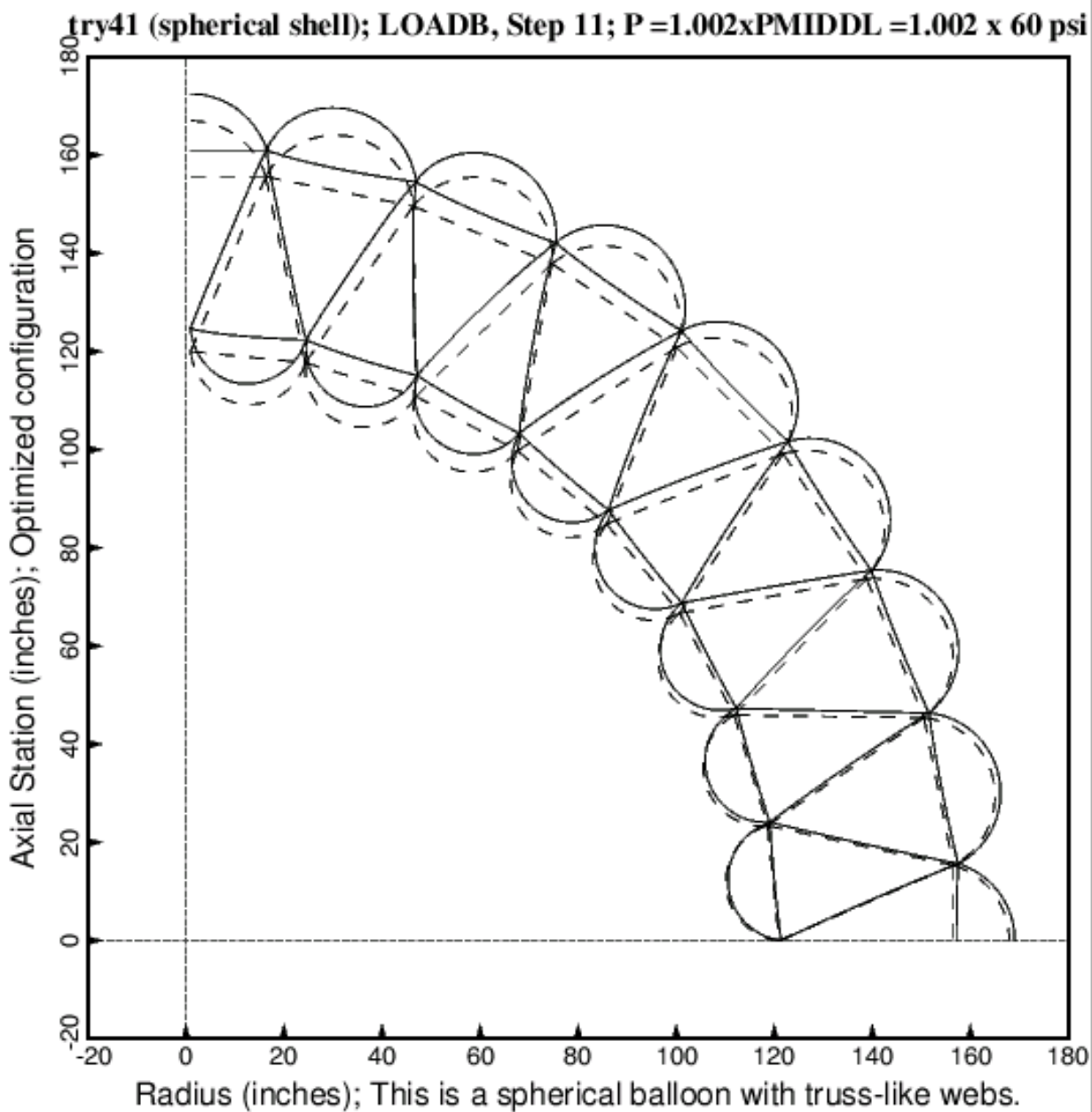


Fig. 6 Pre-buckling axisymmetric deformation of the optimized spherical balloon with 8 modules over 90 degrees of the meridian and with truss-like (slanted) webs. The loading is pressure between the innermost and outermost walls equal to $P = 1.002 \times PMIDDLE = 1.002 \times 60$ psi. See Item 6, Load Step 11 in Table 9. Compare with the previous figure. A different displacement scale factor is used to produce this figure than that used to produce the previous figure. Therefore, the maximum displacement in the structure appears to be about the same in both figures. Notice that the spherical balloon elongates in the axial direction much more than in the radial direction, becoming slightly egg shaped. This non-uniform axisymmetric deformation occurs because the balloon, having only circumferential webs, is not isotropic.

□ Maximum displacement (inches) in optimized spherical balloon with radial webs at 6.12 psi

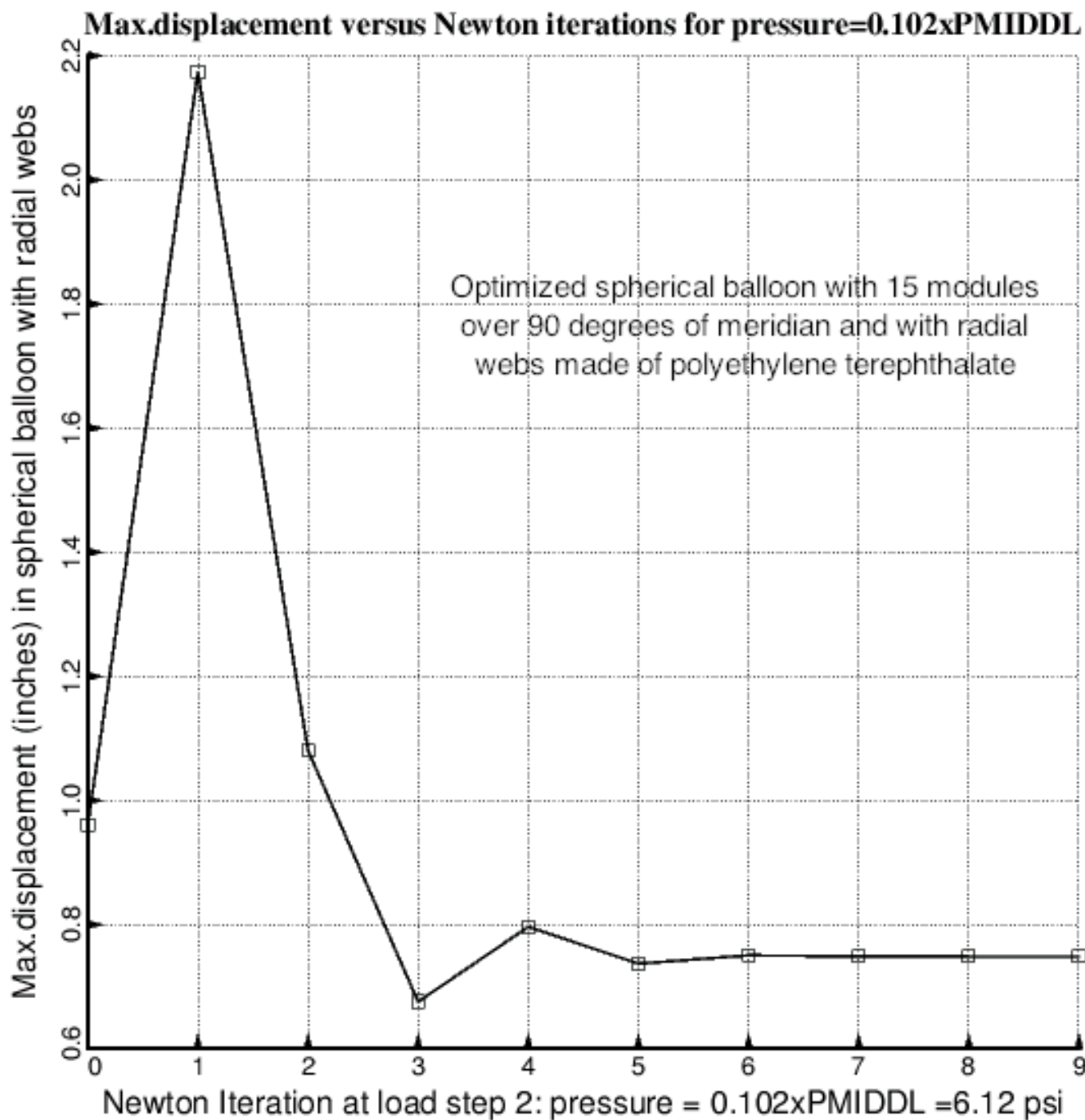


Fig. 7 Maximum displacement in the spherical balloon with 15 modules and radial webs (Fig.1) versus Newton iteration for the solution of the nonlinear pre-buckling equilibrium equations at Load Step 2 in the analysis of the spherical balloon with pressure between the innermost and outermost wall equal to $P = 0.102 \times \text{PMIDDLE} = 0.102 \times 60 \text{ psi}$. Load Step 2 typically (but not always) requires the most Newton iterations to achieve convergence. (See Item 6, Load Step 2 of Table 9, for example.)

□ Axial displacement, UV (inches), at Node 1, Segment 1 in spherical balloon with radial webs

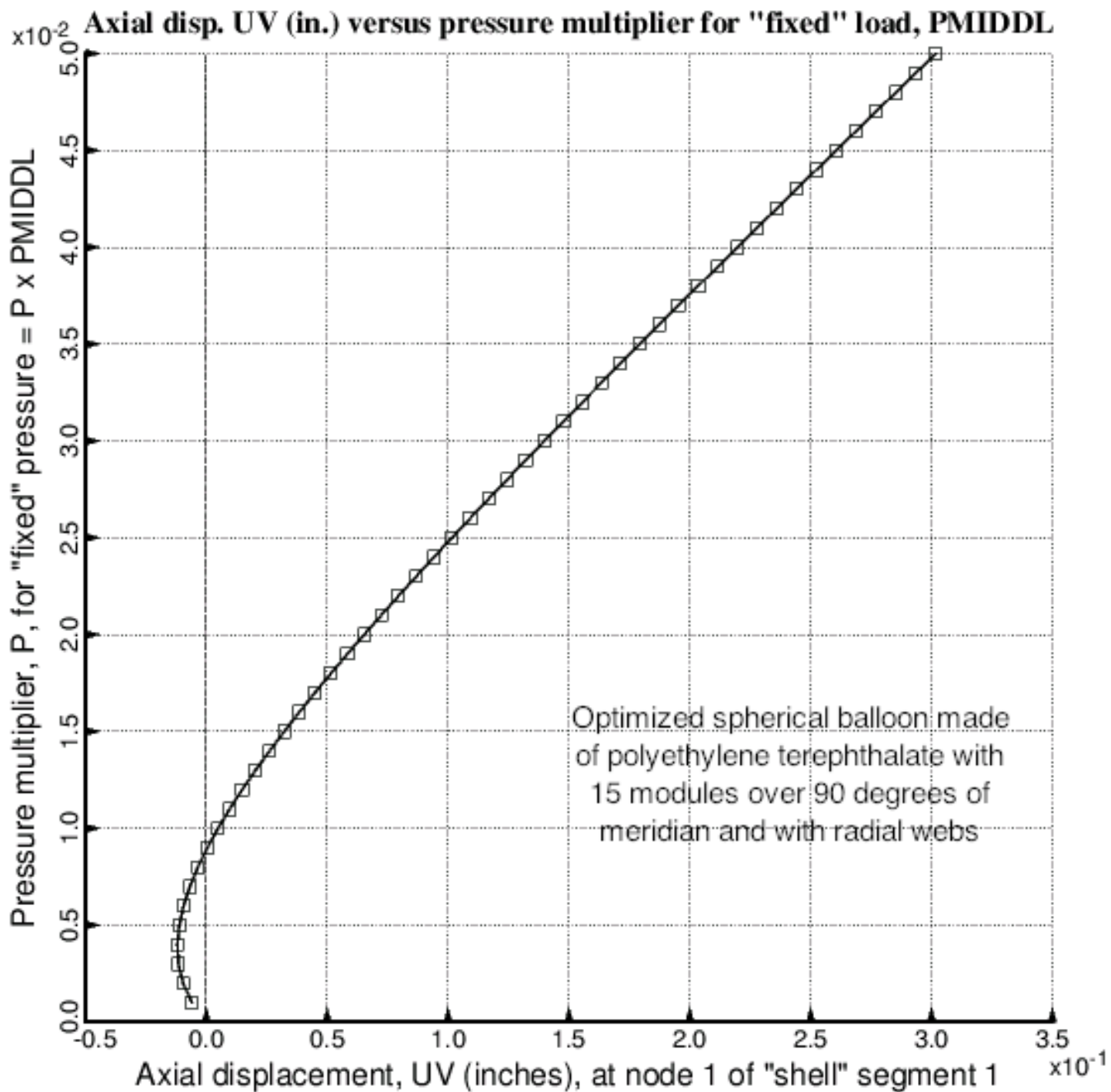


Fig. 8 Axial displacement at the apex of the spherical balloon with 15 modules and radial webs (Fig.1) versus pressure multiplier, P , for the low-load range, $0 < P < 0.05$, of pressure between the innermost and outermost walls. The behavior during this low-load range is very nonlinear. Compare with the next figure.

□ Axial displacement, UV (inches), at Node 1, Segment 1 in spherical balloon with radial webs

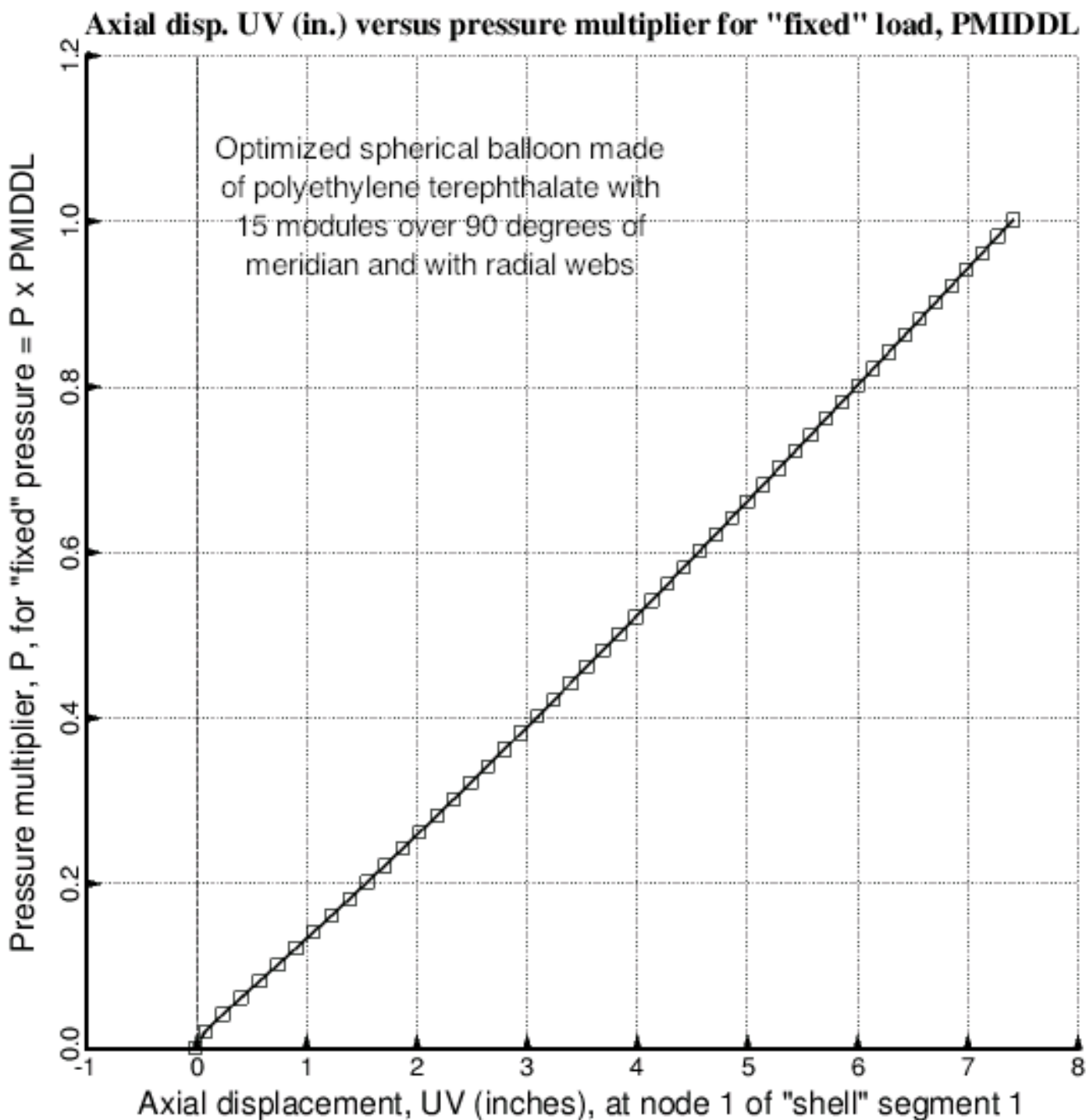


Fig. 9 Axial displacement at the apex of the spherical balloon with 15 modules and radial webs (Fig.1) versus pressure multiplier, P, for the high-load range of pressure between the innermost and outermost walls. The behavior during this high-load range is almost linear. Compare with the previous figure.

— — Undeformed; There are 8 modules over 90 degrees of the meridian of the spherical balloon.
 — Deformed: Axisymmetric ($N=0$ circumferential waves) buckling mode from BIGBOSOR4

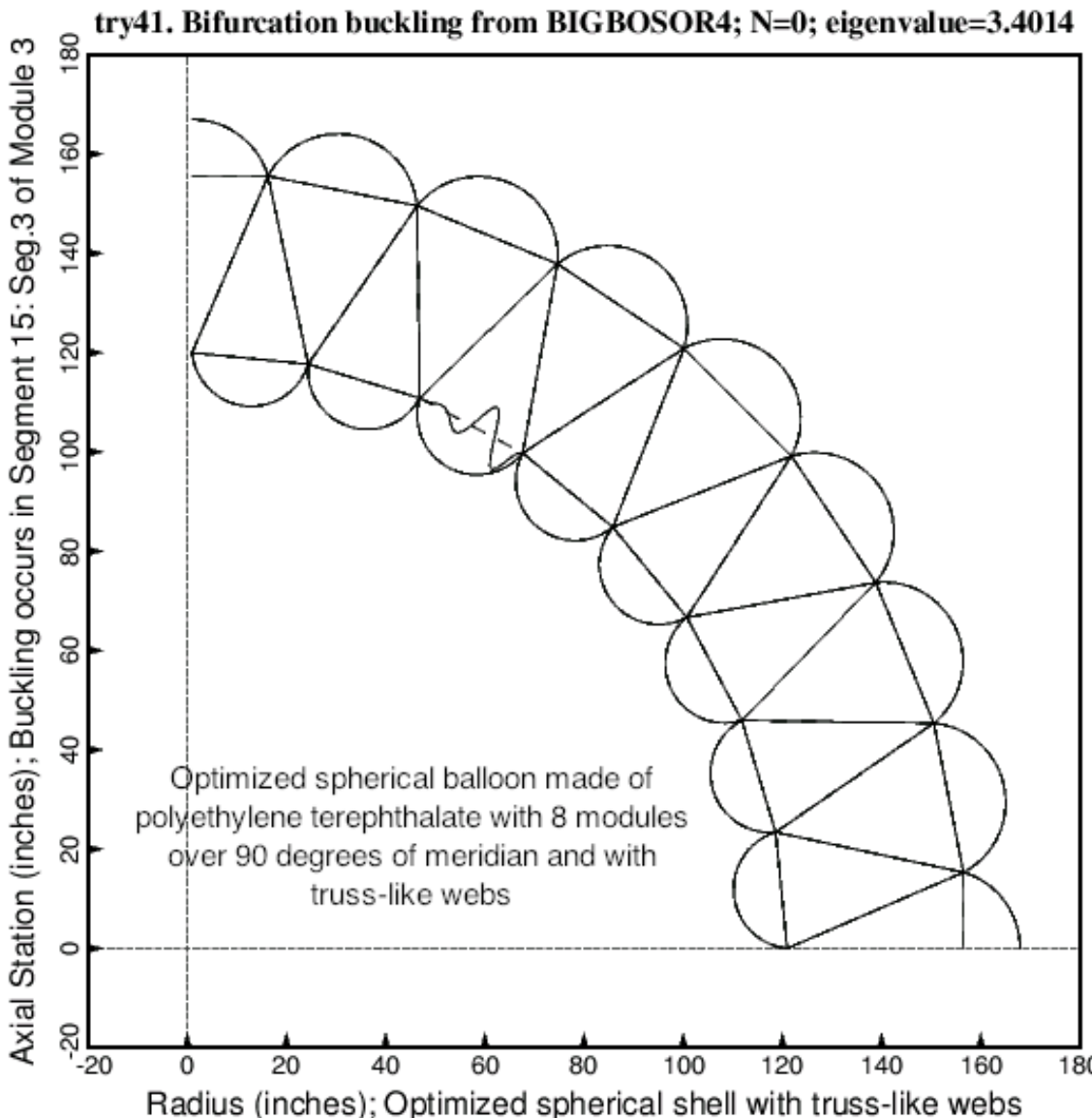


Fig. 10a Buckling mode shape of the optimized spherical balloon with 8 modules and truss-like (slanted) webs. This buckling mode, obtained from BIGBOSOR4, corresponds to $N = 0$ circumferential waves (axisymmetric buckling). Buckling first occurs in Segment 15, that is, in Segment 3 of Module 3. (Segment 15 = (2 modules) \times 6 segments per module) + (3rd segment in Module 3). This location of the $N = 0$ buckling mode obtained from the BIGBOSOR4 stability analysis agrees with the prediction of the location of the initial loss of meridional tension as listed in **Item 10** of Table 9. During optimization cycles (ITYPE = 1 in the *.OPT file) only the $N = 0$ buckling mode from BIGBOSOR4 is computed in order to save computer time and because often there exist, especially for balloons made of strong material such as carbon fiber cloth, spurious non-axisymmetric buckling modes with very low eigenvalues. With ITYPE = 2 (analysis of a fixed design) a critical (minimum) buckling load factor is sought over a wide range of numbers of circumferential waves, N , as listed in **Item 9** of Table 9.

— — Undeformed; There are 8 modules over 90 degrees of the meridian of the spherical balloon.
—— Deformed: Nonsymmetric (N=8 circumferential waves) buckling mode from BIGBOSOR4

try41. Bifurcation buckling from BIGBOSOR4; N=8; eigenvalue=3.3378

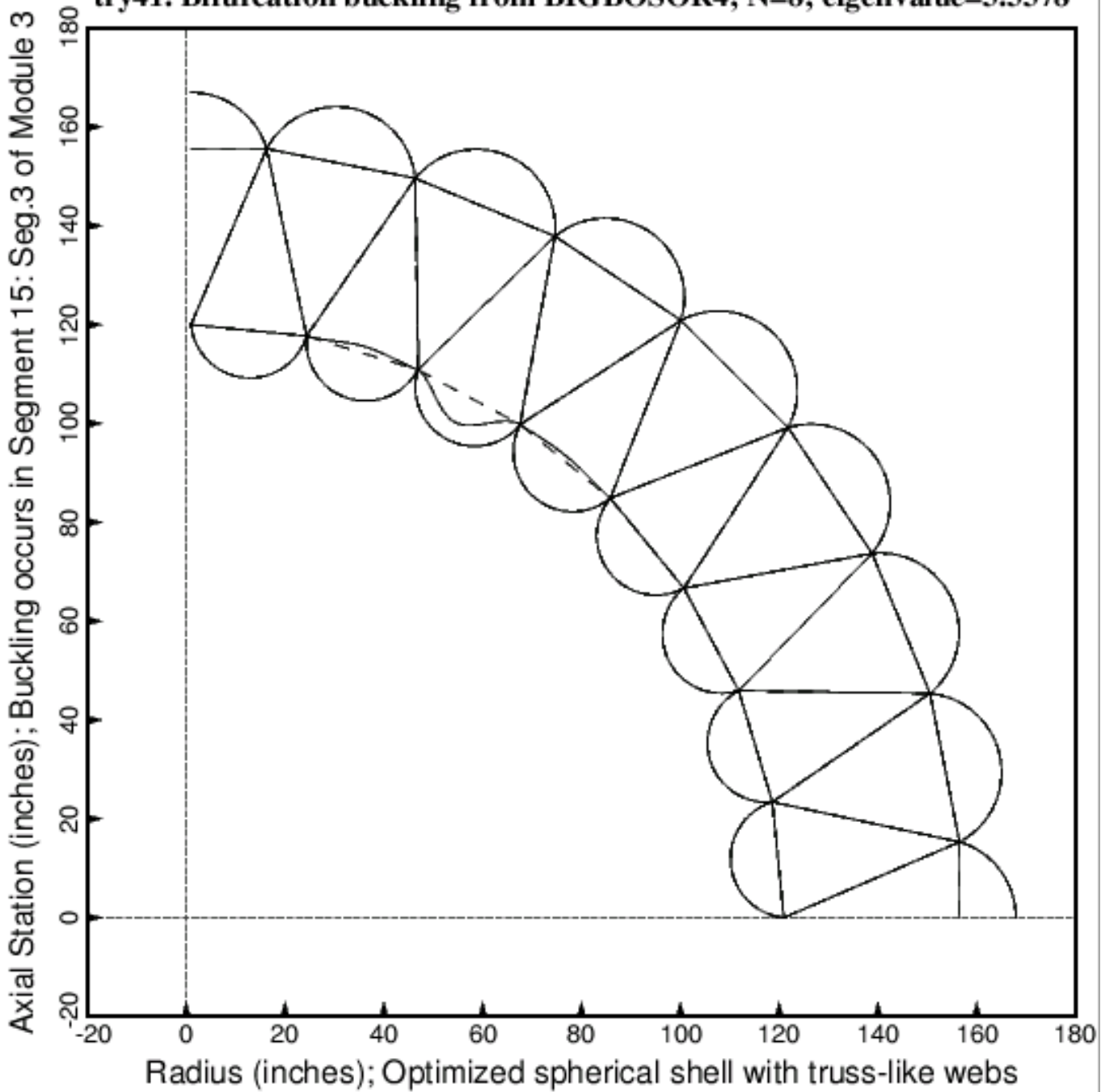


Fig. 10b Buckling mode shape of the optimized spherical balloon with 8 modules and truss-like (slanted) webs. This buckling mode, obtained from BIGBOSOR4, corresponds to $N = 8$ circumferential waves (non-axisymmetric buckling). Buckling first occurs primarily in Segment 15, that is, in Segment 3 of Module 3. (Segment 15 = (2 modules) \times 6 segments per module) + (3rd segment in Module 3).

— — Undeformed; There are 8 modules over 90 degrees of the meridian of the spherical balloon.
— Deformed: Nonsymmetric ($N=16$ circumferential waves) buckling mode from BIGBOSOR4

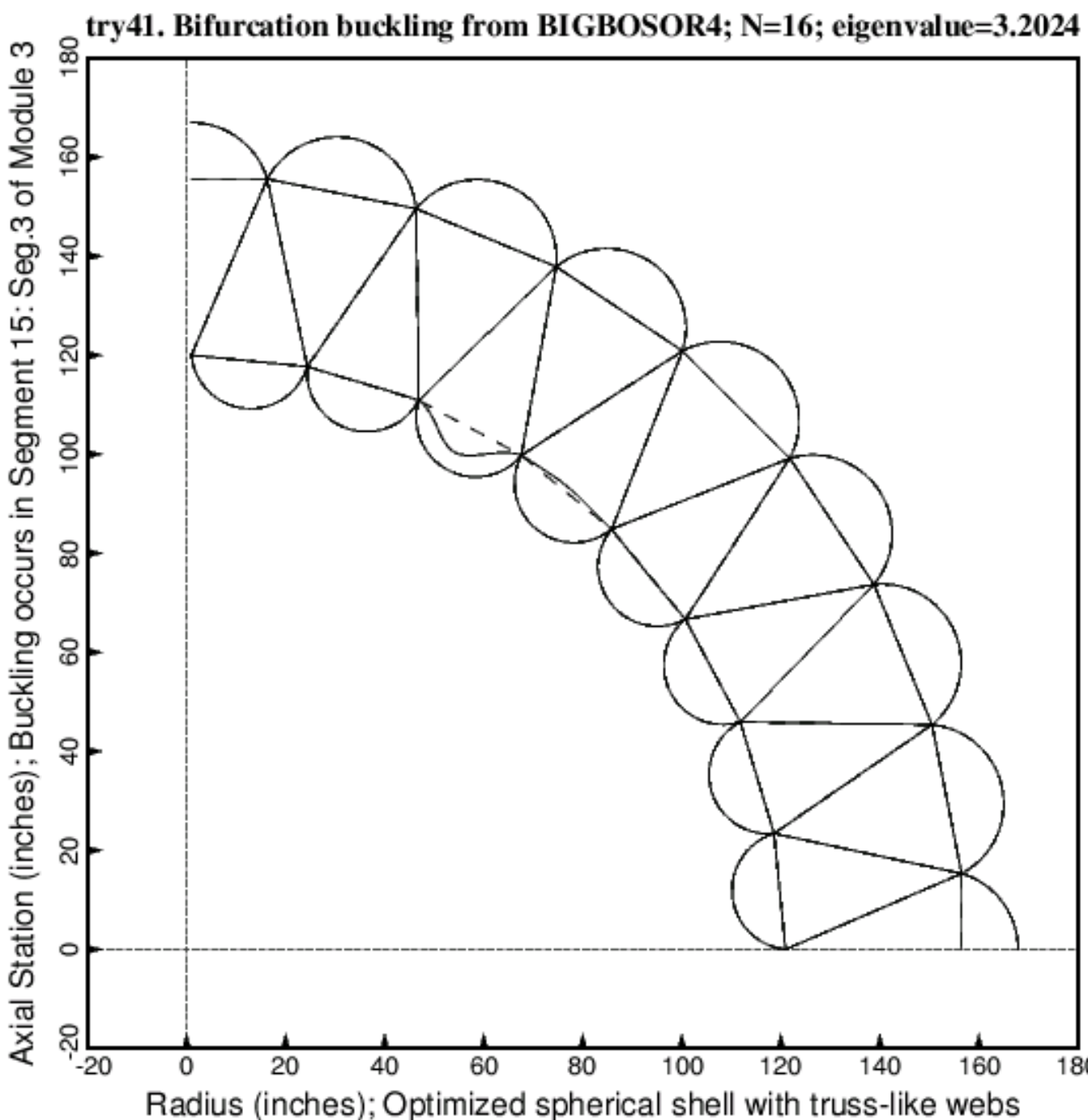


Fig. 10c Buckling mode shape of the optimized spherical balloon with 8 modules and truss-like (slanted) webs. This buckling mode, obtained from BIGBOSOR4, corresponds to $N = 16$ circumferential waves (non-axisymmetric buckling). Buckling first occurs in Segment 15, that is, in Segment 3 of Module 3. (Segment 15 = (2 modules) \times 6 segments per module) + (3rd segment in Module 3).

— — Undeformed; There are 8 modules over 90 degrees of the meridian of the spherical balloon.
—— Deformed: Nonsymmetric ($N=24$ circumferential waves) buckling mode from BIGBOSOR4

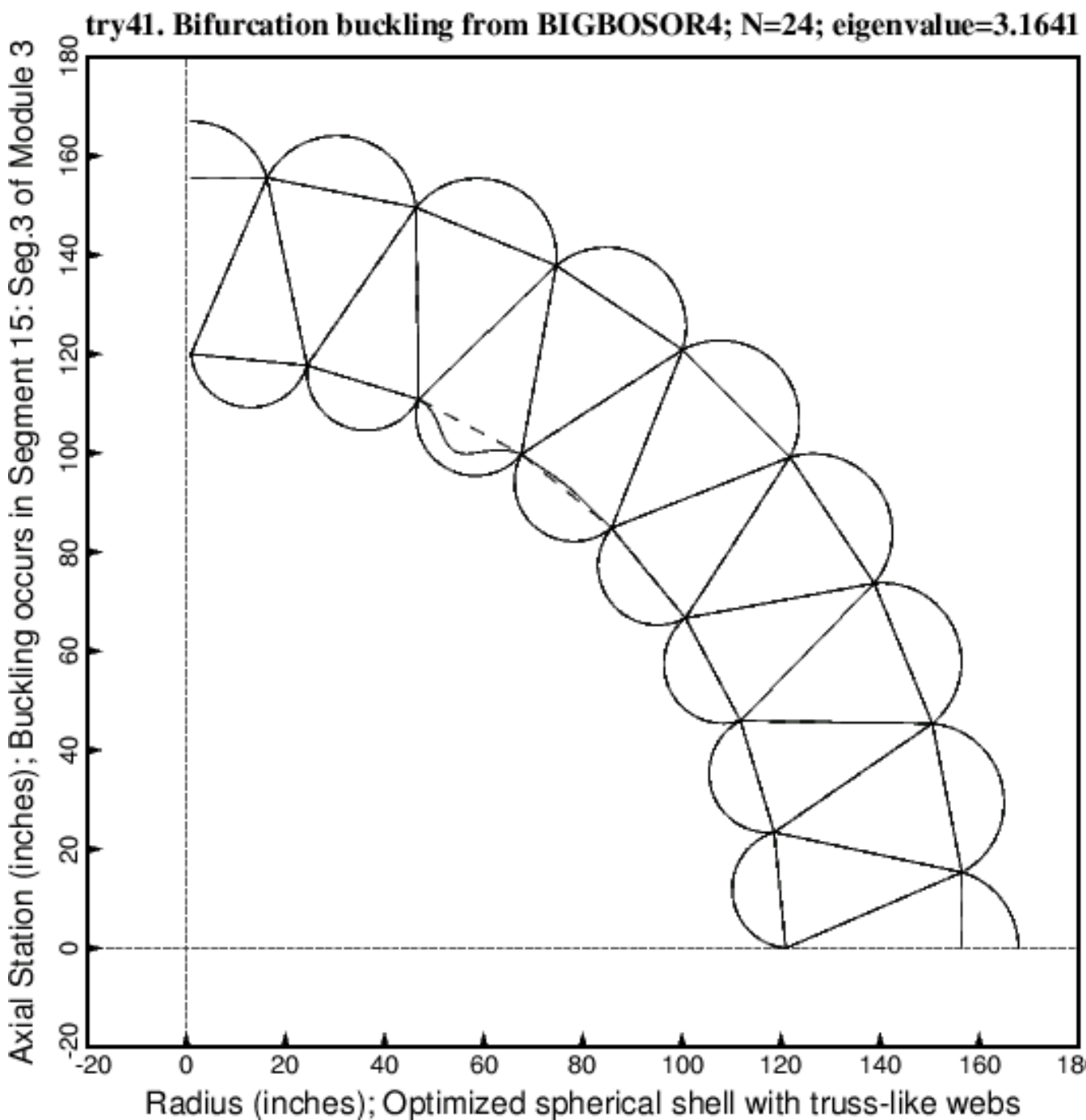


Fig. 10d Buckling mode shape of the optimized spherical balloon with 8 modules and truss-like (slanted) webs. This buckling mode, obtained from BIGBOSOR4, corresponds to $N = 24$ circumferential waves (non-axisymmetric buckling). Buckling first occurs in Segment 15, that is, in Segment 3 of Module 3. (Segment 15 = (2 modules) \times 6 segments per module) + (3rd segment in Module 3).

— — Undeformed; There are 8 modules over 90 degrees of the meridian of the spherical balloon.
— Deformed: Nonsymmetric ($N=32$ circumferential waves) buckling mode from BIGBOSOR4

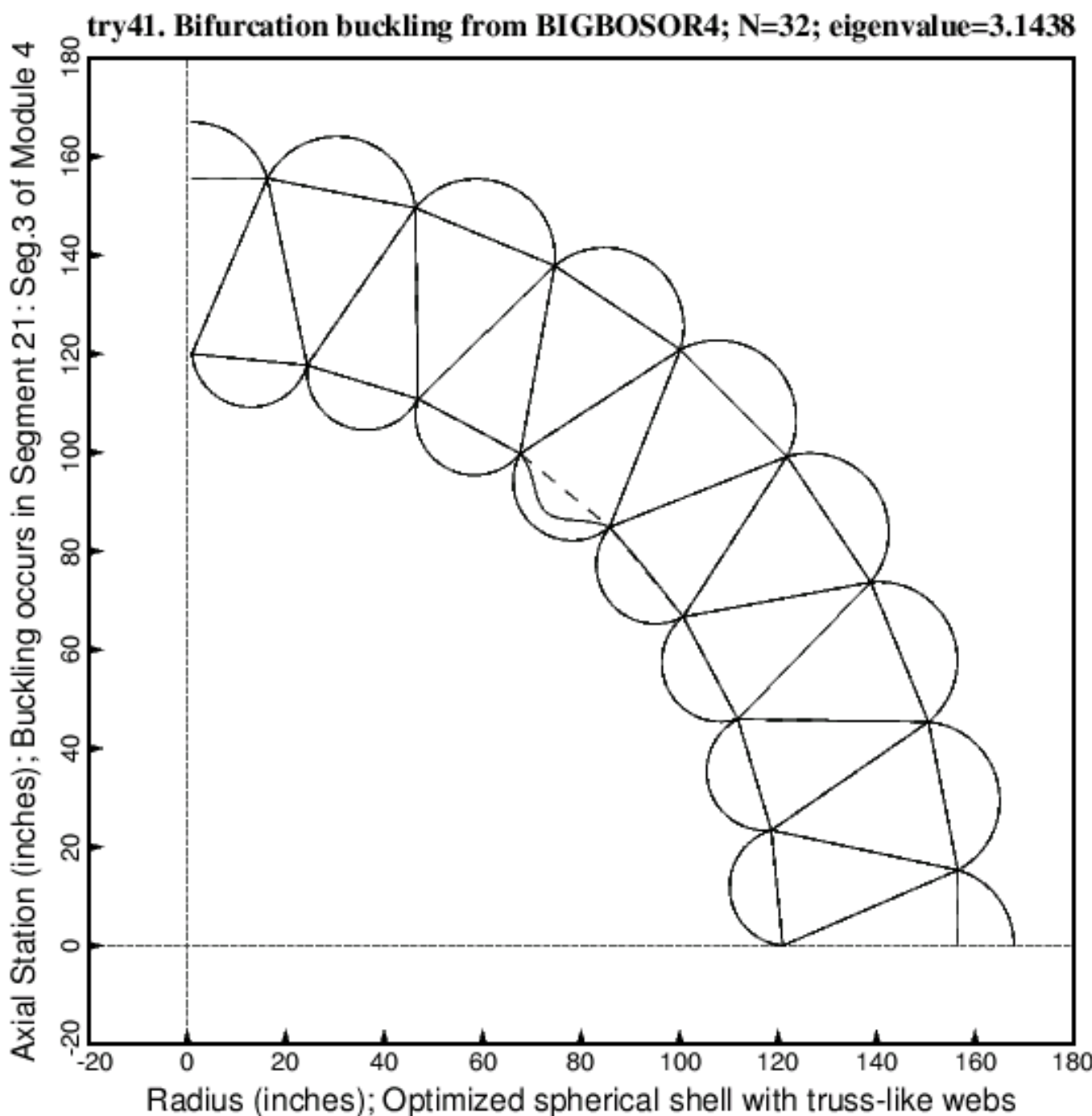


Fig. 10e Buckling mode shape of the optimized spherical balloon with 8 modules and truss-like (slanted) webs. This buckling mode, obtained from BIGBOSOR4, corresponds to $N = 32$ circumferential waves (non-axisymmetric buckling). Buckling first occurs in Segment 21, that is, in Segment 3 of Module 4. (Segment 21 = (3 modules) \times 6 segments per module) + (3rd segment in Module 4).

-- Undeformed; There are 8 modules over 90 degrees of the meridian of the spherical balloon.
— Deformed: Nonsymmetric ($N=40$ circumferential waves) buckling mode from BIGBOSOR4

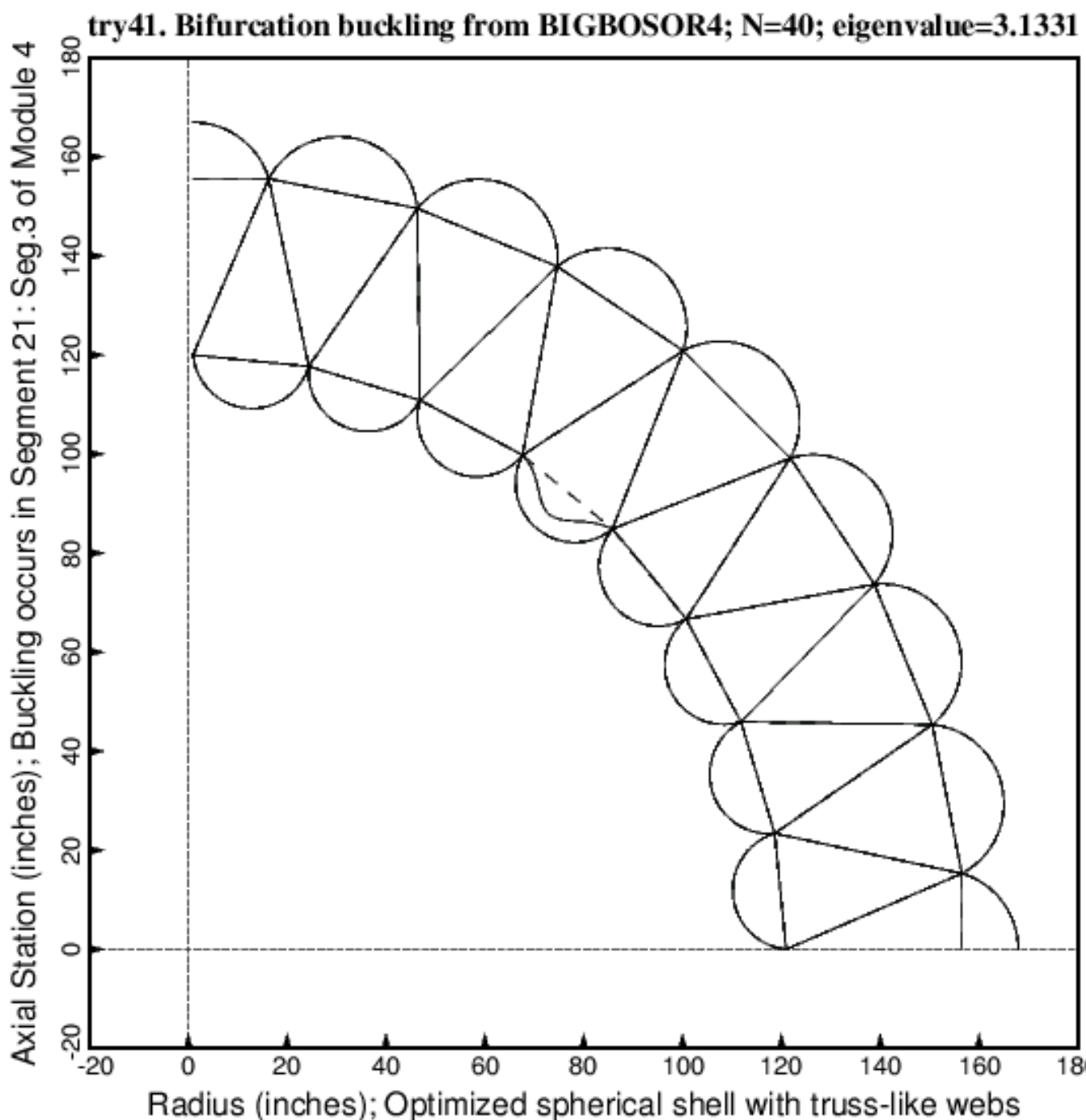


Fig. 10f Buckling mode shape of the optimized spherical balloon with 8 modules and truss-like (slanted) webs. This buckling mode, obtained from BIGBOSOR4, corresponds to $N = 40$ circumferential waves (non-axisymmetric buckling). Buckling first occurs in Segment 21, that is, in Segment 3 of Module 4. (Segment 21 = (3 modules) \times 6 segments per module) + (3rd segment in Module 4).

— — Undeformed; There are 8 modules over 90 degrees of the meridian of the spherical balloon.
— Deformed: Nonsymmetric ($N=48$ circumferential waves) buckling mode from BIGBOSOR4

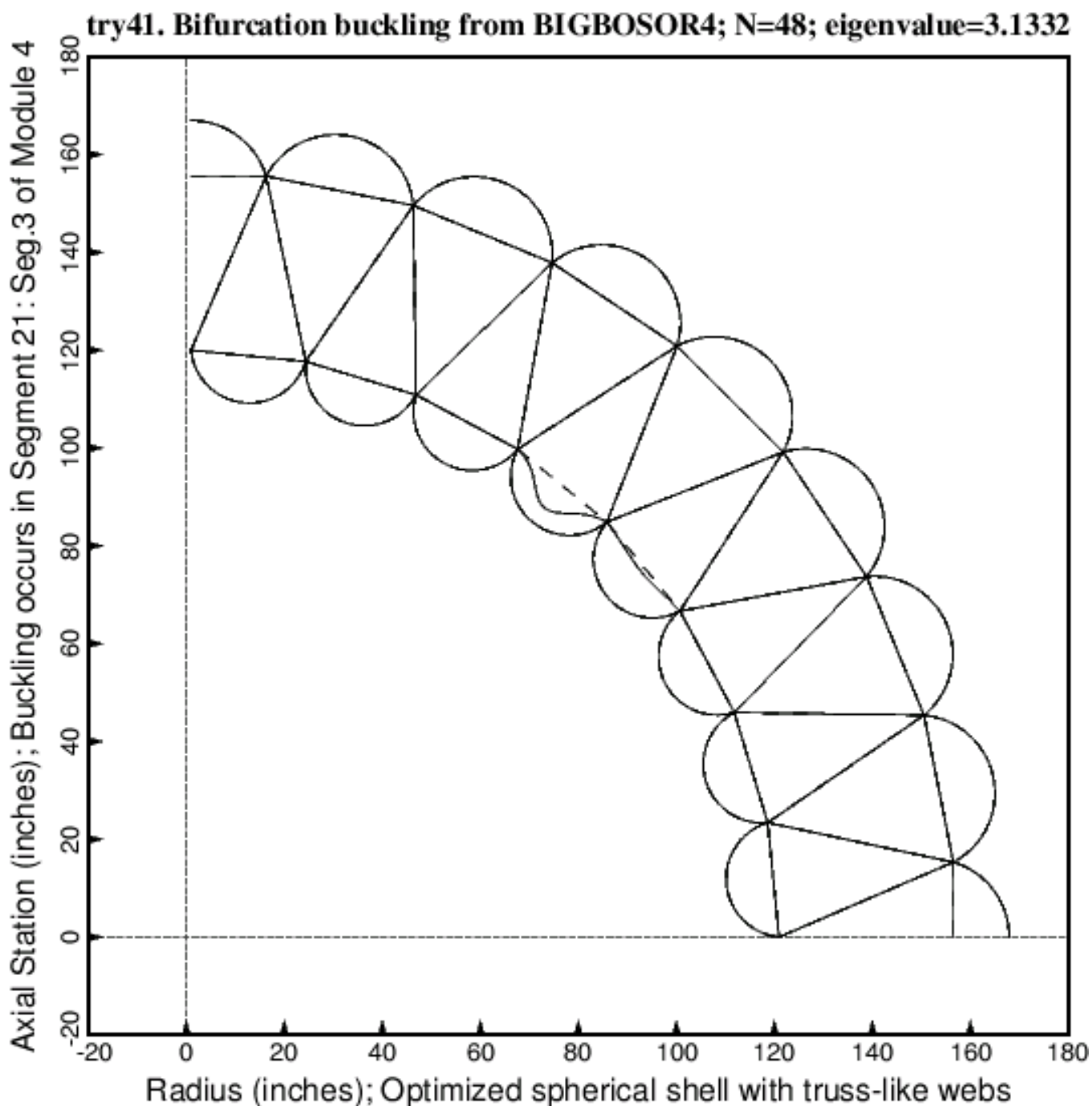


Fig. 10g Buckling mode shape of the optimized spherical balloon with 8 modules and truss-like (slanted) webs. This buckling mode, obtained from BIGBOSOR4, corresponds to $N = 48$ circumferential waves (non-axisymmetric buckling). Buckling first occurs in Segment 21, that is, in Segment 3 of Module 4. (Segment 21 = (3 modules) \times 6 segments per module) + (3rd segment in Module 4).

-- Undeformed; There are 8 modules over 90 degrees of the meridian of the spherical balloon.
— Deformed: Nonsymmetric ($N=56$ circumferential waves) buckling mode from BIGBOSOR4

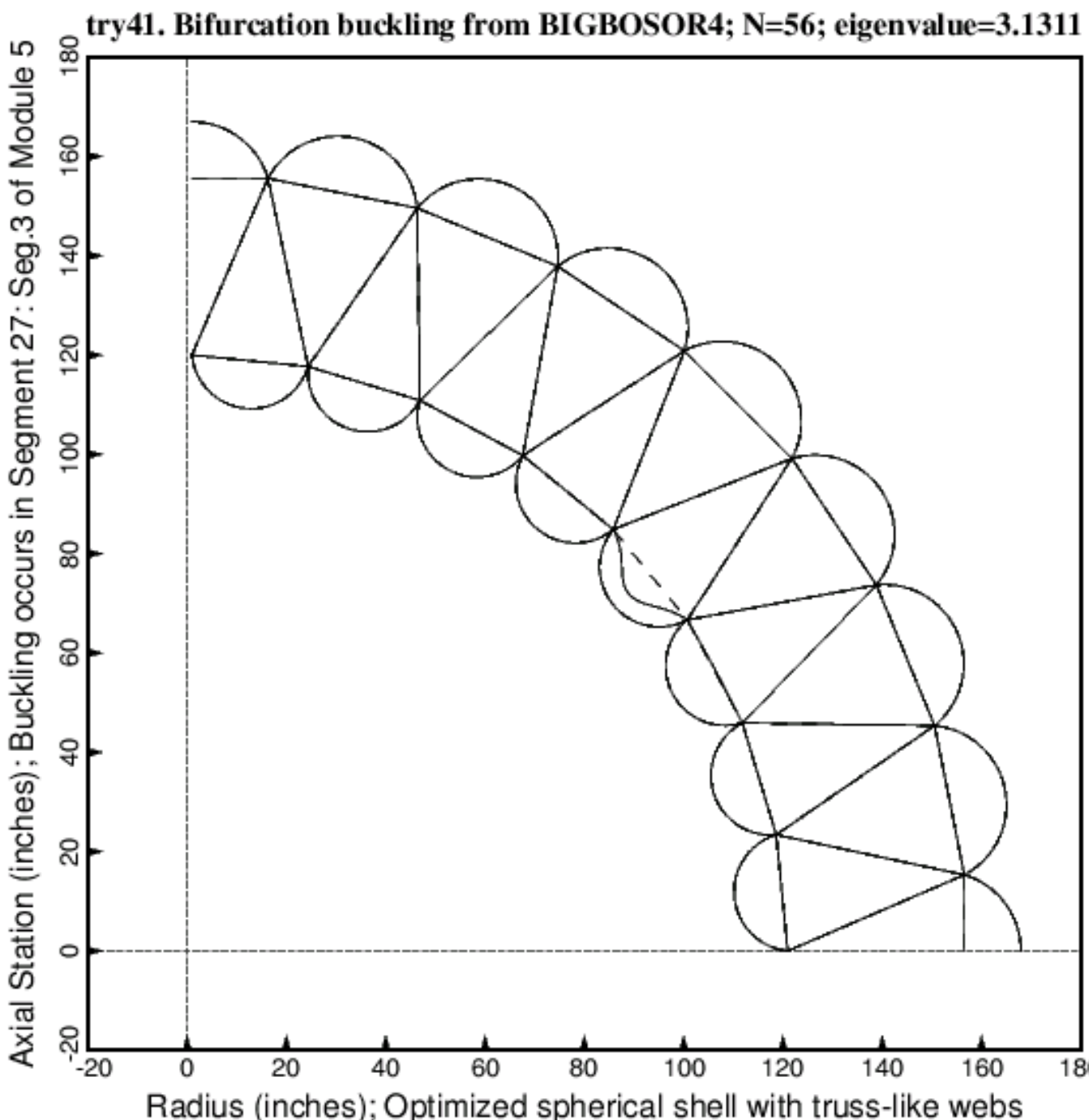


Fig. 10h Buckling mode shape of the optimized spherical balloon with 8 modules and truss-like (slanted) webs. This buckling mode, obtained from BIGBOSOR4, corresponds to $N = 56$ circumferential waves (non-axisymmetric buckling). Buckling first occurs in Segment 27, that is, in Segment 3 of Module 5. (Segment 27 = (4 modules) \times 6 segments per module) + (3rd segment in Module 5).

— — Undeformed; There are 8 modules over 90 degrees of the meridian of the spherical balloon.
— Deformed: Nonsymmetric ($N=64$ circumferential waves) buckling mode from BIGBOSOR4

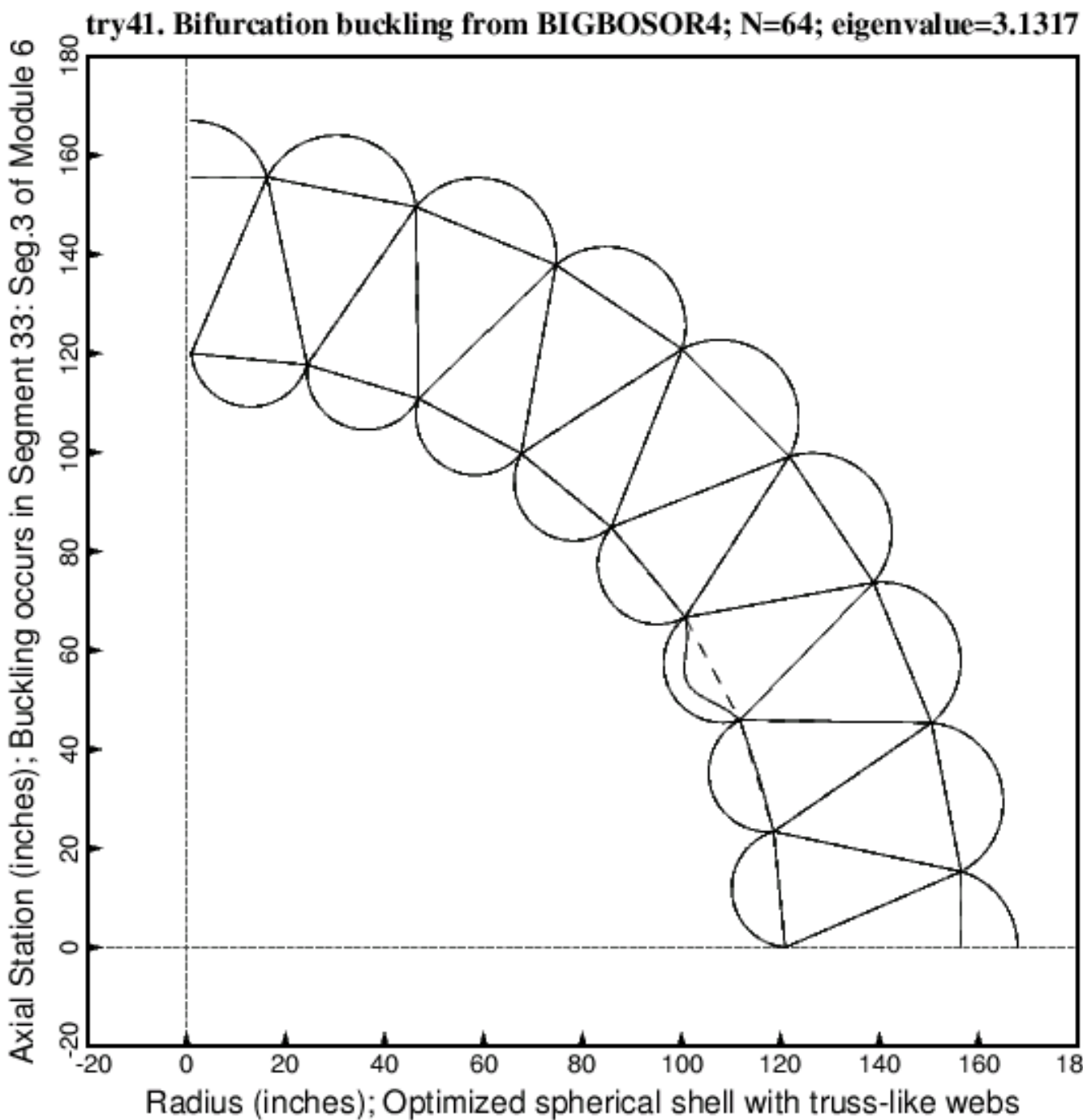


Fig. 10i Buckling mode shape of the optimized spherical balloon with 8 modules and truss-like (slanted) webs. This buckling mode, obtained from BIGBOSOR4, corresponds to $N = 64$ circumferential waves (non-axisymmetric buckling). Buckling first occurs in Segment 33, that is, in Segment 3 of Module 6. (Segment 33 = (5 modules) \times 6 segments per module) + (3rd segment in Module 6).

— — Undeformed; There are 8 modules over 90 degrees of the meridian of the spherical balloon.
— Deformed: Nonsymmetric ($N=72$ circumferential waves) buckling mode from BIGBOSOR4

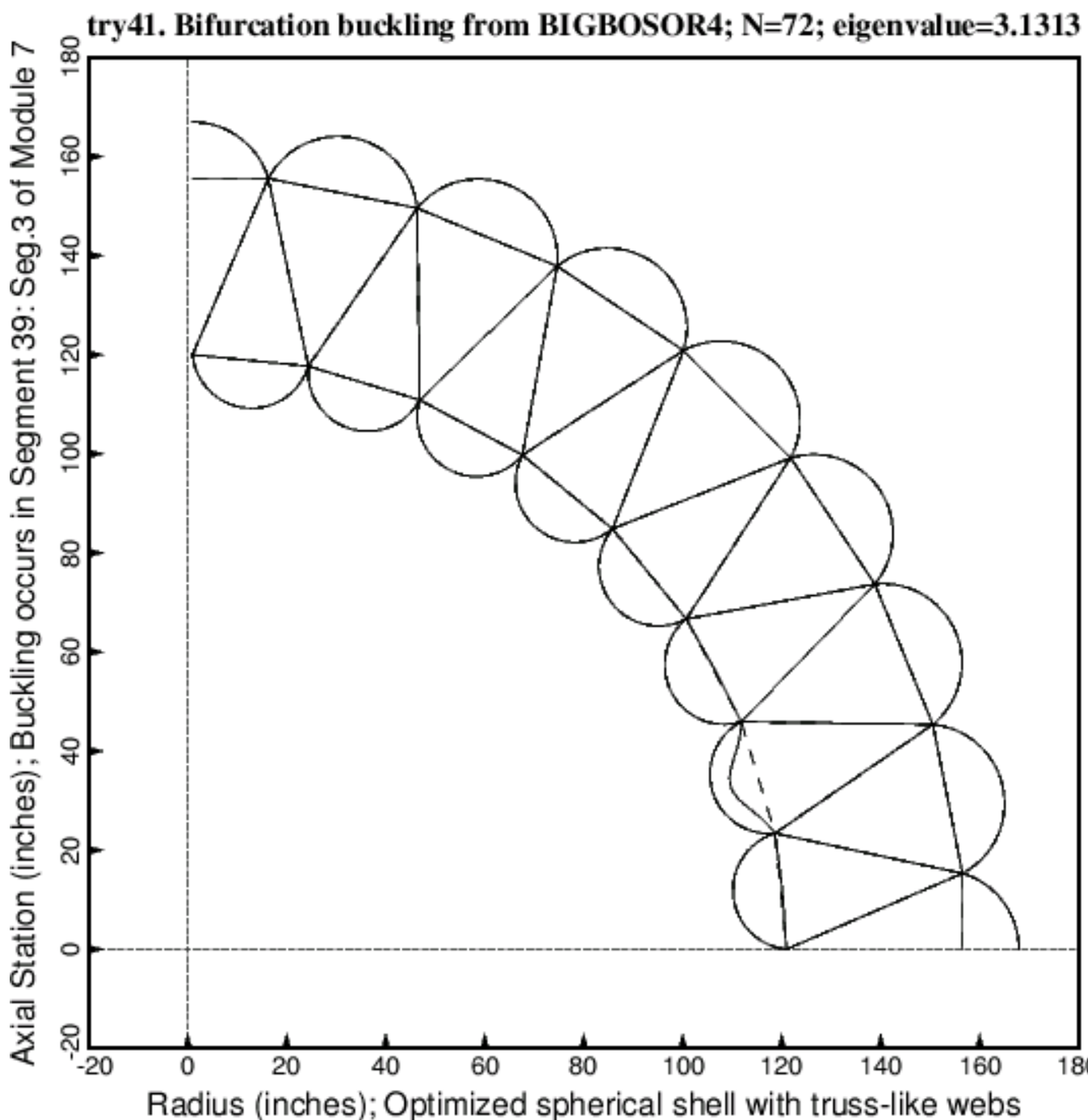


Fig. 10j Buckling mode shape of the optimized spherical balloon with 8 modules and truss-like (slanted) webs. This buckling mode, obtained from BIGBOSOR4, corresponds to $N = 72$ circumferential waves (non-axisymmetric buckling). Buckling first occurs in Segment 39, that is, in Segment 3 of Module 7. (Segment 39 = (6 modules) \times 6 segments per module) + (3rd segment in Module 7).

— Undeformed; There are 8 modules over 90 degrees of the meridian of the spherical balloon.
 — Deformed: Nonsymmetric ($N=80$ circumferential waves) buckling mode from BIGBOSOR4

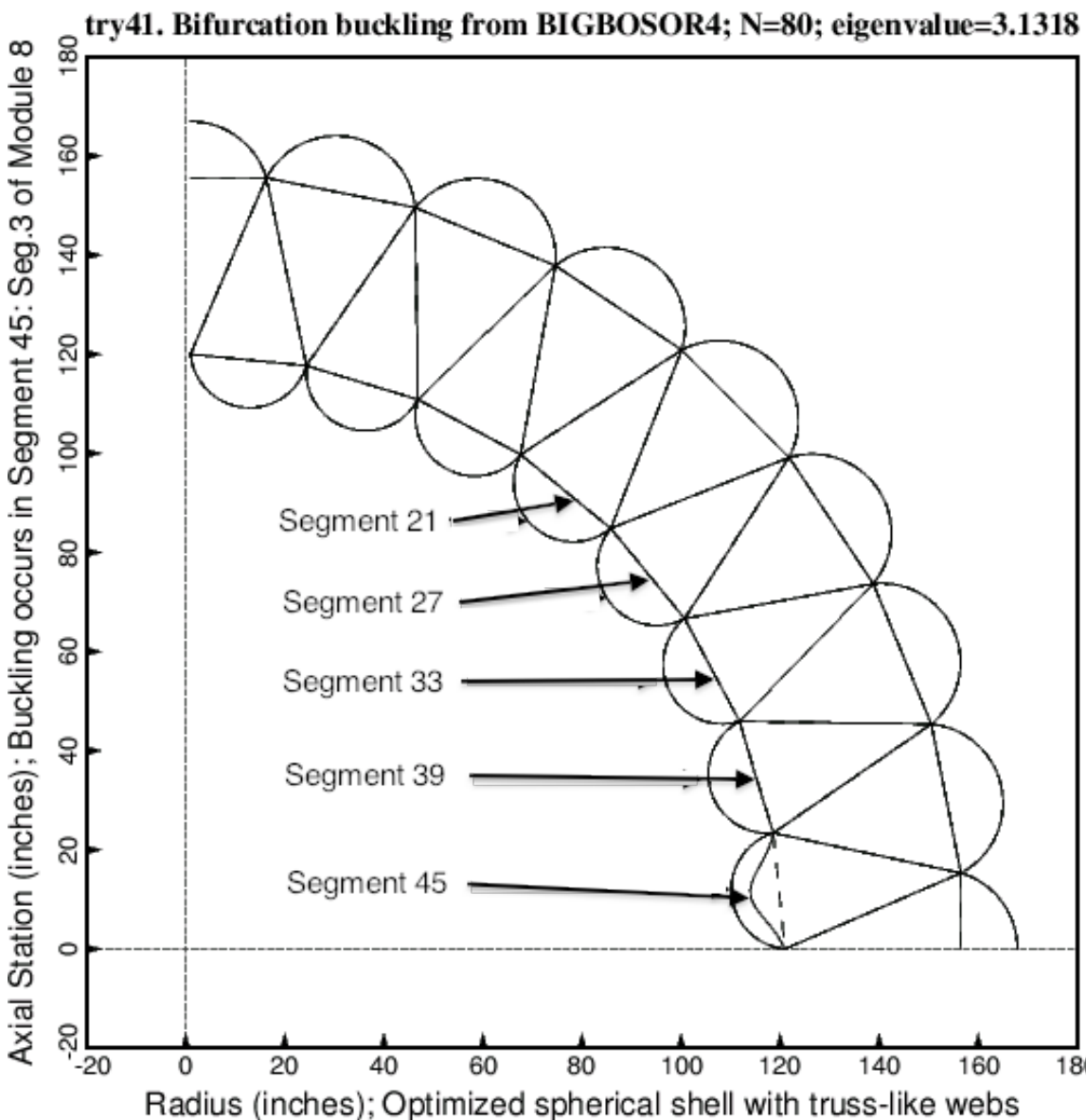


Fig. 10k Buckling mode shape of the optimized spherical balloon with 8 modules and truss-like (slanted) webs. This buckling mode, obtained from BIGBOSOR4, corresponds to $N = 80$ circumferential waves (non-axisymmetric buckling). Buckling first occurs in Segment 45, that is, in Segment 3 of Module 8. (Segment 45 = (7 modules) \times 6 segments per module) + (3rd segment in Module 8). This location of the $N = 80$ buckling mode obtained from the BIGBOSOR4 stability analysis agrees with the prediction of the location of the initial loss of circumferential tension as listed in **Item 10** of Table 9. However, note that the buckling load factors obtained from BIGBOSOR4 are very, very close to one another for $N > 32$ circumferential waves. Local buckling, according to Item 9 in Table 9, occurs essentially simultaneously in segments 21, 27, 33, 39, and 45. For every case processed during this study local buckling always occurs first in one or more of the straight segments of the inner wall, that is, in a segment with thickness = TFINNR.

-- Undeformed; There are only 4 modules over 90 degrees of the meridian of the spherical balloon.
 — Deformed; Load set B = PINNER=0 psi, PMIDDLE=60 psi, POUTER=0 psi

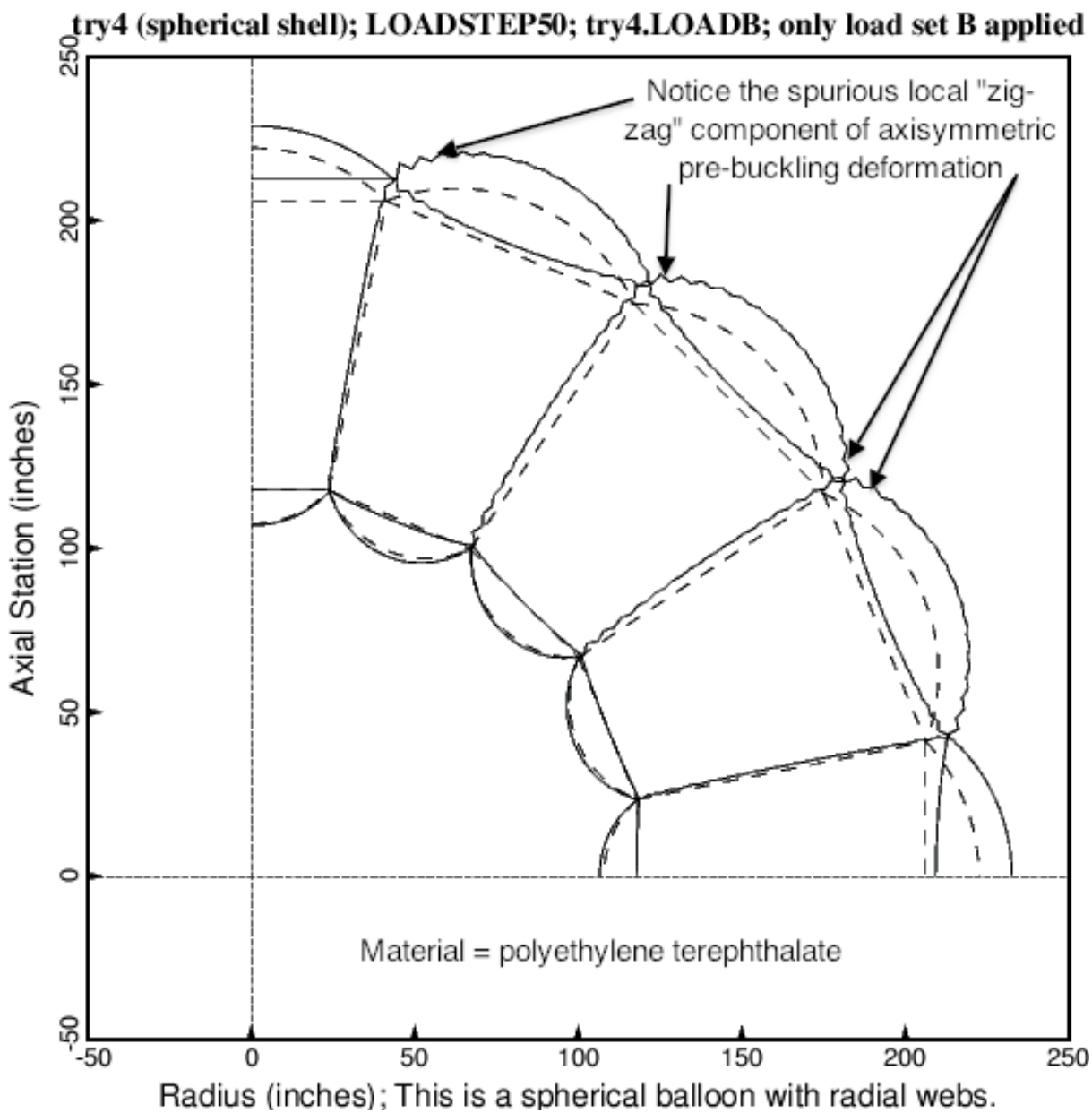


Fig. 11 Axisymmetric pre-buckling displacement of a spherical balloon with only four modules and radial webs under Load B, that is, under the “fixed” (non-eigenvalue) loads, PINNER = 0 psi, PMIDDLE = 60 psi, POUTER = 0 psi. There is a spurious local “zig-zag” component of the pre-buckling deformation that does not occur in the spherical balloons with more modules except in the optimized balloons made of carbon fiber cloth such as those displayed in Figs. 33a and Fig. 58. Those optimized spherical and cylindrical balloons have much thinner wall segments because the carbon fiber cloth is much stronger than the polyethylene terephthalate material. The spurious “zig-zag” component of displacement seems to occur more frequently in “shell” segments that are very thin.

- - - Undeformed; There are 8 modules over 90 degrees of the meridian of the spherical balloon.
 — Deformed; Load set B = PINNER=0 psi, PMIDDLE=60 psi, POUTER=0 psi

try42. Pre-buckled state of spherical shell. Only Load Set B is applied.

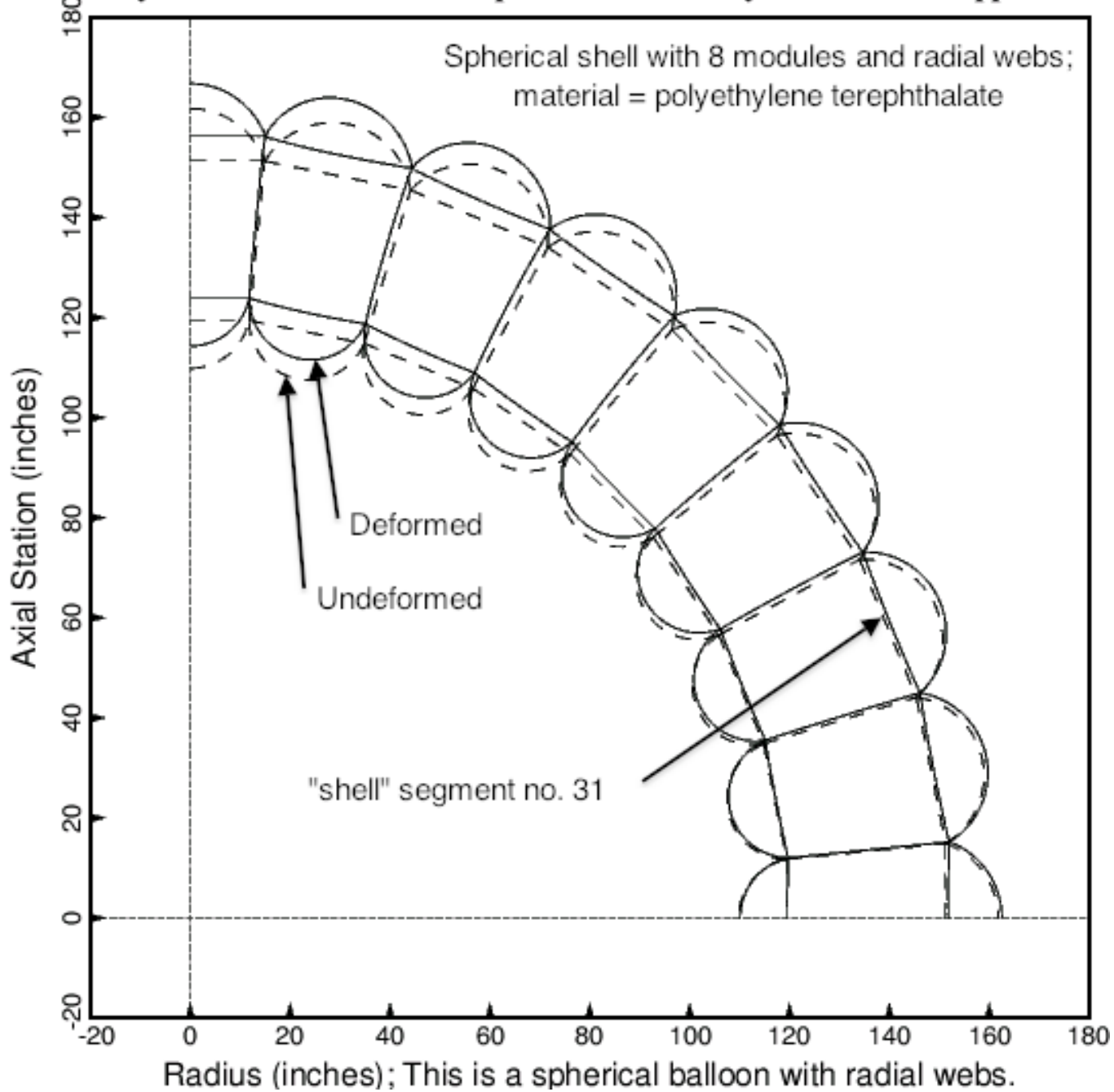


Fig. 12 Spherical balloon with 8 modules and radial webs. This figure shows the axisymmetric pre-buckling deformation caused by Load B (the "fixed", non-eigenvalue loads: PINNER = 0 psi, PMIDDLE = 60 psi, POUTER = 0 psi). This figure is analogous to Fig. 6. The next five figures concentrate on "shell" segment no. 31. The axisymmetric pre-buckling displacement is non-uniform because the spherical balloon is not isotropic.

- See the previous figure for an overall view of the pre-buckling deformation

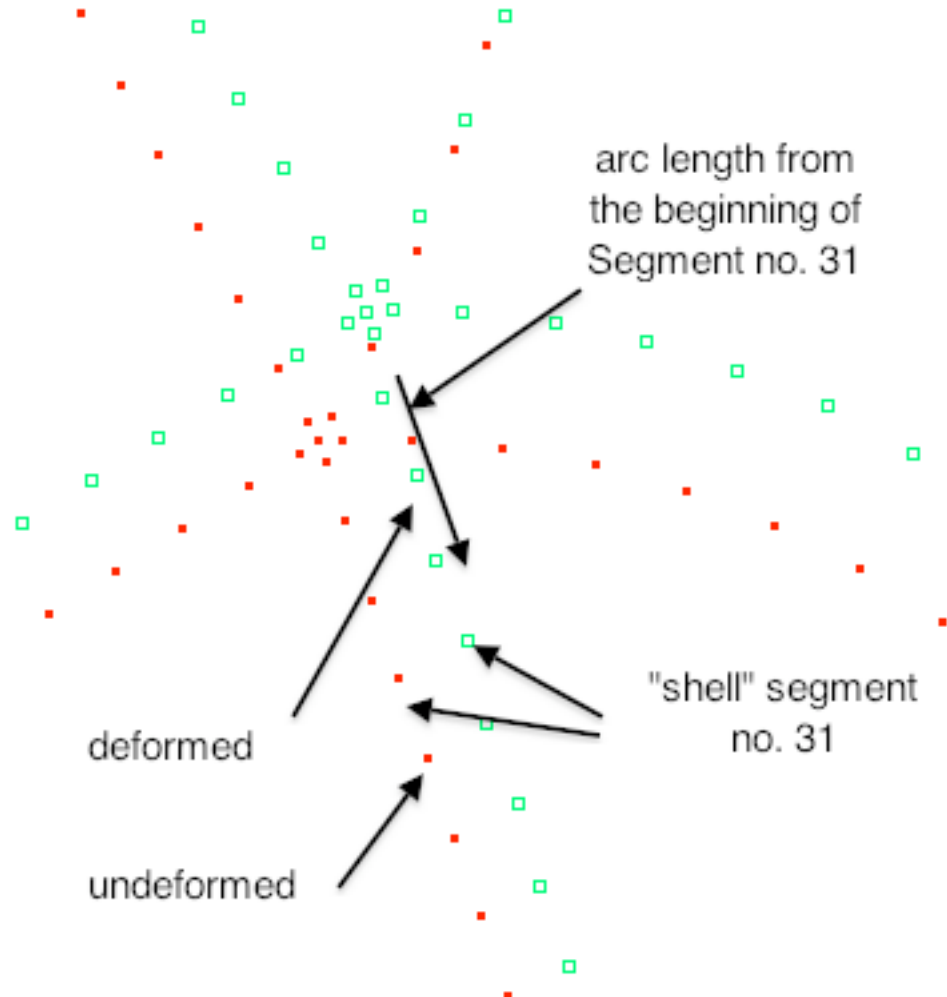


Fig. 13 The nodal point discretization near the beginning of "shell" segment no. 31 (see the previous figure) in the optimized spherical balloon with 8 modules and radial webs. This figure shows the axisymmetric pre-buckling deformation caused by Load B (the "fixed", non-eigenvalue loads: PINNER = 0 psi, PMIDDLE = 60 psi, POUTER = 0 psi) in this local region of the spherical balloon. The axisymmetric pre-buckling deformation of the entire model of the spherical balloon is displayed in the previous figure. There are 31 nodal points in each segment of the balloon. The next figure shows the extreme fiber meridional strain plotted versus the arc length starting from the junction of Segment 31 with previous segments in the balloon.

- Left-most fiber meridional stress in Seg.1, Module 7 of 8; radial webs; PMIDDLE=60 psi, POUTER=0
- Right-most fiber meridional stress in Seg.1, Module 7 of 8; radial webs; PMIDDLE=60 psi, POUTER=0

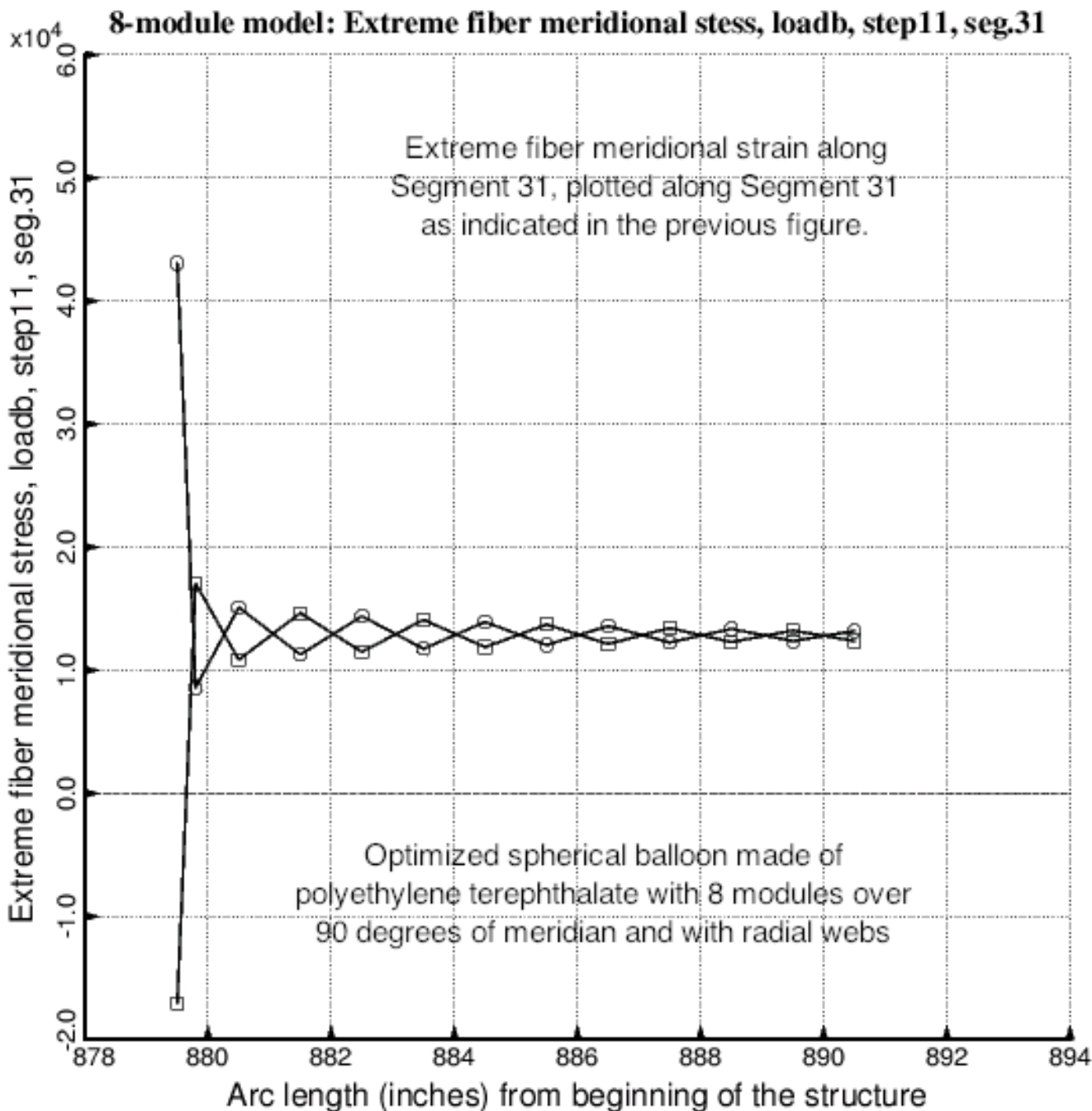


Fig. 14 Extreme fiber meridional stress along the beginning of "shell" Segment No. 31 of the optimized spherical balloon with 8 modules and with radial webs. The pre-buckling axisymmetric stress is generated by Load B, the "fixed", non-eigenvalue loads: PINNER = 0 psi, PMIDDLE = 60 psi, POUTER = 0 psi. The axisymmetric pre-buckling deformation is depicted in the previous two figures. These extreme fiber meridional stresses are derived from the model in which there are 31 nodal points in each segment of the model.

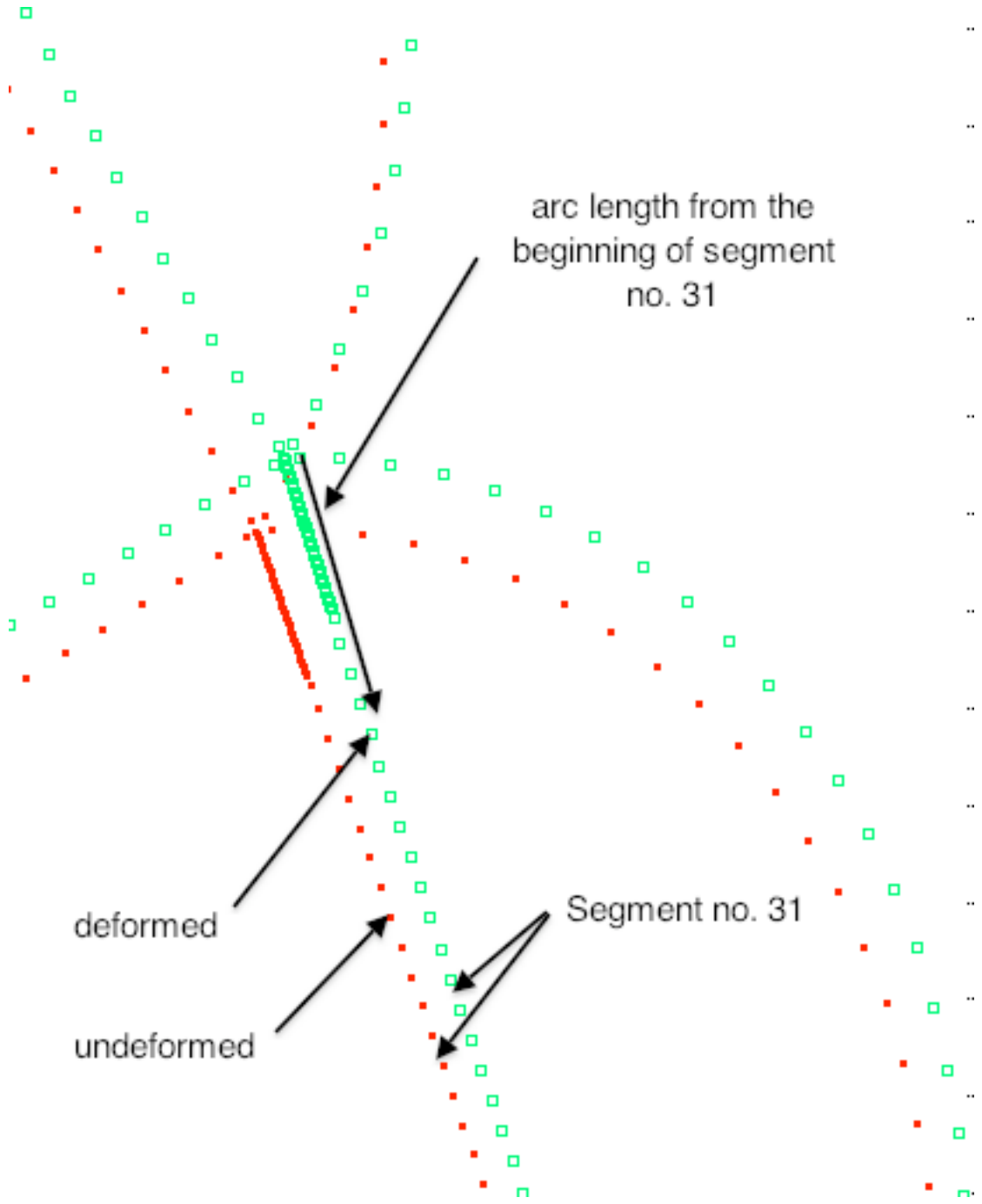


Fig. 15 This figure is analogous to Fig. 13. Axisymmetric pre-buckling deformation of the spherical balloon subjected to Load B, the “fixed”, non-eigenvalue loads, PINNER = 0 psi, PMIDDLE = 60 psi, POUTER = 0 psi. The optimized spherical balloon has 8 modules and radial webs. In this model there are 97 nodal points in Segment No. 31, with nodal points concentrated along the first part of the “shell” segment, which is nearest the junction of Segment 31 with the previous segments in the structure. All the other segments in the model have 31 nodal points.

- Left-most fiber meridional stress in Seg.1, Module 7 of 8; radial webs; PMIDDLE=60 psi, POUTER=0
- Right-most fiber meridional stress in Seg.1, Module 7 of 8; radial webs; PMIDDLE=60 psi, POUTER=0

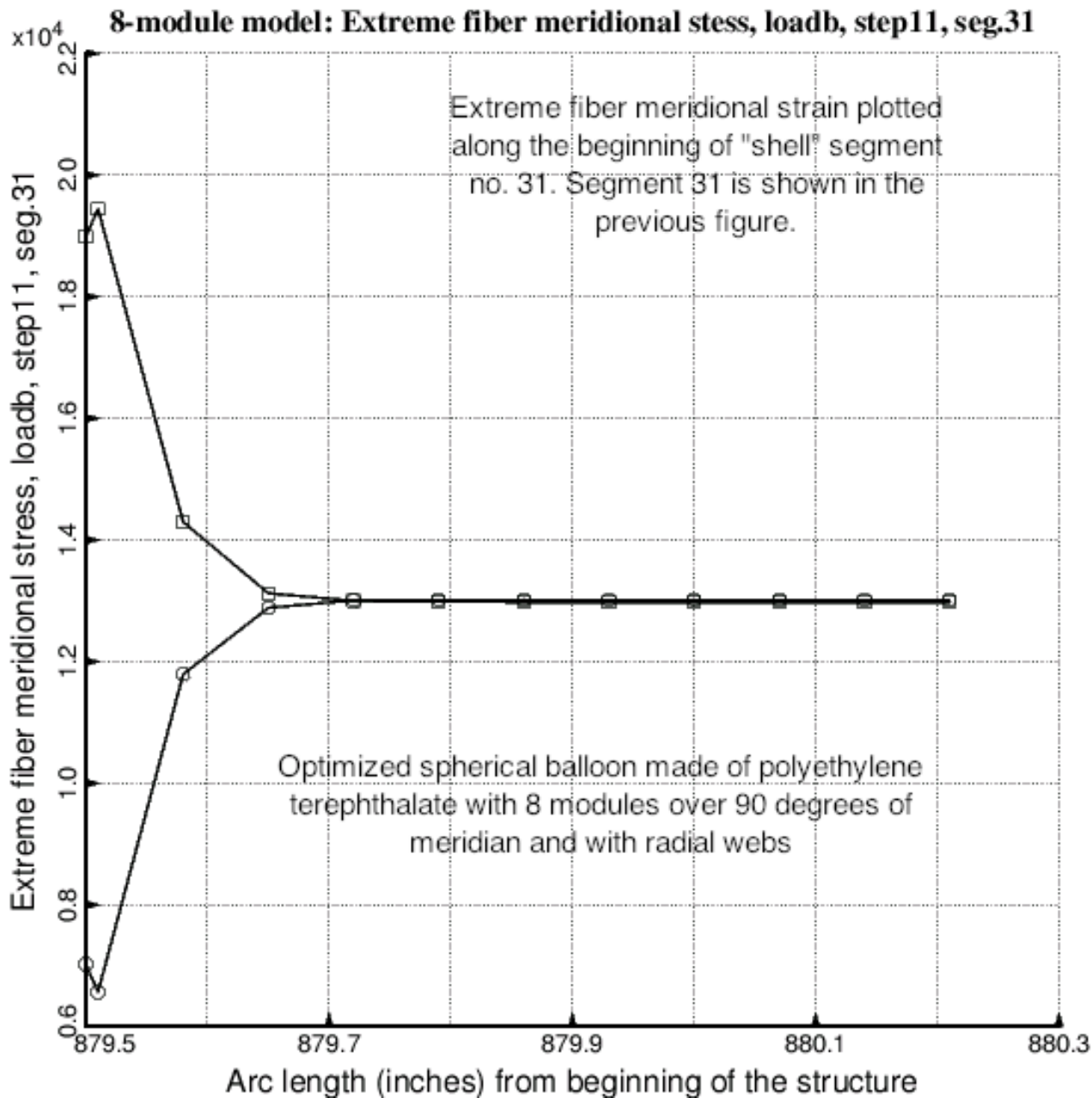


Fig. 16 Extreme fiber meridional stress along the beginning of "shell" Segment No. 31 of the optimized spherical balloon with 8 modules and with radial webs. The pre-buckling axisymmetric stress is generated by Load B, the "fixed", non-eigenvalue loads: PINNER = 0 psi, PMIDDLE = 60 psi, POUTER = 0 psi. The axisymmetric pre-buckling deformation is depicted in the previous figure. These predictions are derived from the model in which there are 97 nodal points in Segment 31 and 31 nodal points in all the other segments of the model. Nodal points are especially concentrated near the beginning of Segment 31, as displayed in the previous figure.

- Left-most fiber meridional stress in Seg.1, Module 7 of 8; radial webs; PMIDDLE=60 psi, POUTER=0
- Right-most fiber meridional stress in Seg.1, Module 7 of 8; radial webs; PMIDDLE=60 psi, POUTER=0
- △ Left-most fiber meridional stress in Seg.1, Module 7 of 8; radial webs; refined Seg.31
- + Right-most fiber meridional stress in Seg.1, Module 7 of 8; radial webs; refined Seg.31

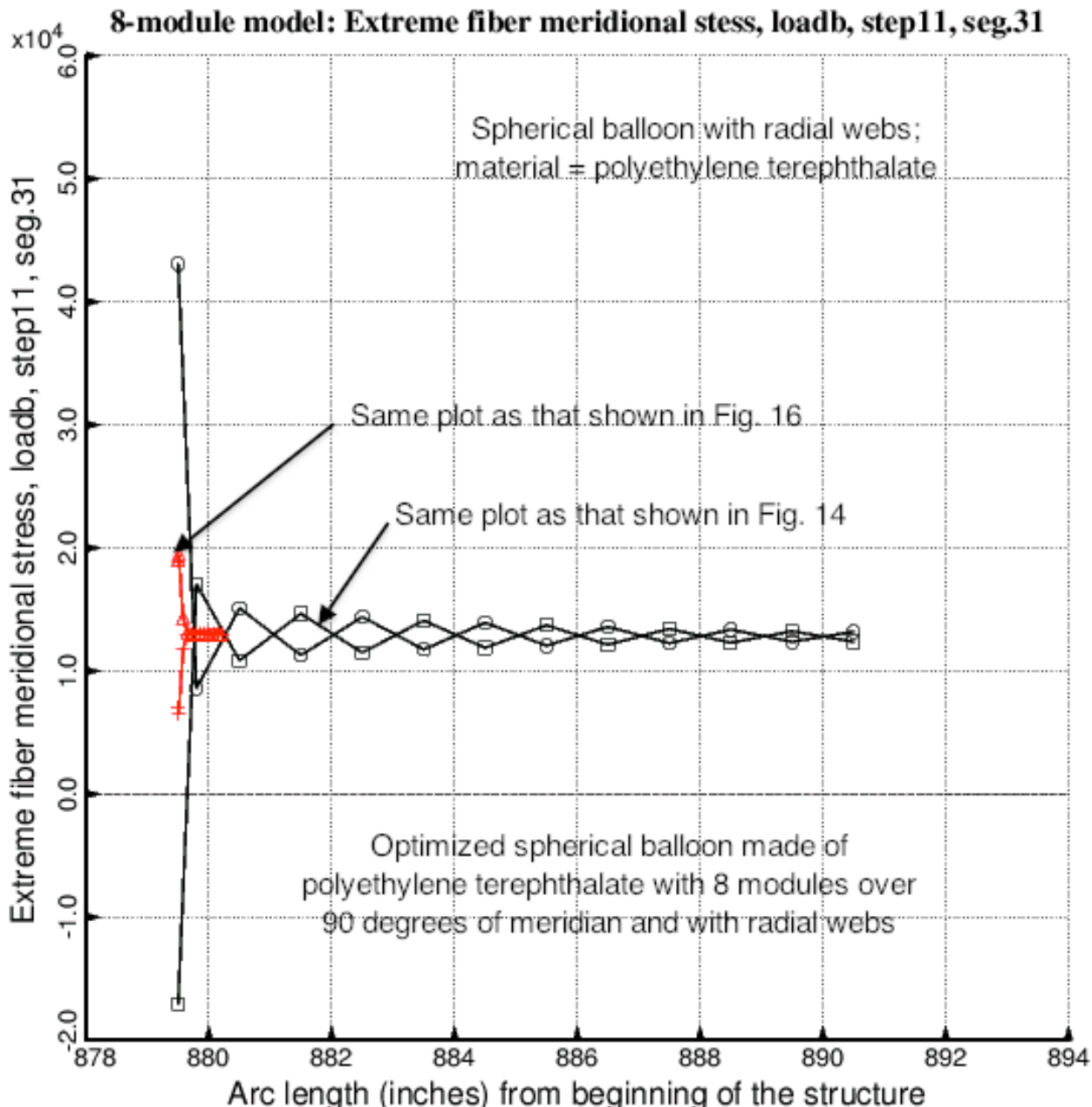


Fig. 17 Axisymmetric pre-buckling extreme fiber meridional stress along the beginning of Segment 31 in the spherical balloon with 8 modules and radial webs. The loading is Load B, the “fixed”, non-eigenvalue loads: PINNER = 0 psi, PMIDDLE = 60 psi, POUTER = 0 psi. The entire model and deformation are shown in Fig. 12. Note that the amplitude of the meridional stress concentration decreases dramatically with the increase in nodal point density in the immediate neighborhood of the junction of Segment 31 with the previous segments of the model.

-- Undeformed; There are 8 modules over 90 degrees of the meridian of the spherical balloon.
— Deformed: Axisymmetric ($N=0$ circumferential waves) buckling mode from BIGBOSOR4

try42. Bifurcation buckling from BIGBOSOR4; $N=0$; eigenvalue=3.6727

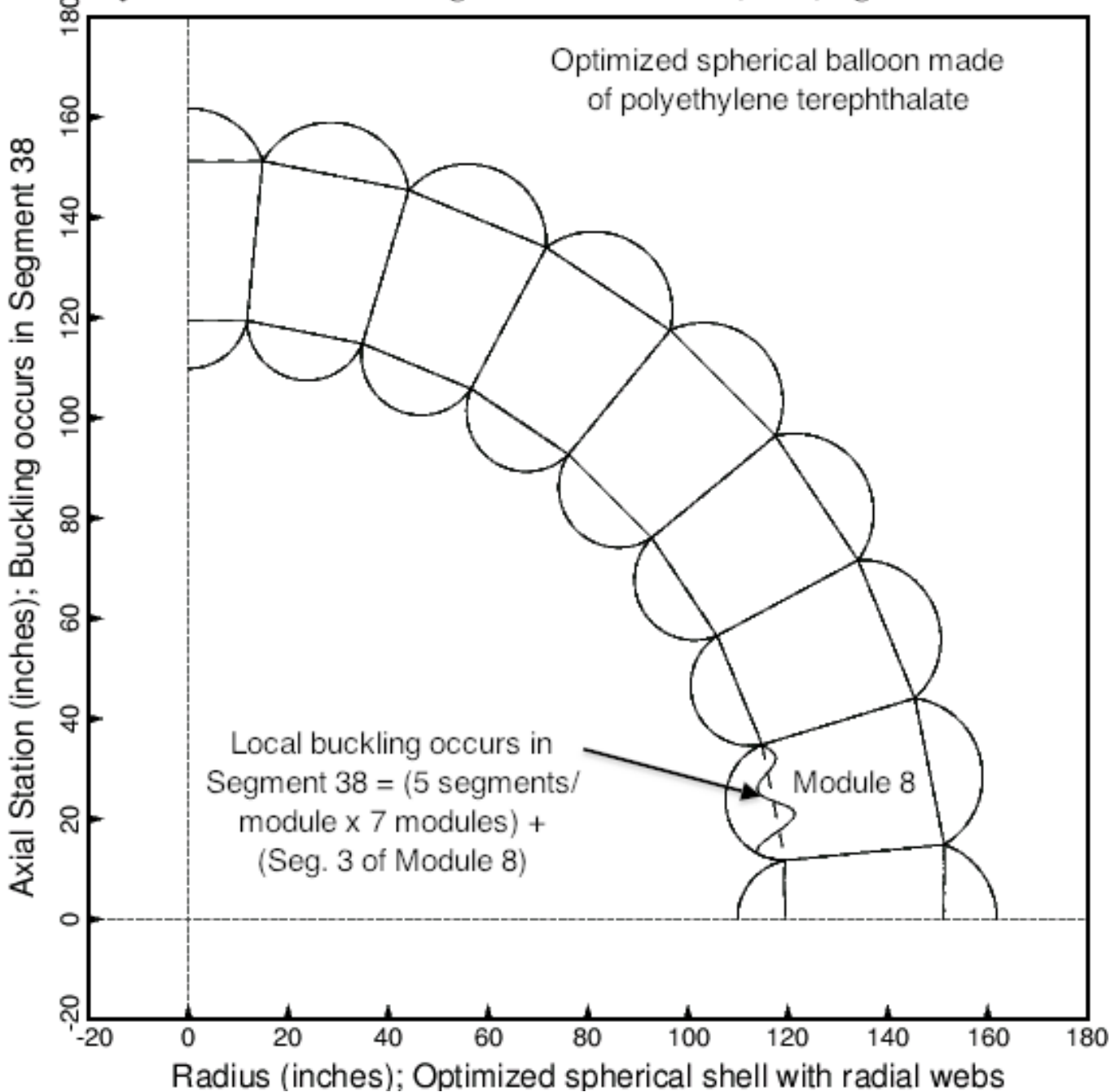


Fig. 18 Axisymmetric ($N = 0$ circumferential waves) bifurcation buckling from BIGBOSOR4 of the optimized spherical balloon with 8 modules and radial webs. Local buckling occurs in the inner wall straight segment that has thickness = TFINNR. No general buckling mode of any optimized or non-optimized spherical balloon was ever found during the work that produced this paper.

— — Undeformed; There are 8 modules over 90 degrees of the meridian of the spherical balloon.
— Deformed: Nonsymmetric ($N=64$ circumferential waves) buckling mode from BIGBOSOR4

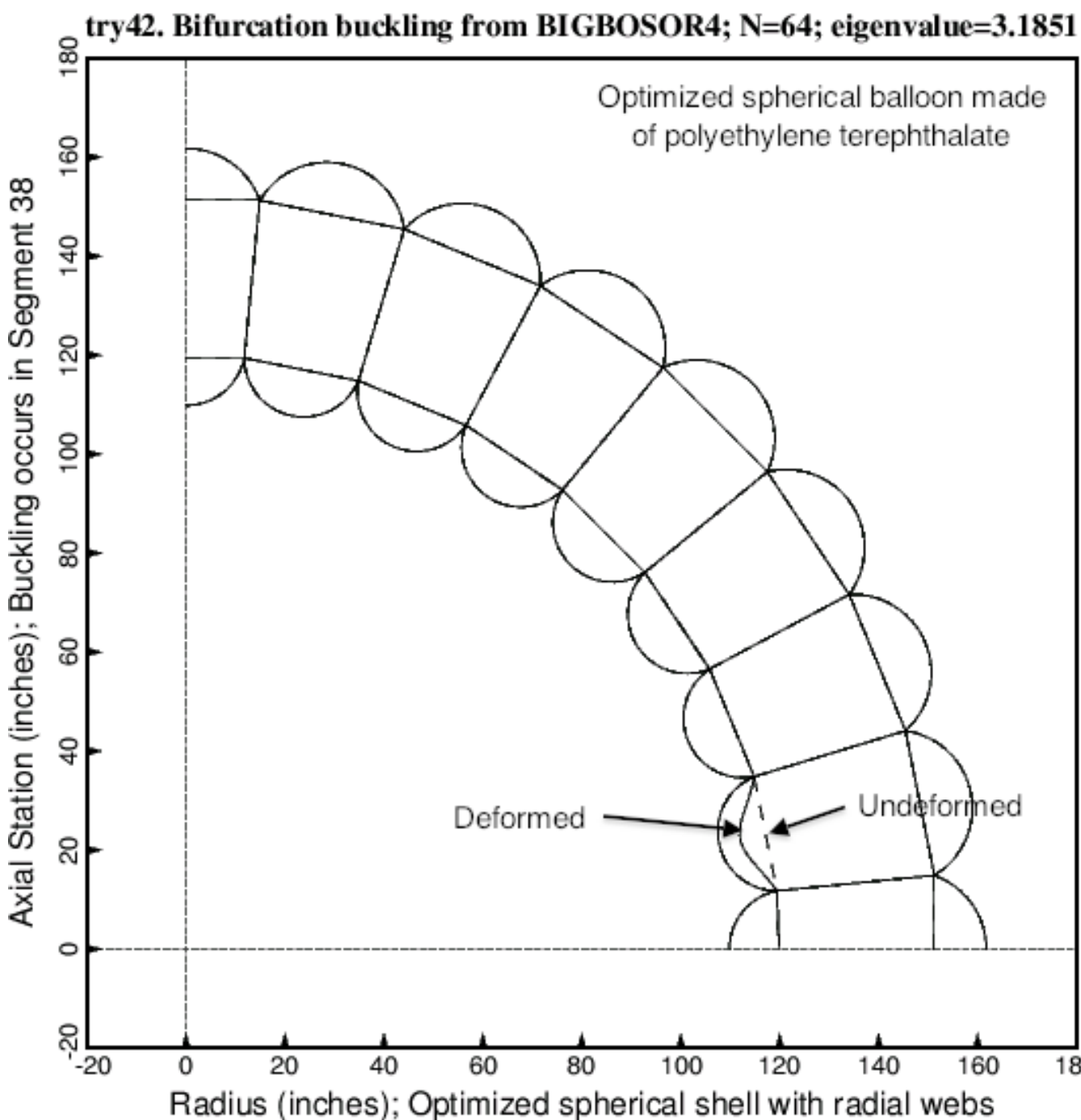


Fig. 19 Non-axisymmetric bifurcation buckling with $N = 64$ circumferential waves from BIGBOSOR4 of the optimized spherical balloon with 8 modules and radial webs. Local buckling occurs in the inner wall straight segment that has thickness = TFINNR. This is the fundamental buckling mode. No general buckling mode of any spherical balloon was ever found during the work that produced this paper.

— Undeformed; There are 8 modules over 90 degrees of the meridian of the spherical balloon.
 — Deformed: Axisymmetric (N=0 circumferential waves) 45th N=0 buckling mode from BIGBOSOR4

try42. Bifurcation buckling from BIGBOSOR4; N=0; eigenvalue45=3.885

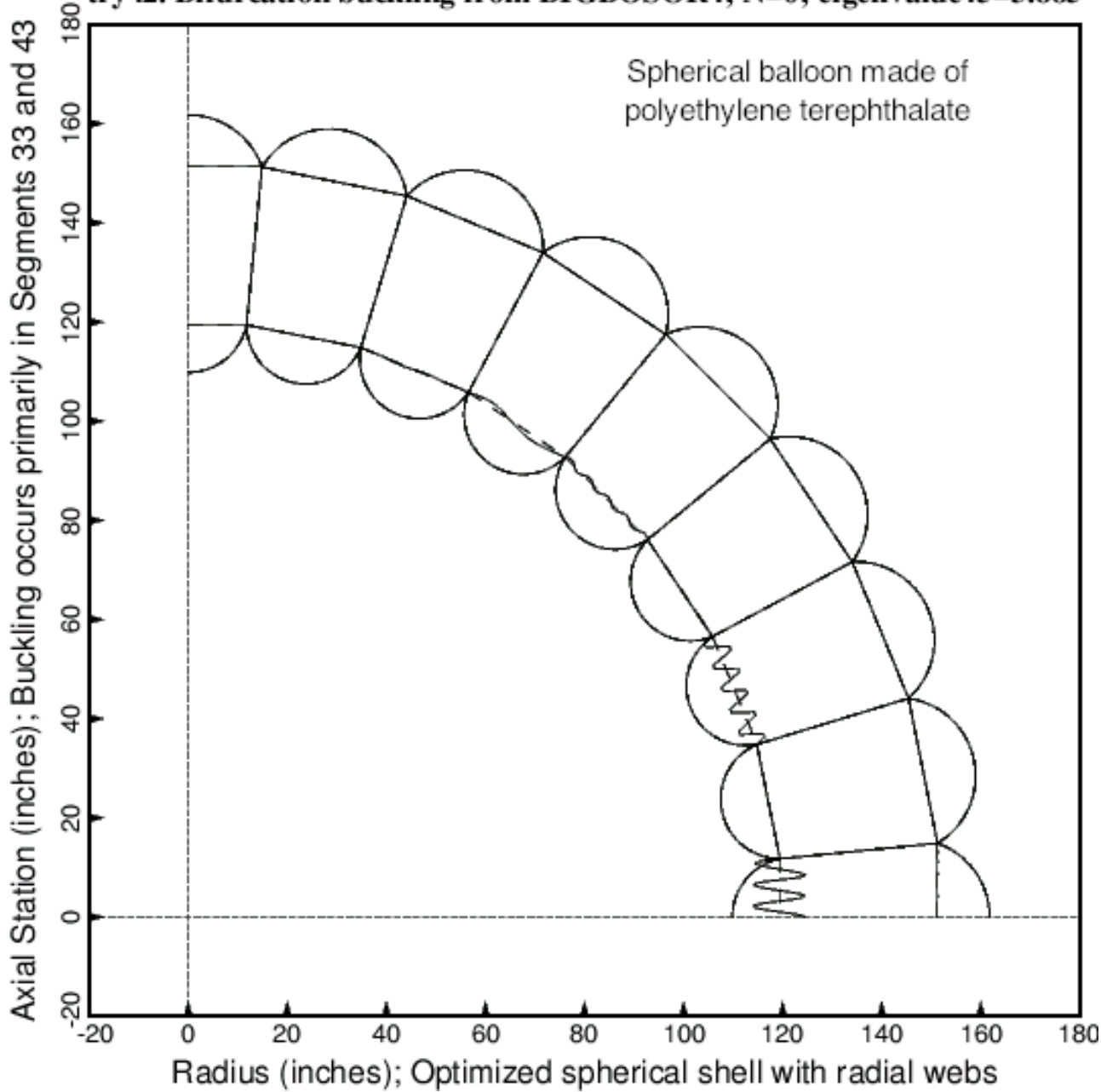


Fig. 20 Axisymmetric bifurcation buckling from BIGBOSOR4 of the optimized spherical balloon with 8 modules and radial webs. Local buckling occurs in the inner wall straight segments that have thickness = TFINNR. This is the 45th axisymmetric buckling mode. Note that there are many, many local buckling eigenvalues corresponding to axisymmetric buckling modes clustered between 3.67 (Fig.18) and 3.88 (this figure). No general buckling mode of any spherical balloon was ever found during the work that produced this paper.

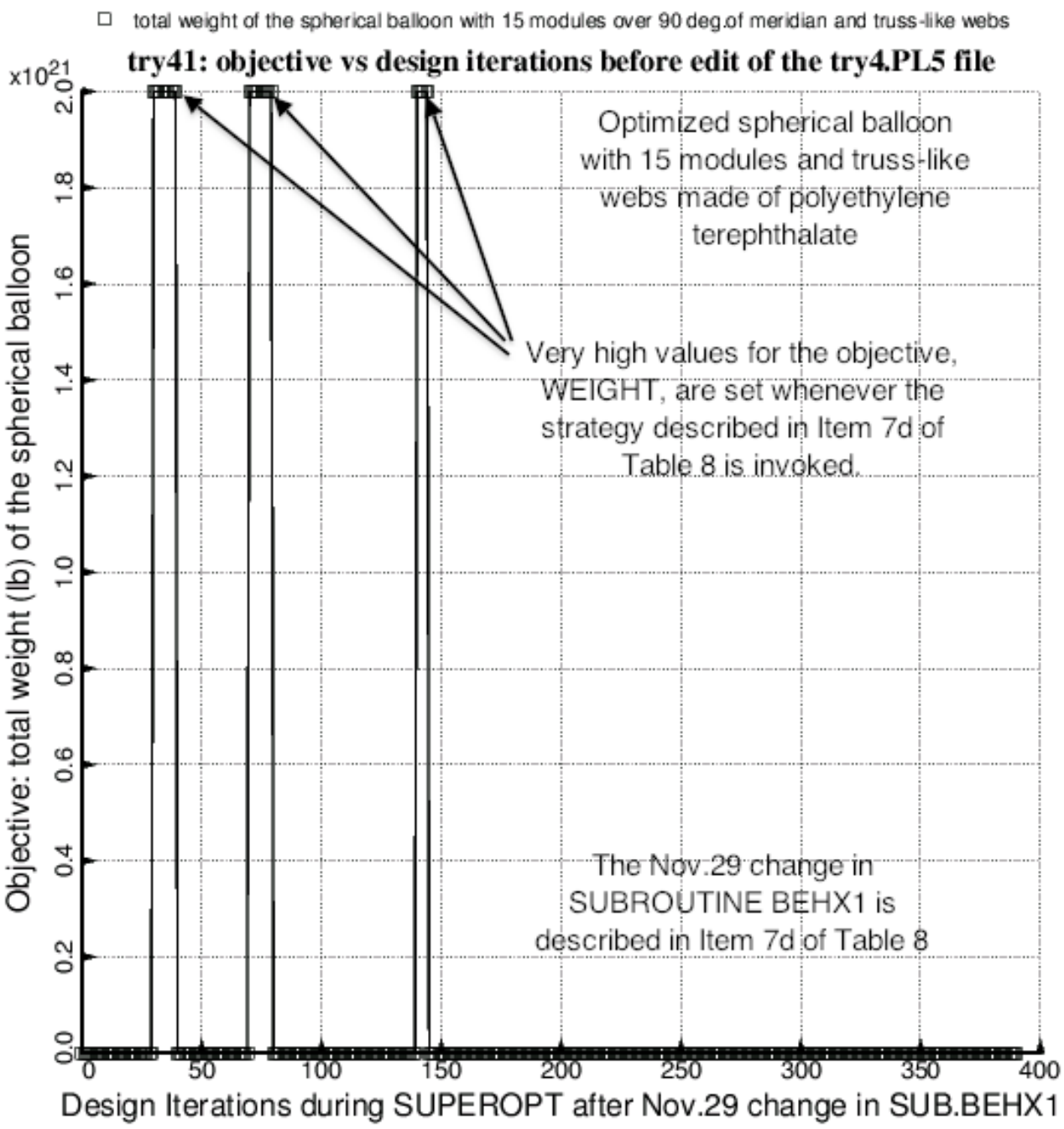


Fig. 21 Optimization of the spherical balloon with 15 modules and truss-like (slanted) webs (Fig. 2) during a partial execution of SUPEROPT. The purpose of the strategy described in Item 7d of Table 8 is to prevent lack of convergence of the Newton method for the solution of the nonlinear pre-buckling equilibrium equations from causing the execution of SUPEROPT to terminate prematurely. SUPEROPT “keeps truckin” in spite of failure of BIGBOSOR4 to obtain the nonlinear pre-buckled state of the spherical balloon. This figure demonstrates that lack of convergence occurred on three occasions during this execution of SUPEROPT. The next figure shows the evolution of the objective with the very high values edited out of the try4.PL5 file.

□ total weight of the spherical balloon with 15 modules over 90 deg.of meridian and truss-like webs

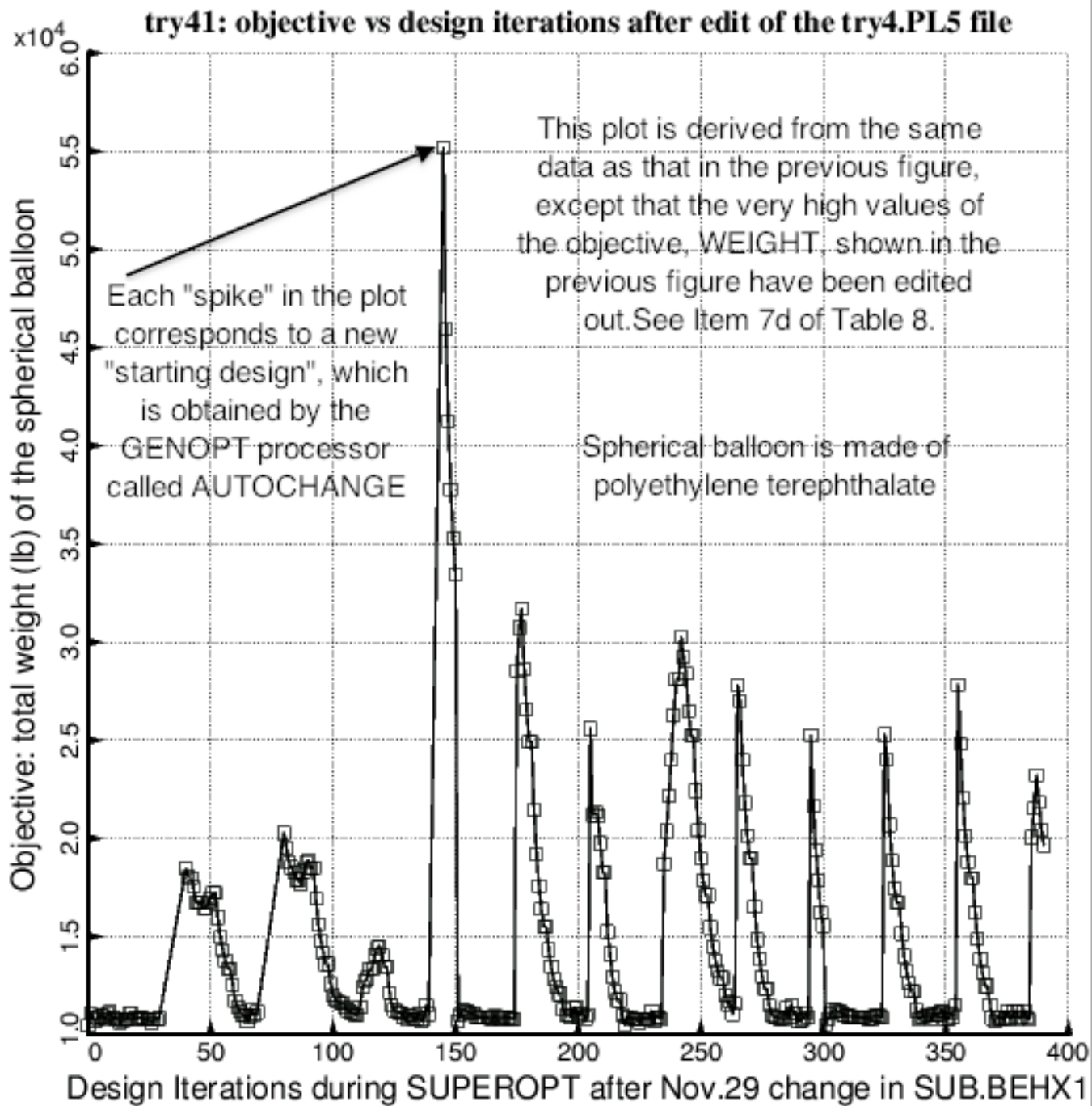


Fig. 22 Optimization of the spherical balloon with 15 modules and truss-like (slanted) webs (Fig. 2) during a partial execution of SUPEROPT. This figure is obtained by editing the try4.PL5 file – removing the very high values of WEIGHT shown in the previous figure – and then executing the GENOPT processor called DIPLOT with the edited file, try4.PL5, used as input. Each “spike” in the plot corresponds to a new “starting design”, generated automatically and randomly by the GENOPT processor called AUTOCHANGE [12].

- weight (lb) of the spherical balloon with truss-like (slanted) webs; "ALMOST FEASIBLE" designs
- weight (lb) of the spherical balloon with radial webs; "ALMOST FEASIBLE" designs
- △ weight (lb) of the spherical balloon with truss-like (slanted) webs; "FEASIBLE" designs
- + weight (lb) of the spherical balloon with radial webs; "FEASIBLE" designs

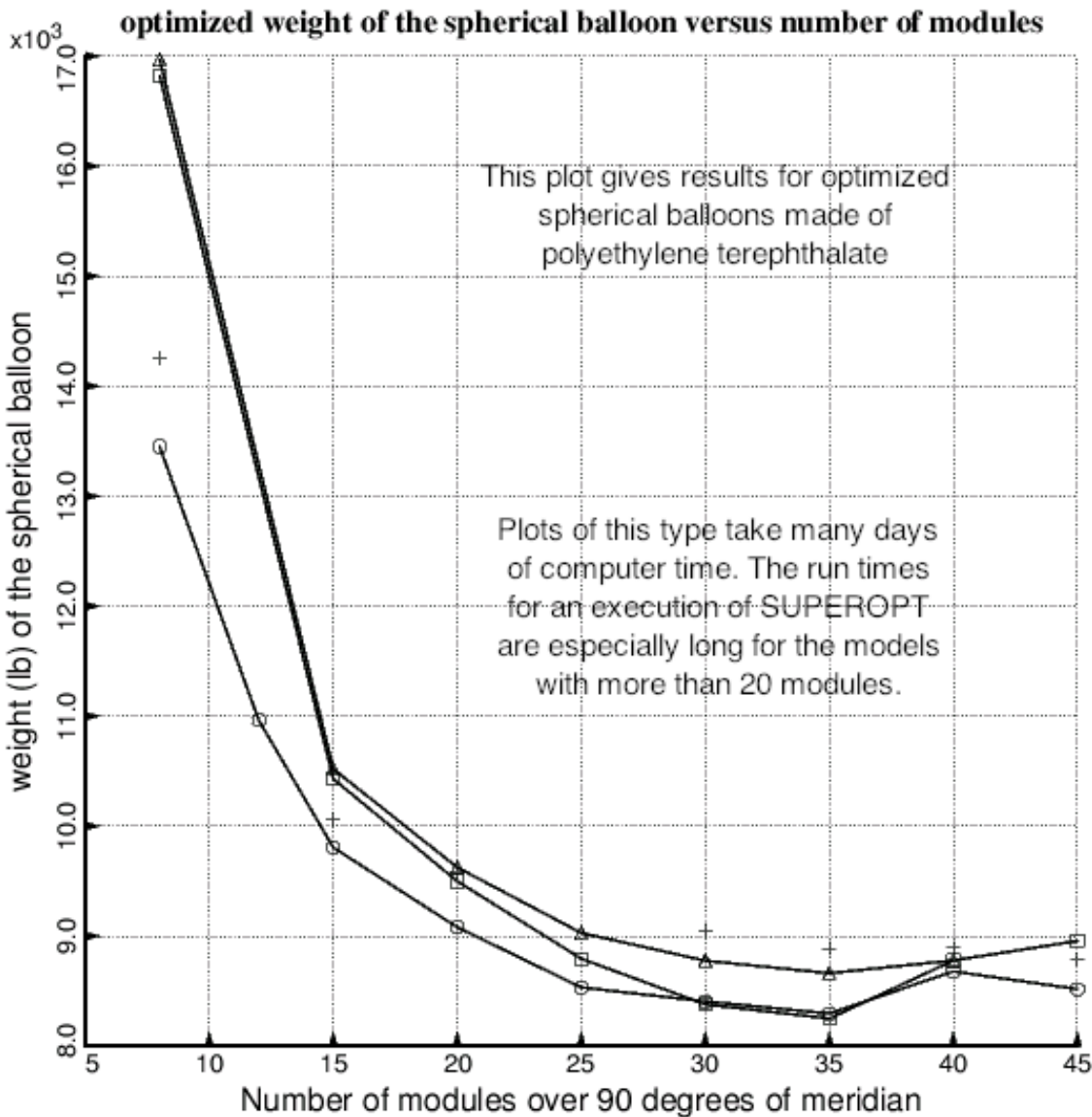


Fig. 23 The weight of optimized spherical balloons made of polyethylene terephthalate as a function of the number of modules over 90 degrees of meridian. All of the results in this figure were obtained with models in which there are 31 nodal points in each segment of the multi-module model. For the models with truss-like webs there are six segments per module plus two additional segments near the equator (Fig. 4). For models with radial webs there are five segments per module plus four additional segments near the equator (Fig.3). BIGBOSOR4 can handle up to 45 modules for models with truss-like webs and up to 55 modules for models with radial webs. For models with large numbers of modules the number of nodal points per segment is limited by the total number of degrees of freedom permitted by BIGBOSOR4 for pre-buckling analysis (20000 d.o.f) and for bifurcation buckling analysis (30000 d.o.f.). Compare this figure with Fig. 28.

— — Undeformed; There are 35 modules over 90 degrees of the meridian of the spherical balloon.
— Deformed: axisymmetric ($N=0$ circumferential waves) buckling mode from BIGBOSOR4

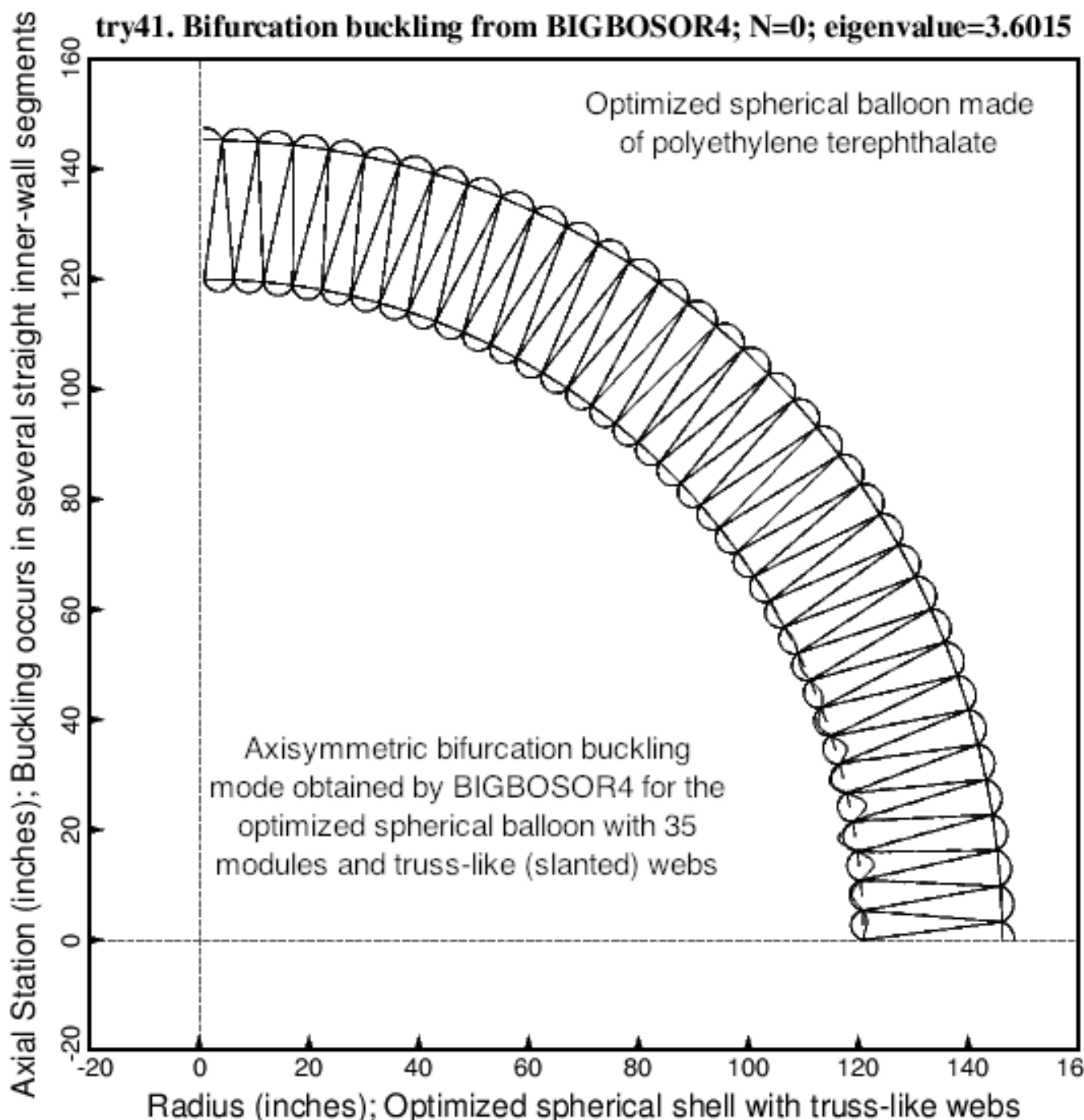


Fig. 24 Axisymmetric ($N = 0$ circumferential waves) buckling of the optimized spherical balloon with 35 modules over 90 degrees of meridian and with truss-like webs. As seen from the previous figure this configuration (35 modules, truss-like webs) corresponds to the spherical balloon with truss-like webs with the smallest optimized weight as a function of the number of modules.

— — Undeformed; There are 35 modules over 90 degrees of the meridian of the spherical balloon.
— Deformed: non-axisymmetric ($N=105$ circumferential waves) buckling mode from BIGBOSOR4

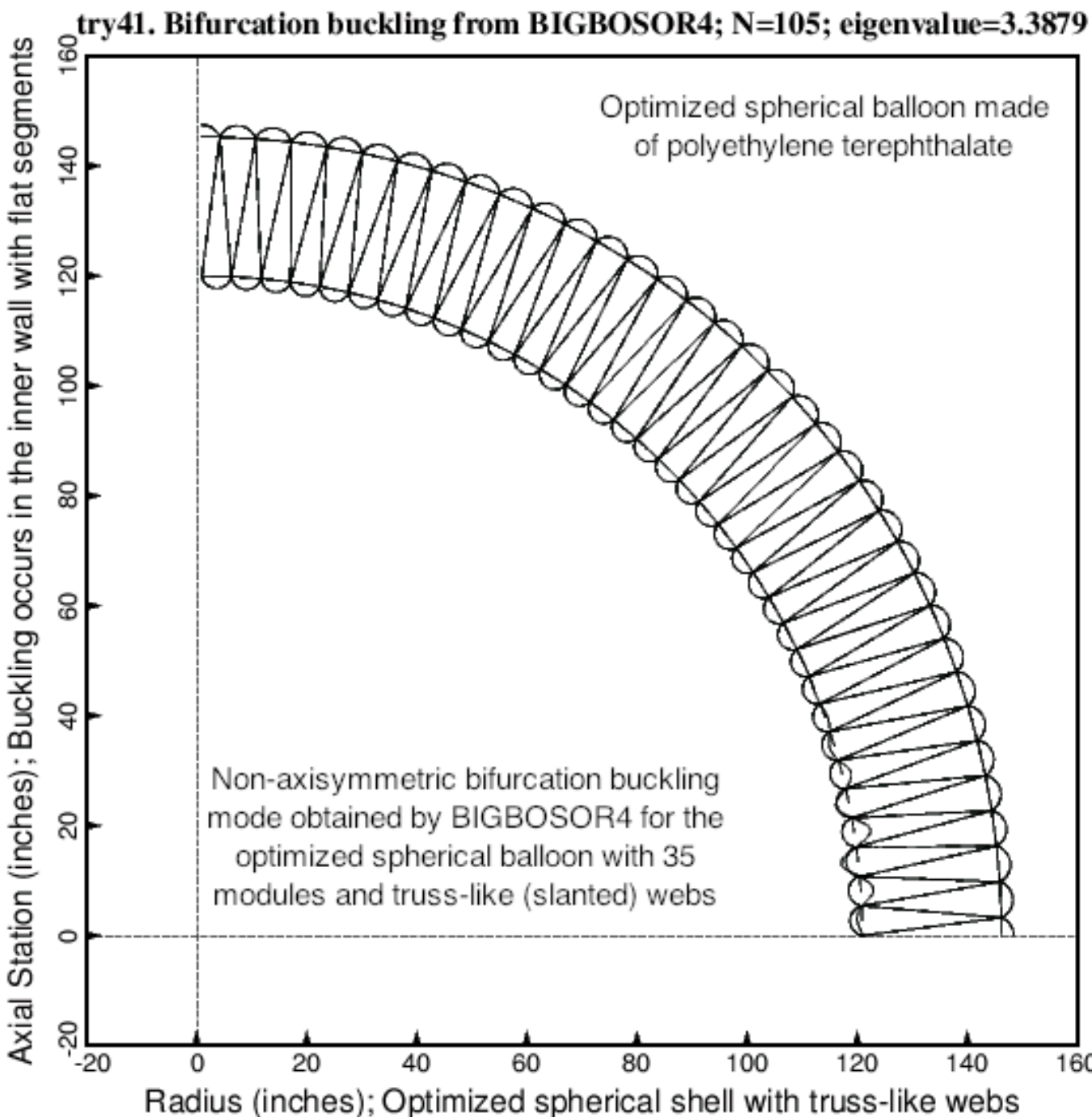


Fig. 25 Non-axisymmetric ($N = 105$ circumferential waves) buckling of the optimized spherical balloon with 35 modules over 90 degrees of meridian and with truss-like webs. As seen from Fig. 23 this configuration (35 modules, truss-like webs) corresponds to the spherical balloon with truss-like webs with the smallest optimized weight as a function of the number of modules. Compare with the previous figure.

-- Undeformed; There are 35 modules over 90 degrees of the meridian of the spherical balloon.
— Deformed: axisymmetric ($N=0$ circumferential waves) buckling mode from BIGBOSOR4

try42. Bifurcation buckling from BIGBOSOR4; $N=0$; eigenvalue=3.7817

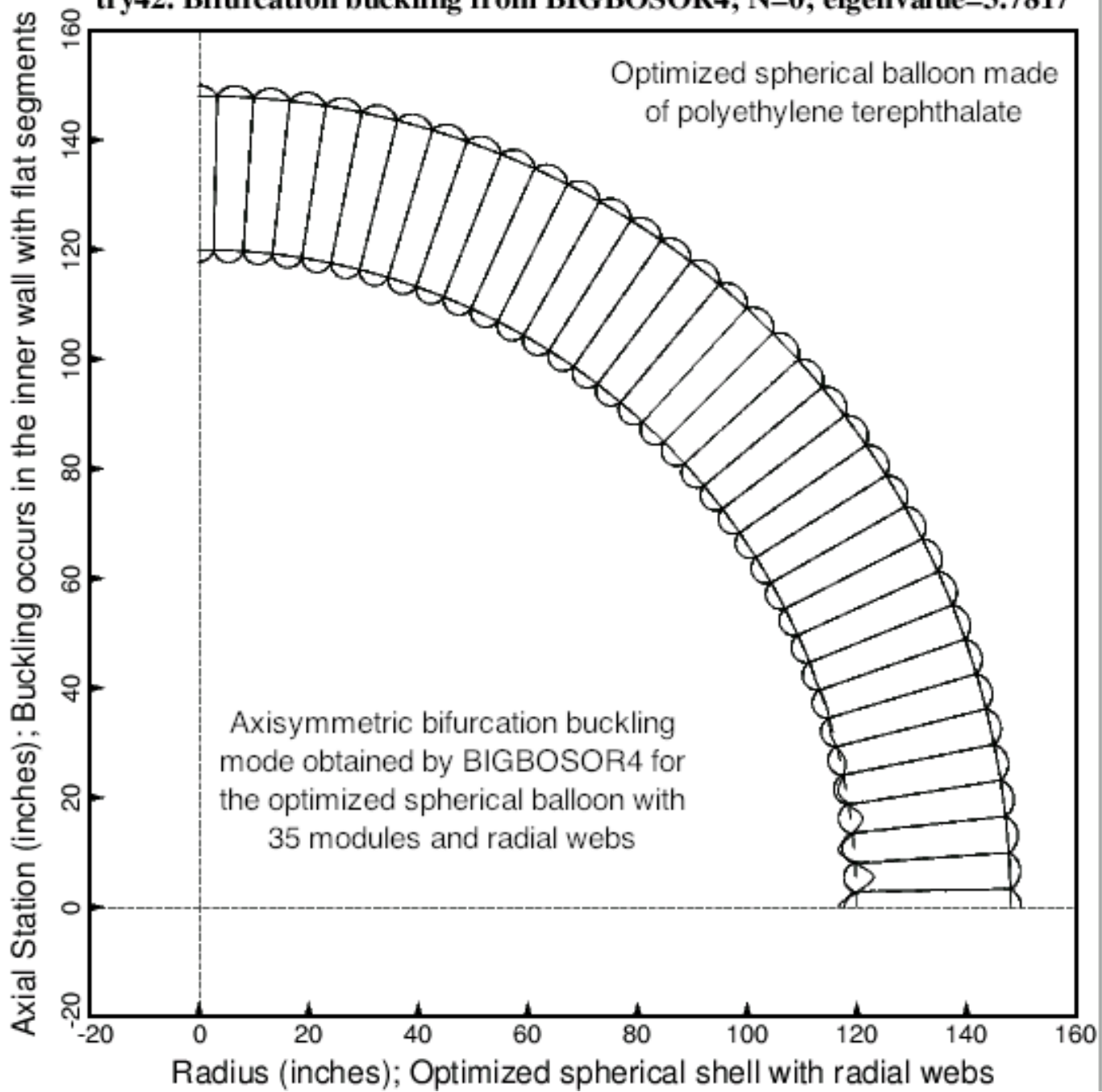


Fig. 26 Axisymmetric ($N = 0$ circumferential waves) buckling of the optimized spherical balloon with 35 modules over 90 degrees of meridian and with radial webs. As seen from Fig. 23 this configuration (35 modules, radial webs) corresponds to the spherical balloon with the smallest optimized weight as a function of the number of modules.

— — Undeformed; There are 35 modules over 90 degrees of the meridian of the spherical balloon.
— Deformed: non-axisymmetric ($N=105$ circumferential waves) buckling mode from BIGBOSOR4

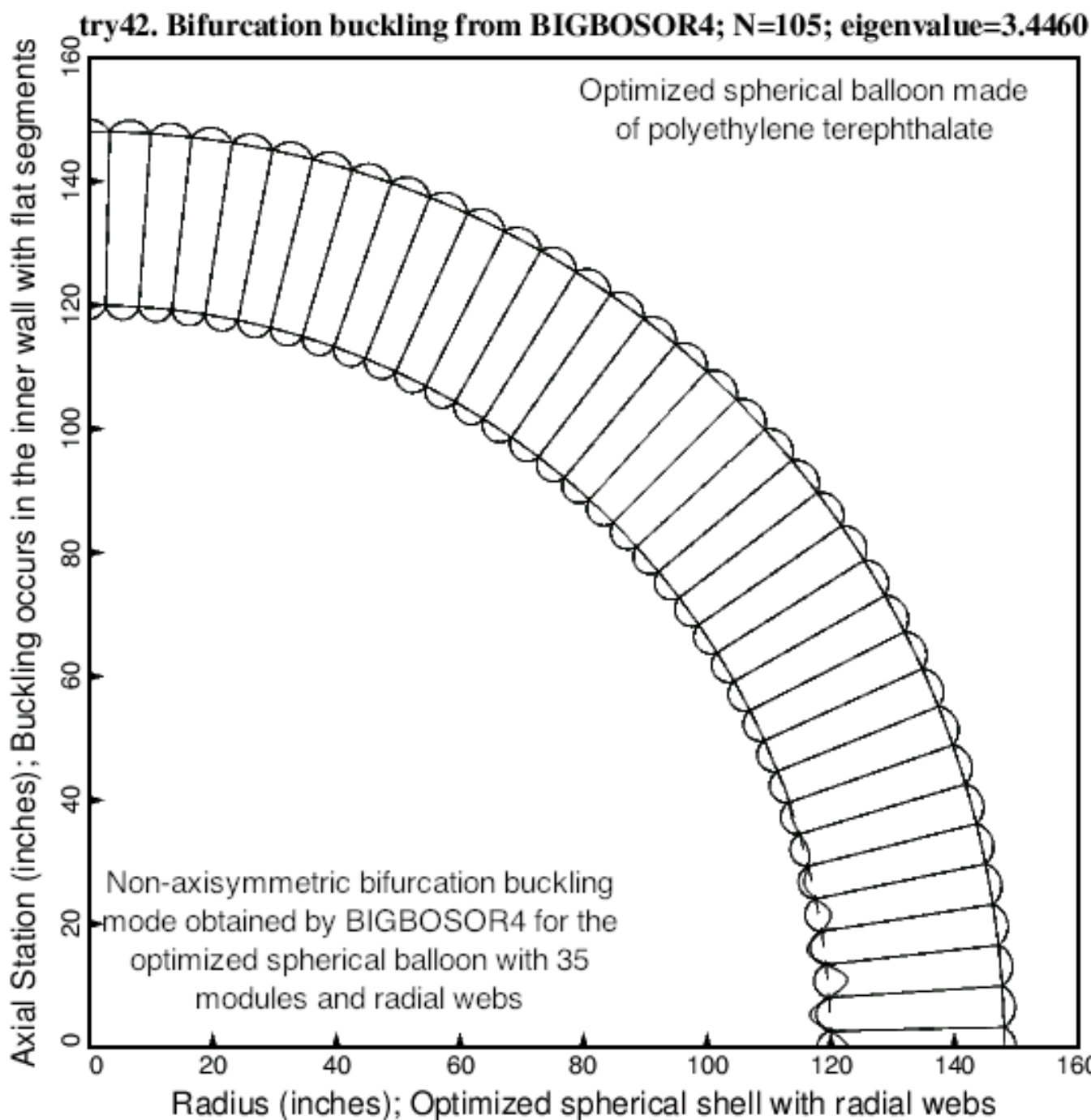


Fig. 27 Non-axisymmetric ($N = 105$ circumferential waves) buckling of the optimized spherical balloon with 35 modules over 90 degrees of meridian and with radial webs. As seen from Fig. 23 this configuration (35 modules, radial webs) corresponds to the spherical balloon with the smallest optimized weight as a function of the number of modules. Compare with the previous figure.

- weight (lb) of the spherical balloon with truss-like (slanted) webs; "ALMOST FEASIBLE" designs
- weight (lb) of the spherical balloon with radial webs; "ALMOST FEASIBLE" designs
- △ weight (lb) of the spherical balloon with truss-like (slanted) webs; "FEASIBLE" designs
- + weight (lb) of the spherical balloon with radial webs; "FEASIBLE" designs
- weight (lb) of the spherical balloon with radial webs; "ALMOST FEASIBLE" designs; dec3

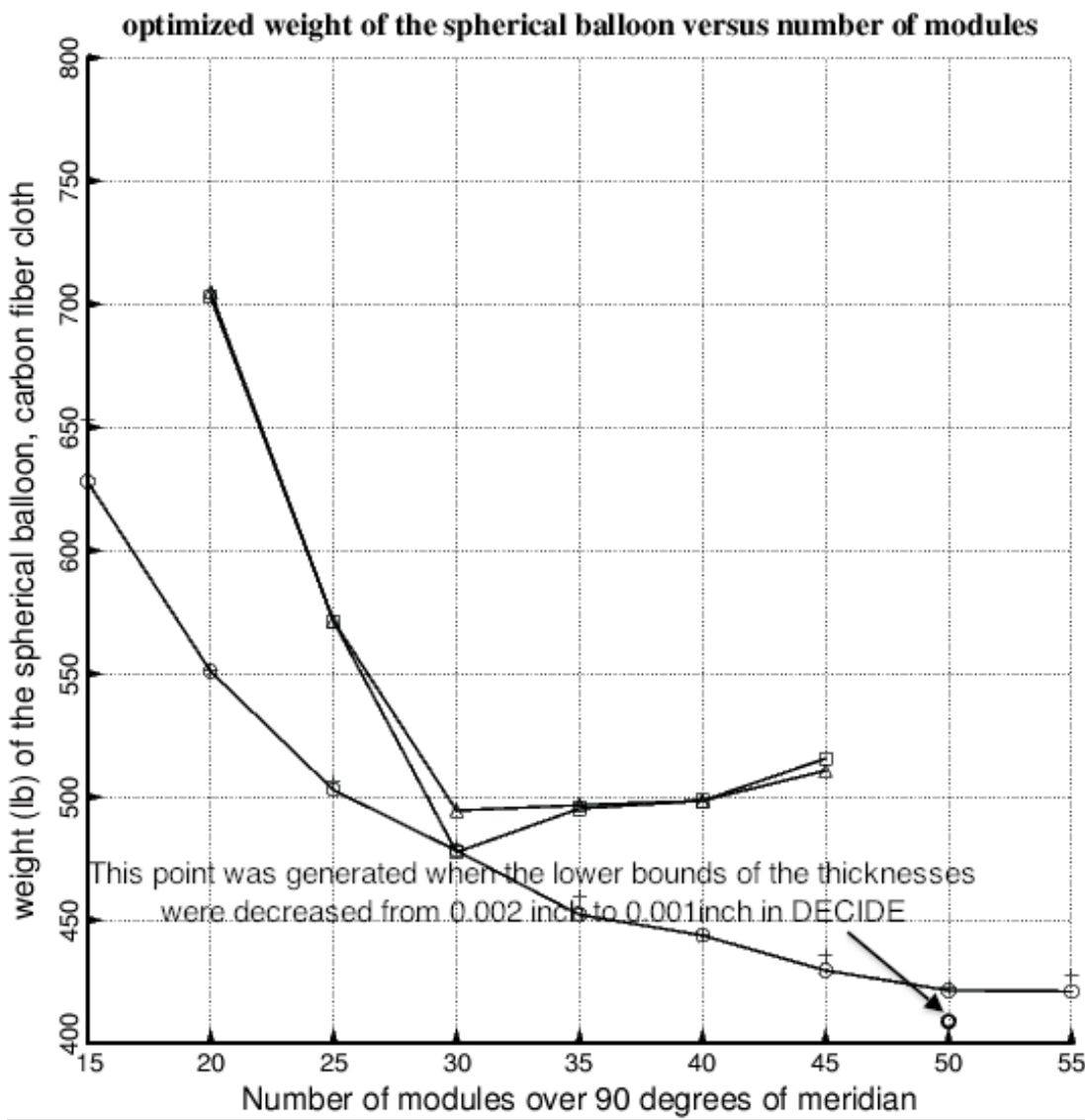


Fig. 28 The weight of optimized spherical balloons made of fictitious carbon fiber cloth as a function of the number of modules over 90 degrees of meridian. All of the results in this figure were obtained with models in which there are 31 nodal points in each segment of the multi-module model. For the models with truss-like webs there are six segments per module plus two additional segments near the equator (Fig. 4). For models with radial webs there are five segments per module plus four additional segments near the equator (Fig.3). BIGBOSOR4 can handle up to 45 modules for models with truss-like webs and up to 55 modules for models with radial webs. For models with large numbers of modules the number of nodal points per segment is limited by the total number of degrees of freedom permitted by BIGBOSOR4 for pre-buckling analysis (20000 d.o.f) and for bifurcation buckling analysis (30000 d.o.f.). Compare this figure with Fig. 23.

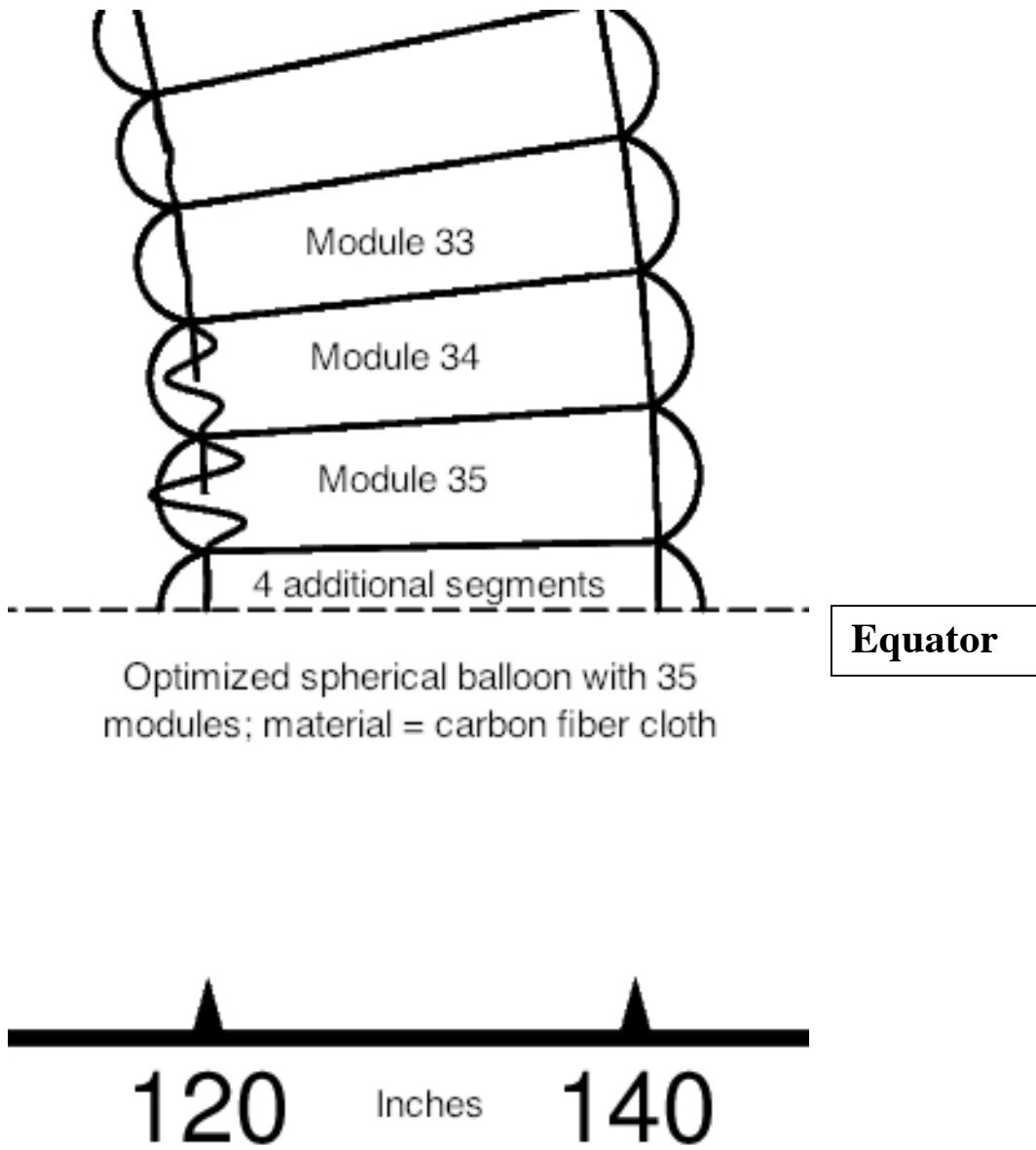


Fig. 29 Axisymmetric ($N = 0$ circumferential waves) local buckling of the optimized spherical balloon with 35 modules over 90 degrees of meridian and with radial webs. The material is carbon fiber cloth, the properties of which are listed in Table 13. The buckling load factor obtained from BIGBOSOR4 is 2.9541 (Table 14). This is a real buckling mode, not a spurious buckling mode of the types shown in the next three figures. In optimization runs (ITYPE = 1 in the *.OPT file) ONLY the buckling load factor (eigenvalue) corresponding to $N = 0$ circumferential waves is used in the computation of the buckling constraint, BUCKB4, and in the computation of the buckling margin, (BUCKB4(1)/BUCKB4A(1)) / BUCKB4F(1)-1, which is always Margin No. 1 listed in the *.OPM file. This is done in order to avoid the production of overly conservative designs resulting from the use of low buckling load factors that correspond to spurious buckling modes such as that displayed in the next figure. In all the cases run during this project the axisymmetric buckling mode has always been a real buckling mode, not a spurious buckling mode.

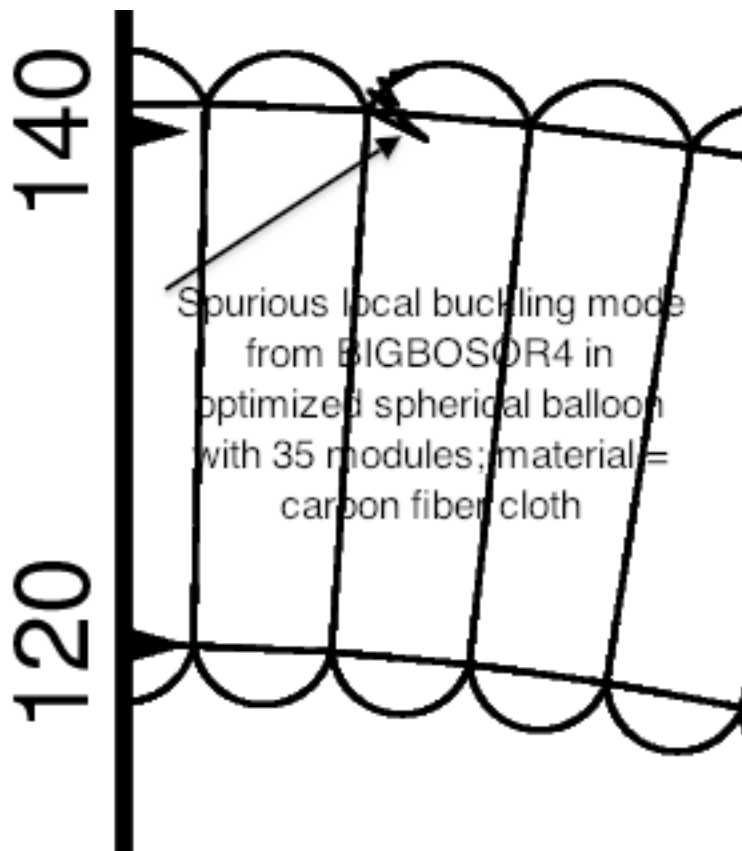


Fig. 30 Non-axisymmetric ($N = 35$ circumferential waves) spurious local buckling of the optimized spherical balloon with 35 modules over 90 degrees of meridian and with radial webs. (See the previous figure.) The material is carbon fiber cloth, the properties of which are listed in Table 13. The spurious buckling load factor obtained from BIGBOSOR4 is 0.35645 (Table 14), which is almost a factor of 10 too small. This is a spurious buckling mode, not a real buckling mode of the type shown in the previous figure for $N = 0$ circumferential waves. **In order to avoid the production of overly conservative designs resulting from the use of low buckling load factors that correspond to spurious buckling modes, in optimization runs (ITYPE = 1 in the *.OPT file) ONLY the buckling load factor (eigenvalue) corresponding to $N = 0$ circumferential waves is used in the computation of the buckling constraint, BUCKB4, and in the computation of the buckling margin, (BUCKB4(1)/BUCKB4A(1)) / BUCKB4F(1)-1, which is always Margin No. 1 listed in the *.OPM file. Non-axisymmetric buckling modes ($N > 0$ circumferential waves) are never used in the computation of BUCKB4, even if these non-axisymmetric modes are real modes. Non-axisymmetric buckling is covered by the initial-loss-of-tension behavioral constraint, TENLOS, and by its corresponding margin, (TENLOS(1)/TENLOSA(1)) / TENLOSF(1)-1, which is always Margin No. 2 in the *.OPM file.**

Close Hdcpy About

try7..R,Z_EIGENMODE_1--N_35

Axial Station

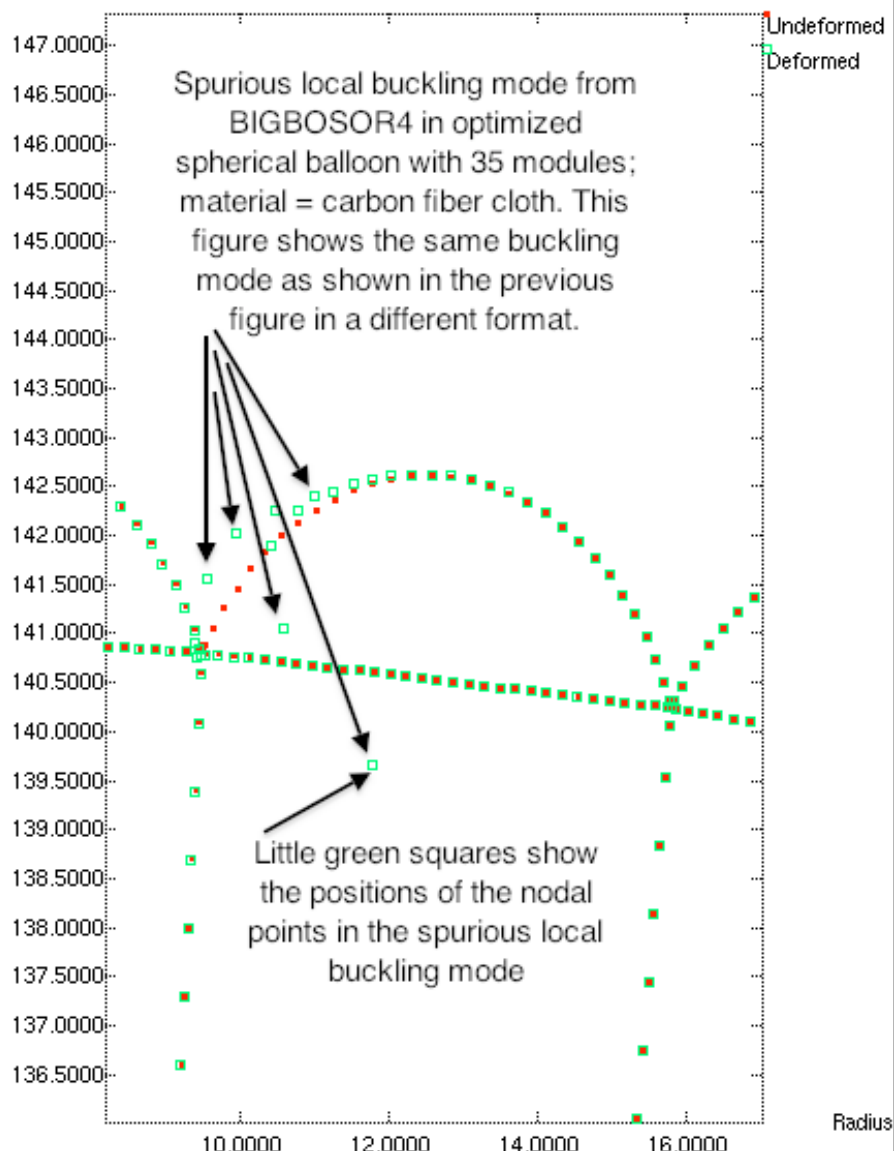


Fig. 31 The same spurious local buckling mode as that shown in the previous figure displayed here in a different format. Non-axisymmetric ($N = 35$ circumferential waves) spurious local buckling of the optimized spherical balloon with 35 modules over 90 degrees of meridian and with radial webs. The material is carbon fiber cloth. This spurious buckling mode would disappear if many more nodal points were used in the shell segment that buckles. However, an analogous spurious buckling mode would then occur in one of the neighboring segments unless the number of nodal points were greatly increased in all segments of the model. Unfortunately, this cannot be done because there would then be many more degrees of freedom than is allowed by BIGBOSOR4.

-- Undeformed; Initial loss of tension occurs in Seg.6 of Module 7 (Segment 42) at load factor=2.9169
 — Deformed; This web buckling mode in Seg.6 of Module 8 (Model Segment 48) appears to be spurious.

try7: N=315 circumferential waves, eigenvalue=2.8134

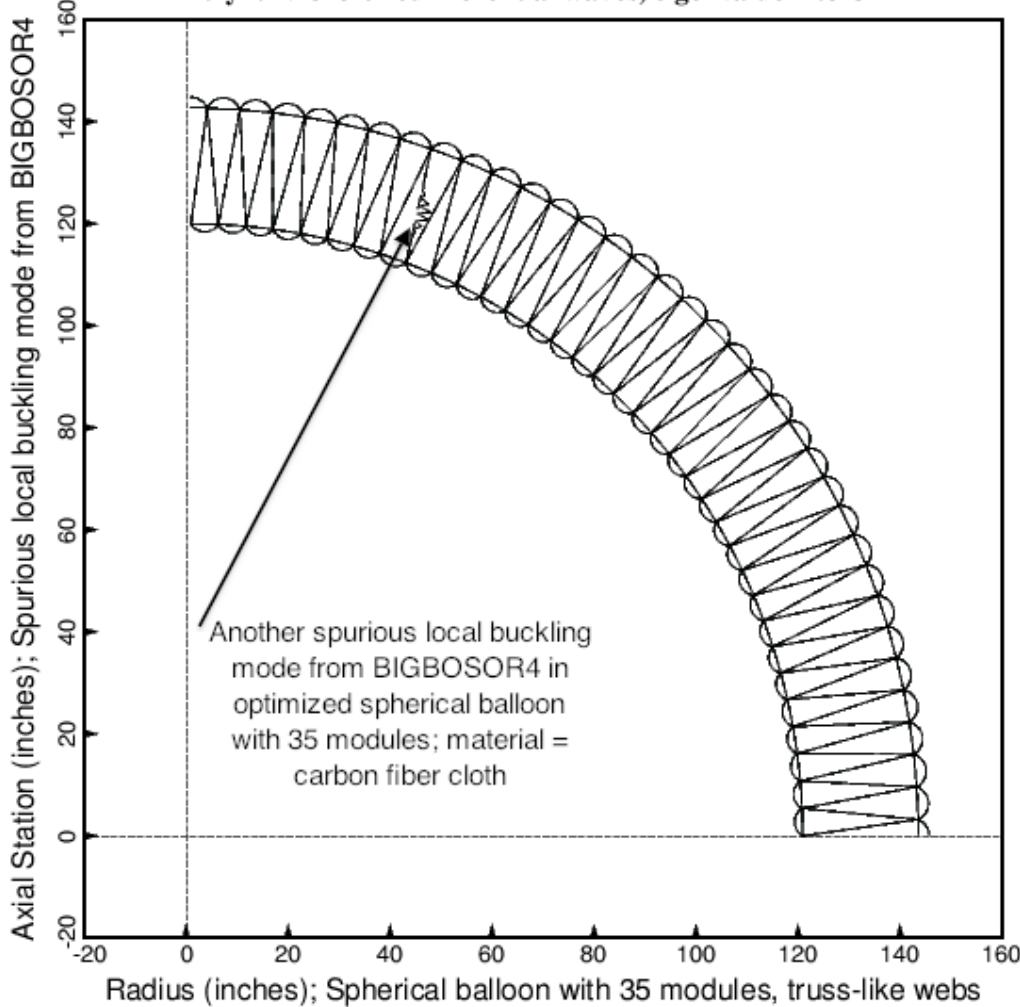


Fig. 32 Non-axisymmetric ($N = 315$ circumferential waves) local buckling of the optimized spherical balloon with 35 modules over 90 degrees of meridian and with truss-like (slanted) webs. The material is carbon fiber cloth, the properties of which are listed in Table 13. The buckling load factor obtained from BIGBOSOR4 is 2.8134 (not listed in any table in this paper). This is a spurious buckling mode, not a real buckling mode of the type shown in Fig. 29 for $N = 0$ circumferential waves. In optimization runs (ITYPE = 1 in the *.OPT file) ONLY the buckling load factor (eigenvalue) corresponding to $N = 0$ circumferential waves is used in the computation of the buckling constraint, BUCKB4, and in the computation of the buckling margin, (BUCKB4(1)/BUCKB4A(1)) / BUCKB4F(1)-1, which is always Margin No. 1 listed in the *.OPM file. In order to avoid the production of overly conservative designs resulting from the use of low buckling load factors that correspond to spurious buckling modes, non-axisymmetric buckling modes ($N > 0$ circumferential waves) are never used in the computation of BUCKB4, even if these non-axisymmetric modes are real modes. Non-axisymmetric buckling is covered by the initial-loss-of-tension behavioral constraint, TENLOS, and by its corresponding margin, (TENLOS(1)/TENLOSA(1)) / TENLOSF(1)-1, which is always Margin No. 2 in the *.OPM file.

Close Hdcpy About
Axial Station inches

try7..R,Z_LOADSTEP11

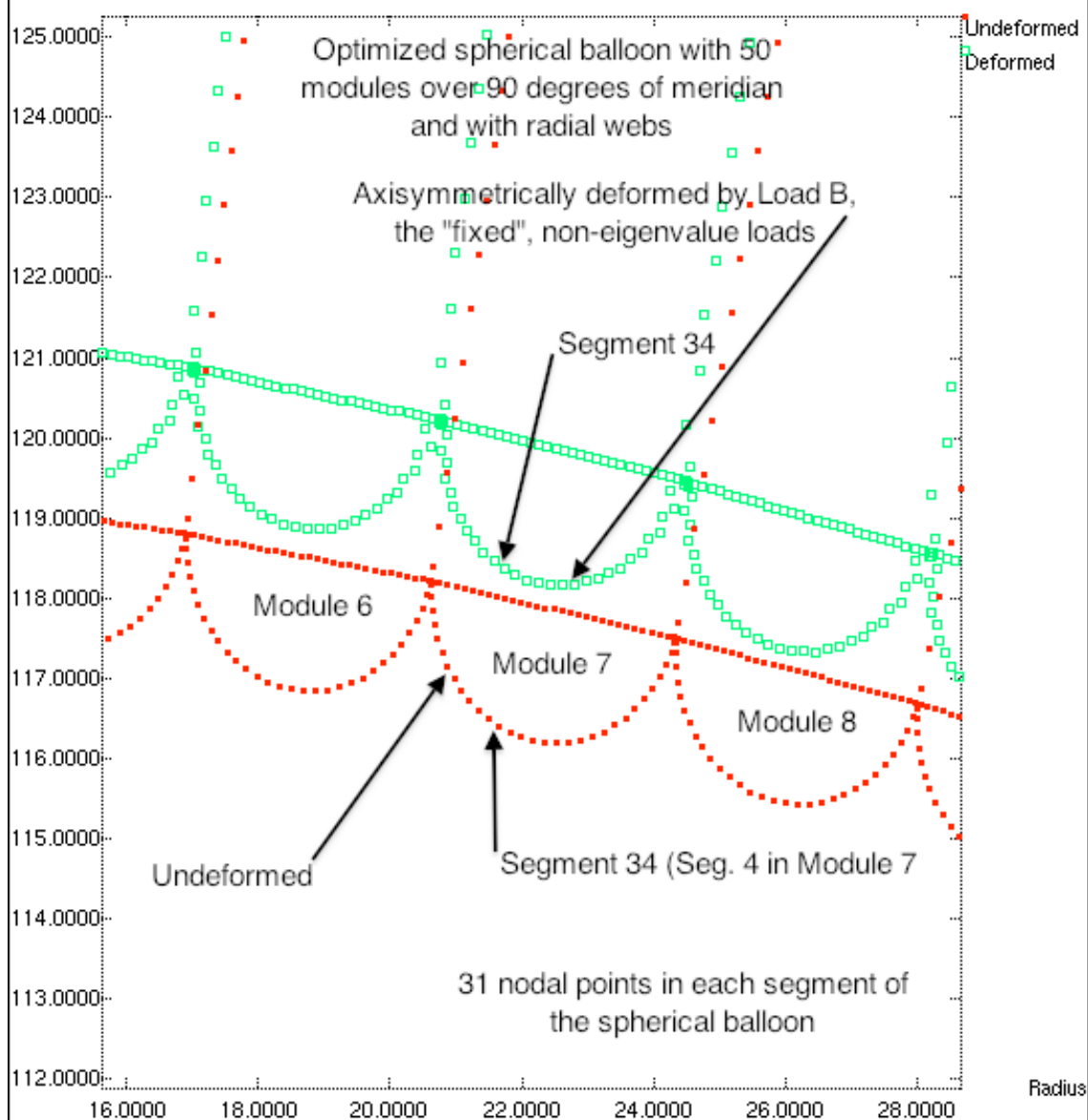


Fig. 33a The nodal point discretization in the neighborhood of Segment 34 in the optimized spherical balloon with 50 modules and with radial webs. The material is carbon fiber cloth the properties of which are listed in Table 13. This figure shows the axisymmetric pre-buckling deformation caused by Load B (the "fixed", non-eigenvalue loads: PINNER = 0 psi, PMIDDLE = 60 psi, POUTER = 0 psi) in this local region of the spherical balloon. The axisymmetric pre-buckling deformation of the entire model of the spherical balloon is analogous to that displayed in Fig. 12. There are 31 nodal points in each segment of the balloon. Notice the spurious local "zig-zag" component of deformation near both ends of each of the curved segments. The amplitude of this spurious local "zig-zag" component decreases with increasing numbers of nodal points, as displayed in the following three figures, for which the number of nodal points in Segment 34 is increased.

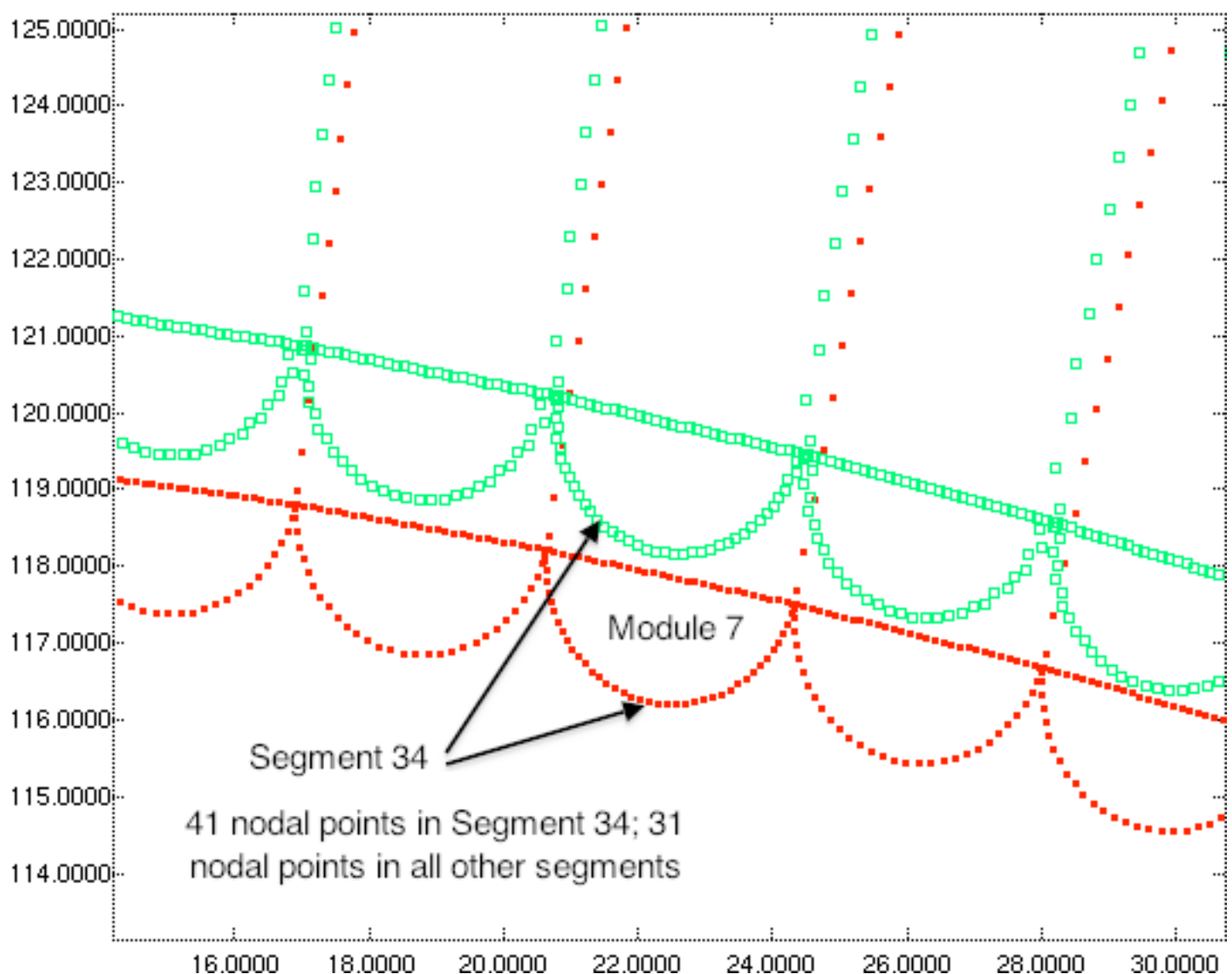


Fig. 33b The nodal point discretization in the neighborhood of Segment 34 in the optimized spherical balloon with 50 modules and with radial webs. The material is carbon fiber cloth the properties of which are listed in Table 13. This figure shows the axisymmetric pre-buckling deformation caused by Load B (the “fixed”, non-eigenvalue loads: PINNER = 0 psi, PMIDDLE = 60 psi, POUTER = 0 psi) in this local region of the spherical balloon. The axisymmetric pre-buckling deformation of the entire model of the spherical balloon is analogous to that displayed in Fig. 12. There are 31 nodal points in each segment of the balloon except for Segment 34, which has 41 nodal points. Notice that the amplitude of the spurious local “zig-zag” component of pre-buckling deformation near both ends of Segment 34 is less than that in the other curved segments, each of which has 31 nodal points.

[Close](#) [Hdcpy](#) [About](#)

try7..R,Z_LOADSTE

Axial Station inches

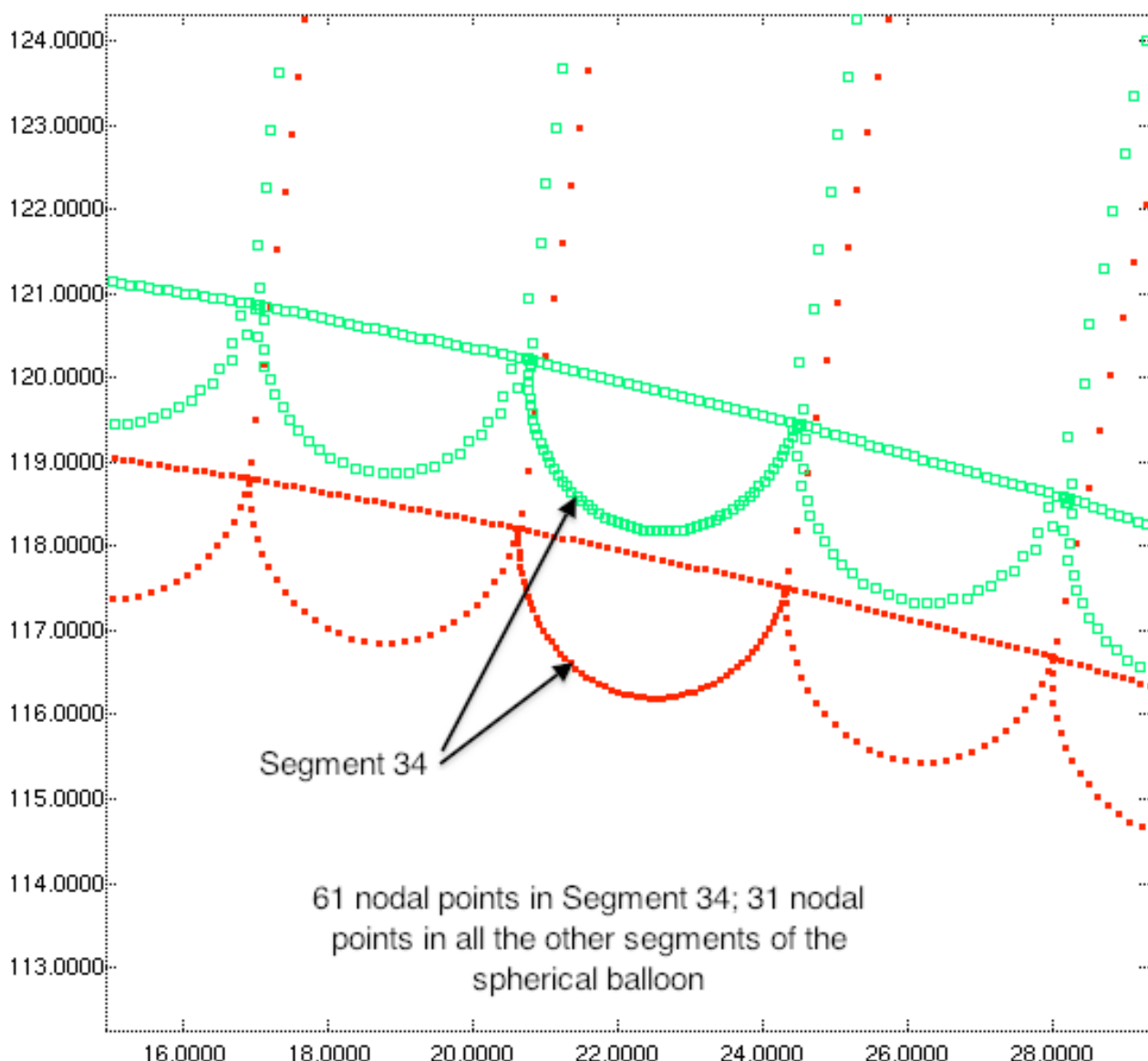


Fig. 33c The nodal point discretization in the neighborhood of Segment 34 in the optimized spherical balloon with 50 modules and with radial webs. The material is carbon fiber cloth the properties of which are listed in Table 13. This figure shows the axisymmetric pre-buckling deformation caused by Load B (the “fixed”, non-eigenvalue loads: PINNER = 0 psi, PMIDDLE = 60 psi, POUTER = 0 psi) in this local region of the spherical balloon. The axisymmetric pre-buckling deformation of the entire model of the spherical balloon is analogous to that displayed in Fig. 12. There are 31 nodal points in each segment of the balloon except for Segment 34, which has 61 nodal points. Notice that the amplitude of the spurious local “zig-zag” component of pre-buckling deformation near both ends of Segment 34 is much less than that in the other curved segments, each of which has 31 nodal points.

[Close](#) [Hdcpy](#) [About](#)

Axial Station inches

try7..R,Z_LOADSTE

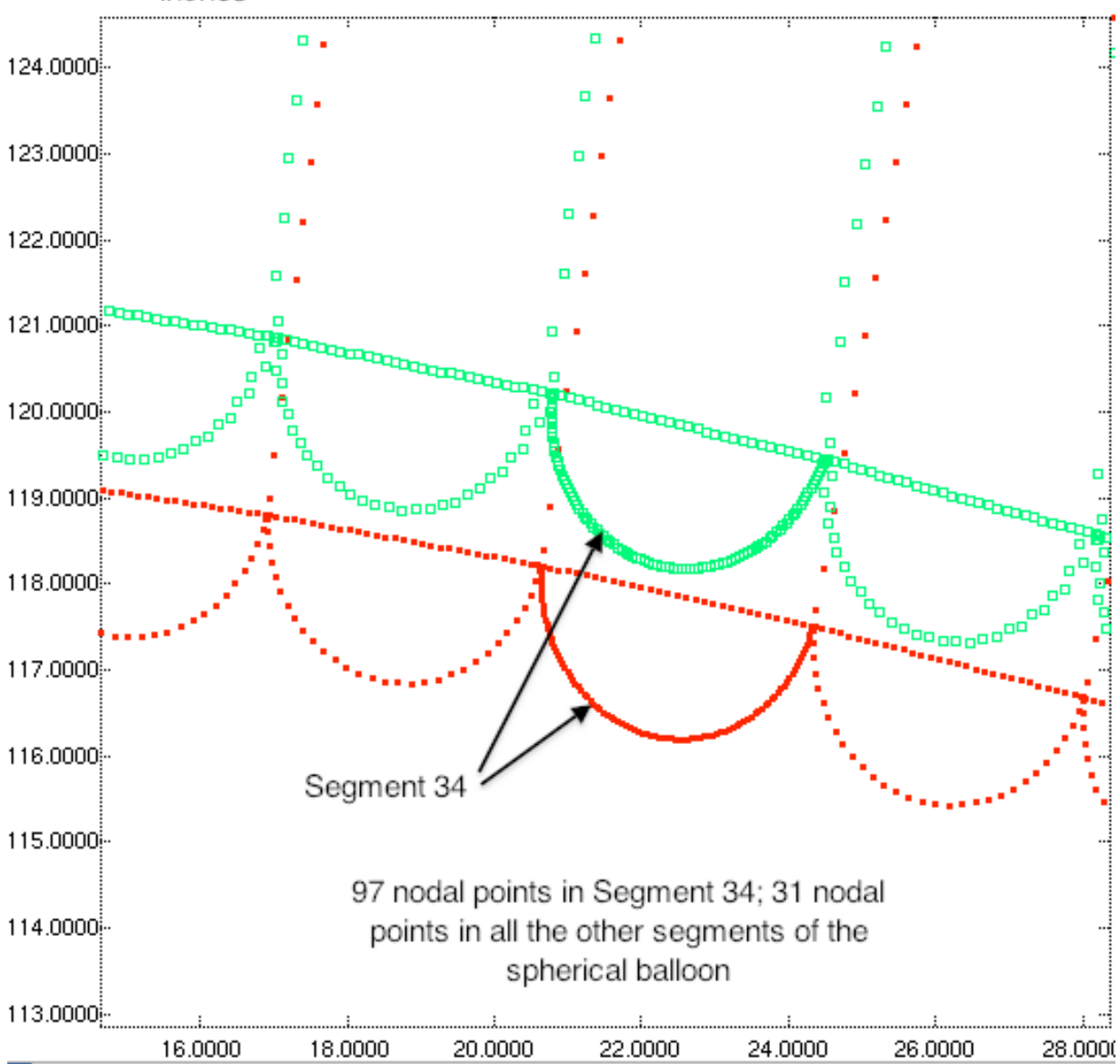


Fig. 33d The nodal point discretization in the neighborhood of Segment 34 in the optimized spherical balloon with 50 modules and with radial webs. The material is carbon fiber cloth the properties of which are listed in Table 13. This figure shows the axisymmetric pre-buckling deformation caused by Load B (the “fixed”, non-eigenvalue loads: PINNER = 0 psi, PMIDDLE = 60 psi, POUTER = 0 psi) in this local region of the spherical balloon. The axisymmetric pre-buckling deformation of the entire model of the spherical balloon is analogous to that displayed in Fig. 12. There are 31 nodal points in each segment of the balloon except for Segment 34, which has 97 nodal points. Notice that the amplitude of the spurious local “zig-zag” component of pre-buckling deformation near both ends of Segment 34 is much less than that in the other curved segments, each of which has 31 nodal points.

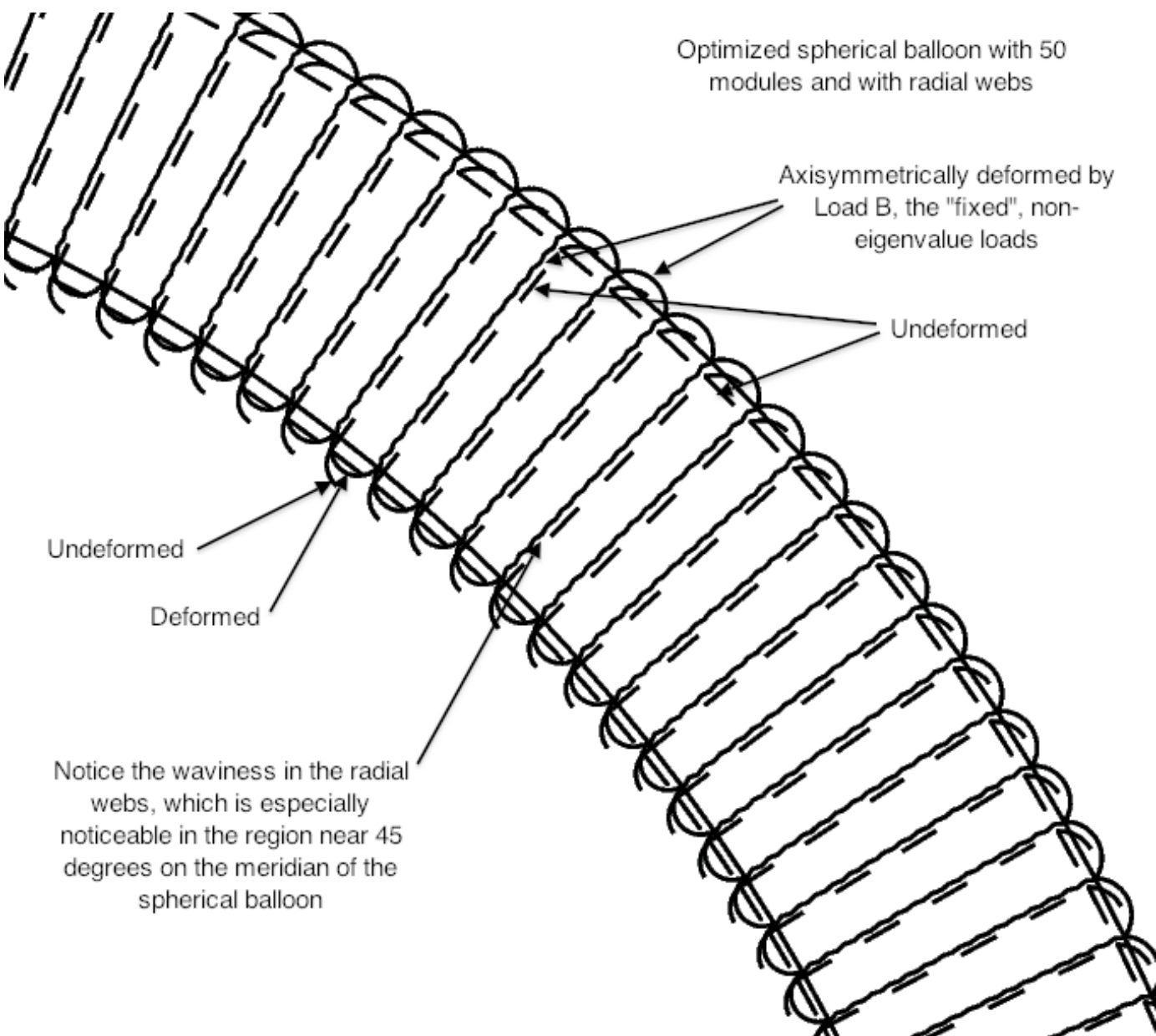


Fig. 34 The optimized spherical balloon with 50 modules and with radial webs. The material is carbon fiber cloth the properties of which are listed in Table 13. This figure shows the axisymmetric pre-buckling deformation caused by Load B (the “fixed”, non-eigenvalue loads: PINNER = 0 psi, PMIDDLE = 60 psi, POUTER = 0 psi) in the region of the spherical balloon in the neighborhood of 45 degrees along its meridian. The axisymmetric pre-buckling deformation of the entire model of the spherical balloon is analogous to that displayed in Fig. 12. There are 31 nodal points in each segment of the balloon. Notice the spurious local “zig-zag” component of deformation in the radial webs that is most pronounced at and near 45 degrees. The amplitude of this spurious local “zig-zag” component would decrease with increasing numbers of nodal points. However, it is not possible to increase the number of nodal points in every segment of the model because there would then be too many degrees of freedom for BIGBOSOR4 to handle.

- Meridional resultant, n1 in Seg.34 (Seg. 4 of Module 7 of 50); PMIDDLL=60 psi, POUTER=0
- Circumferential resultant, n2 in Seg.34 (Seg. 4 of Module 7 of 50); PMIDDLL=60 psi, POUTER=0
- △ Average circumferential resultant, $[n2(i)+n2(i+1)]/2$ in Seg.34; PMIDDLL=60 psi, POUTER=0

50-module model; carbon cloth: resultants, n1 & n2, from Load B

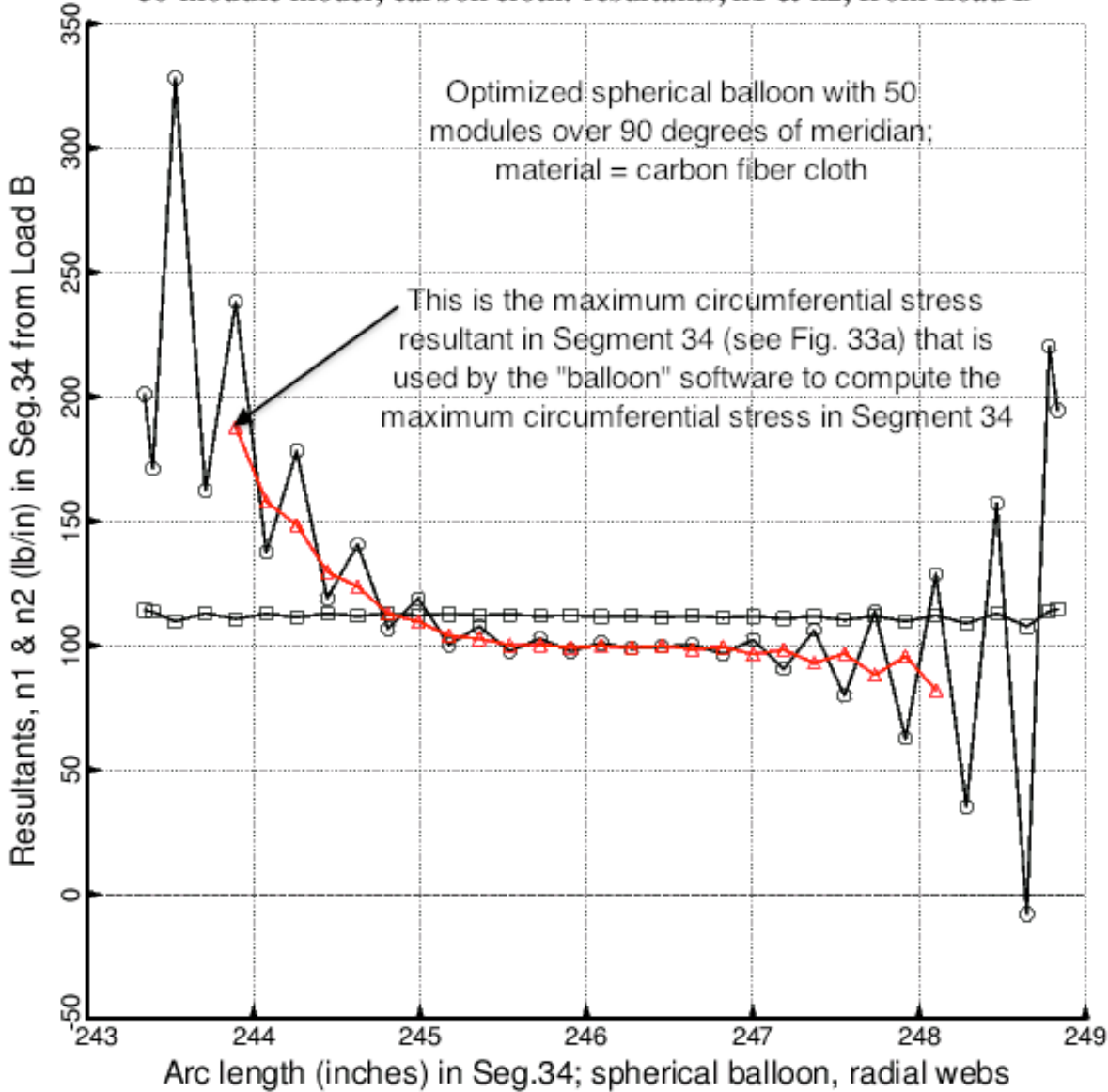


Fig. 35 The meridional and circumferential stress resultants, n1 and n2, in Segment 34 of the optimized spherical balloon with 50 modules and with radial webs. There are 31 nodal points in Segment 34, which is the number of nodal points used in each of the segments of the model for the purpose of optimization. (See Fig.33a.) The material is carbon fiber cloth the properties of which are listed in Table 13. This figure shows the axisymmetric pre-buckling distributions of n1 and n2 in Segment 34 caused by Load B (the "fixed", non-eigenvalue loads: PINNER = 0 psi, PMIDDLL = 60 psi, POUTER = 0 psi). Notice the significant spurious local "zig-zag" component of n2 near both ends of Segment 34. This spurious "zig-zag" component of n2 is dramatically reduced by averaging n2 at neighboring nodal points: n2(effective) = $[n2(i) + n2(i+1)]/2$ (shown in the red curve). That is why the "balloon" software uses n2(effective) instead of n2 during optimization cycles.

- Circumferential resultant, n2 in Seg.34 (Seg. 4 of Module 7 of 50); 33 nodal points
- △ Average circumferential resultant, $[n2(i)+n2(i+1)]/2$ in Seg.34; 33 nodal points
- Circumferential resultant, n2 in Seg.34 (Seg. 4 of Module 7 of 50); 99 nodal points
- + Circumferential resultant, n2 in Seg.34 (Seg. 4 of Module 7 of 50); 43 nodal points
- × Circumferential resultant, n2 in Seg.34 (Seg. 4 of Module 7 of 50); 63 nodal points

50-module model; carbon cloth: hoop resultant, n2, from Load B

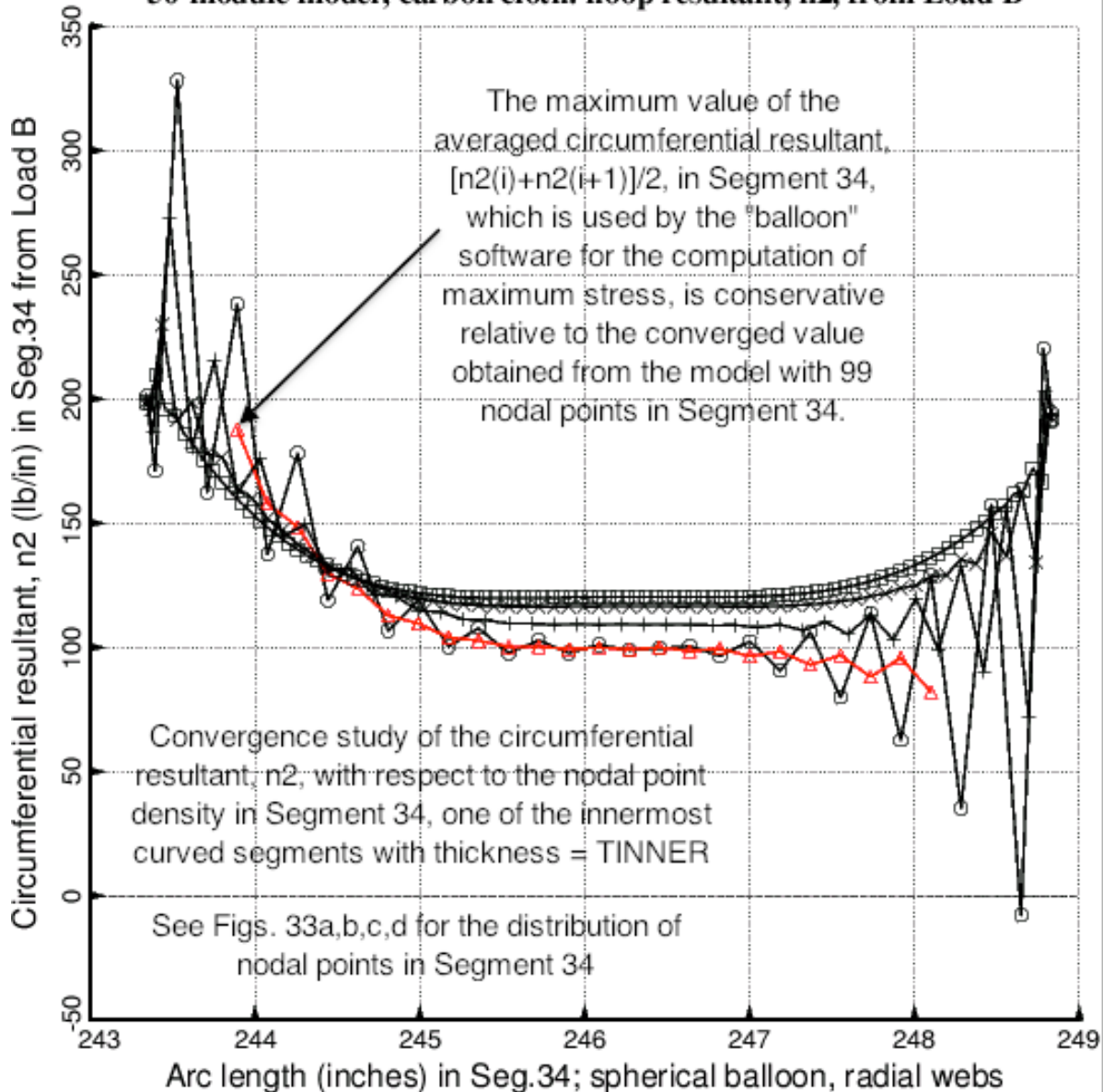


Fig. 36 A convergence study of the circumferential stress resultant, n2, in Segment 34 of the optimized spherical balloon with 50 modules and with radial webs. The material is carbon fiber cloth the properties of which are listed in Table 13. This figure shows the axisymmetric pre-buckling distributions of n2 in Segment 34 caused by Load B (the "fixed", non-eigenvalue loads: PINNER = 0 psi, PMIDDLE = 60 psi, POUTER = 0 psi). Notice that the significant spurious local "zig-zag" component of n2 near both ends of Segment 34 diminishes dramatically with increasing numbers of nodal points in Segment 34. The red curve, which is used by the "balloon" software during optimization cycles, is the same curve as that displayed in the previous figure.

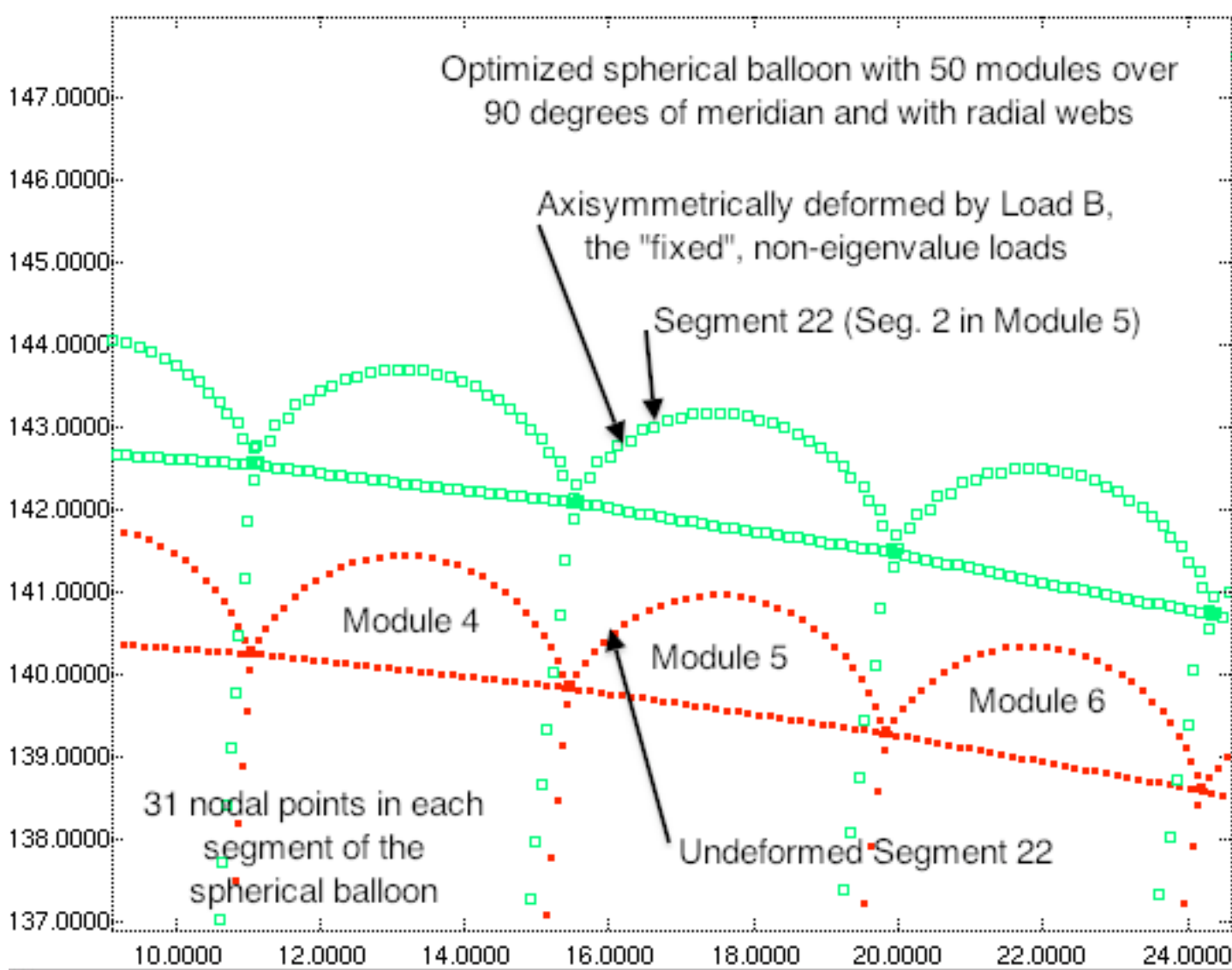


Fig. 37a The nodal point discretization in the neighborhood of Segment 22 in the optimized spherical balloon with 50 modules and with radial webs. The material is carbon fiber cloth the properties of which are listed in Table 13. This figure shows the axisymmetric pre-buckling deformation caused by Load B (the "fixed", non-eigenvalue loads: PINNER = 0 psi, PMIDDLE = 60 psi, POUTER = 0 psi) in this local region of the spherical balloon. The axisymmetric pre-buckling deformation of the entire model of the spherical balloon is analogous to that displayed in Fig. 12. There are 31 nodal points in each segment of the balloon. Notice the spurious local "zig-zag" component of deformation near both ends of each of the curved segments. The amplitude of this spurious local "zig-zag" component decreases with increasing numbers of nodal points, as displayed in the following three figures, for which the number of nodal points in Segment 22 is increased.

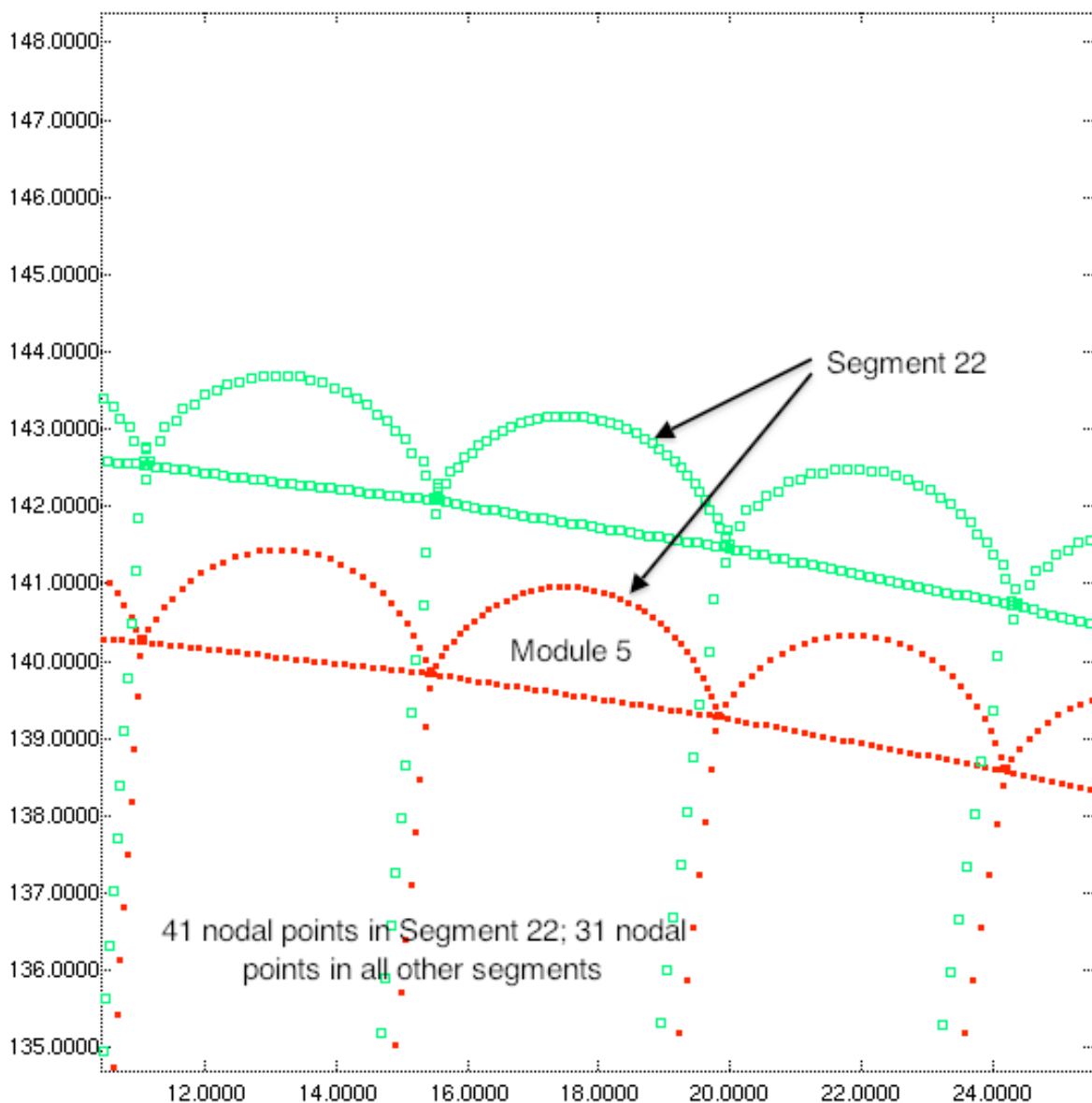


Fig. 37b The nodal point discretization in the neighborhood of Segment 22 in the optimized spherical balloon with 50 modules and with radial webs. The material is carbon fiber cloth the properties of which are listed in Table 13. This figure shows the axisymmetric pre-buckling deformation caused by Load B (the “fixed”, non-eigenvalue loads: PINNER = 0 psi, PMIDDLE = 60 psi, POUTER = 0 psi) in this local region of the spherical balloon. The axisymmetric pre-buckling deformation of the entire model of the spherical balloon is analogous to that displayed in Fig. 12. There are 31 nodal points in each segment of the balloon except for Segment 22, which has 41 nodal points. Notice that the amplitude of the spurious local “zig-zag” component of pre-buckling deformation near both ends of Segment 22 is less than that in the other curved segments, each of which has 31 nodal points.

Axial Station inches

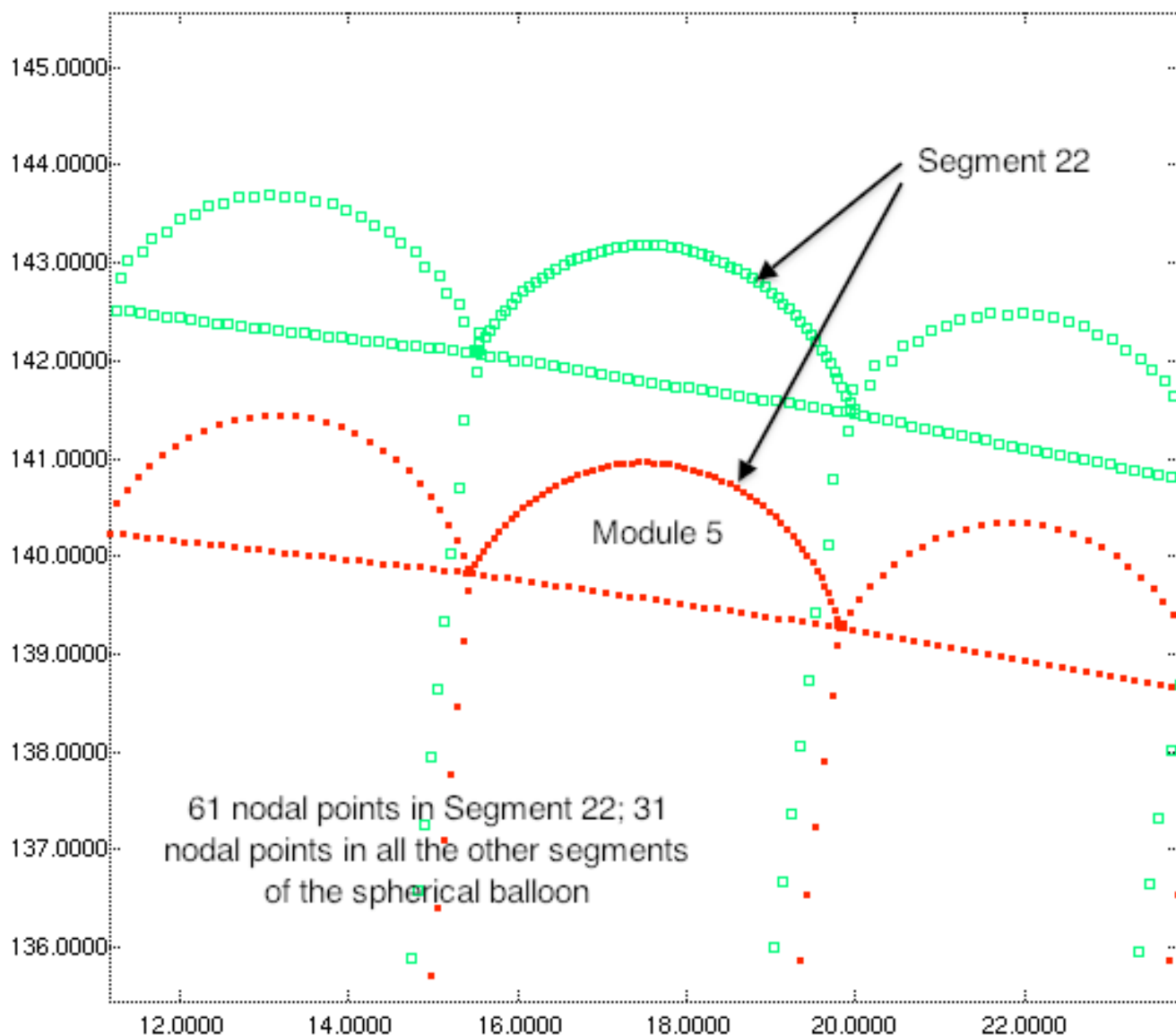


Fig. 37c The nodal point discretization in the neighborhood of Segment 22 in the optimized spherical balloon with 50 modules and with radial webs. The material is carbon fiber cloth the properties of which are listed in Table 13. This figure shows the axisymmetric pre-buckling deformation caused by Load B (the “fixed”, non-eigenvalue loads: PINNER = 0 psi, PMIDDLE = 60 psi, POUTER = 0 psi) in this local region of the spherical balloon. The axisymmetric pre-buckling deformation of the entire model of the spherical balloon is analogous to that displayed in Fig. 12. There are 31 nodal points in each segment of the balloon except for Segment 22, which has 61 nodal points. Notice that the amplitude of the spurious local “zig-zag” component of pre-buckling deformation near both ends of Segment 22 is much less than that in the other curved segments, each of which has 31 nodal points.

Axial Station inches

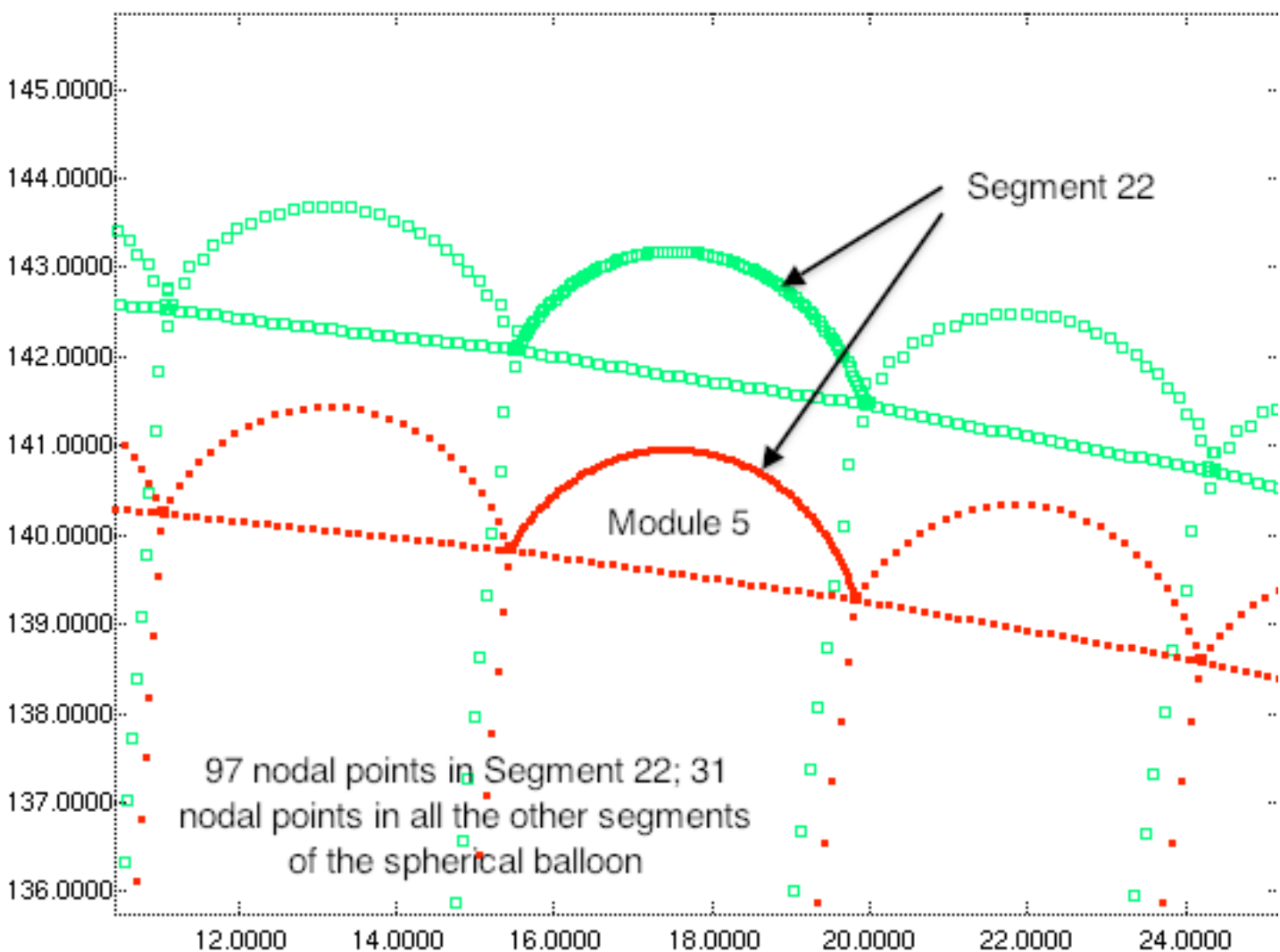


Fig. 37d The nodal point discretization in the neighborhood of Segment 22 in the optimized spherical balloon with 50 modules and with radial webs. The material is carbon fiber cloth the properties of which are listed in Table 13. This figure shows the axisymmetric pre-buckling deformation caused by Load B (the “fixed”, non-eigenvalue loads: PINNER = 0 psi, PMIDDLE = 60 psi, POUTER = 0 psi) in this local region of the spherical balloon. The axisymmetric pre-buckling deformation of the entire model of the spherical balloon is analogous to that displayed in Fig. 12. There are 31 nodal points in each segment of the balloon except for Segment 22, which has 97 nodal points. Notice that the amplitude of the spurious local “zig-zag” component of pre-buckling deformation near both ends of Segment 22 is much less than that in the other curved segments, each of which has 31 nodal points.

- Meridional resultant, n1 in Seg.22 (Seg. 2 of Module 5 of 50); PMIDDLL=60 psi, POUTER=0
- Circumferential resultant, n2 in Seg.22 (Seg. 2 of Module 5 of 50); PMIDDLL=60 psi, POUTER=0
- △ Average circumferential resultant, $[n2(i)+n2(i+1)]/2$ in Seg.22; PMIDDLL=60 psi, POUTER=0

50-module model; carbon cloth: resultants, n1 & n2, from Load B

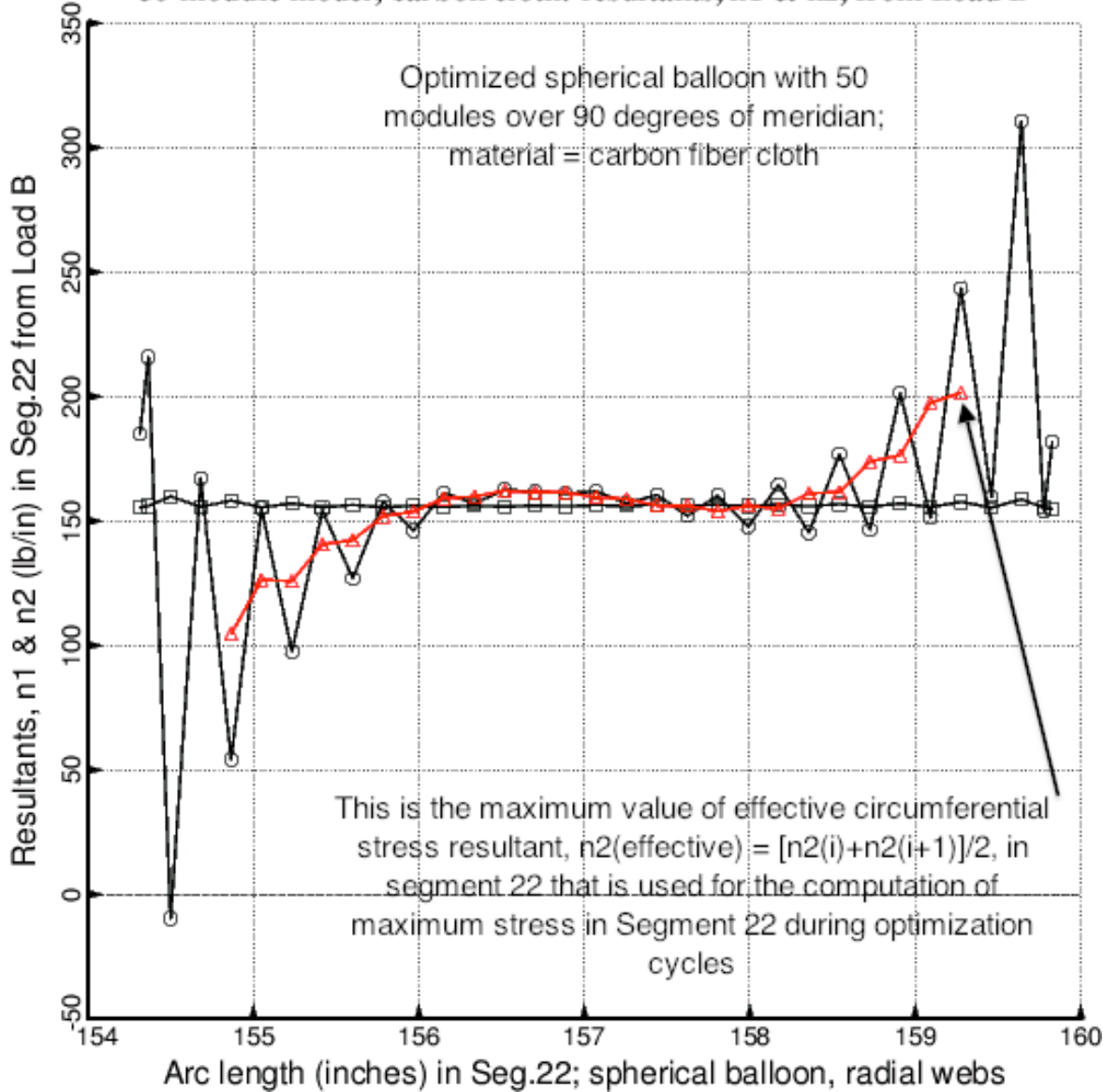


Fig. 38 The meridional and circumferential stress resultants, $n1$ and $n2$, in Segment 22 of the optimized spherical balloon with 50 modules and with radial webs. There are 31 nodal points in Segment 22, which is the number of nodal points used in each of the segments of the model for the purpose of optimization. (See Fig.37a.) The material is carbon fiber cloth the properties of which are listed in Table 13. This figure shows the axisymmetric pre-buckling distributions of $n1$ and $n2$ in Segment 22 caused by Load B (the "fixed", non-eigenvalue loads: PINNER = 0 psi, PMIDDLL = 60 psi, POUTER = 0 psi). Notice the significant spurious local "zig-zag" component of $n2$ near both ends of Segment 22. This spurious "zig-zag" component of $n2$ is dramatically reduced by averaging $n2$ at neighboring nodal points: $n2(\text{effective}) = [n2(i) + n2(i+1)]/2$ (shown in the red curve). That is why the "balloon" software uses $n2(\text{effective})$ instead of $n2$ during optimization cycles.

- Circumferential resultant, n2 in Seg.22 (Seg. 2 of Module 5 of 50); 33 nodal points
- △ Average circumferential resultant, $[n2(i)+n2(i+1)]/2$ in Seg.22; 33 nodal points
- Circumferential resultant, n2 in Seg.22 (Seg. 2 of Module 5 of 50); 99 nodal points
- + Circumferential resultant, n2 in Seg.22 (Seg. 2 of Module 5 of 50); 43 nodal points
- × Circumferential resultant, n2 in Seg.22 (Seg. 2 of Module 5 of 50); 63 nodal points

50-module model; carbon cloth: hoop resultant, n2, from Load B

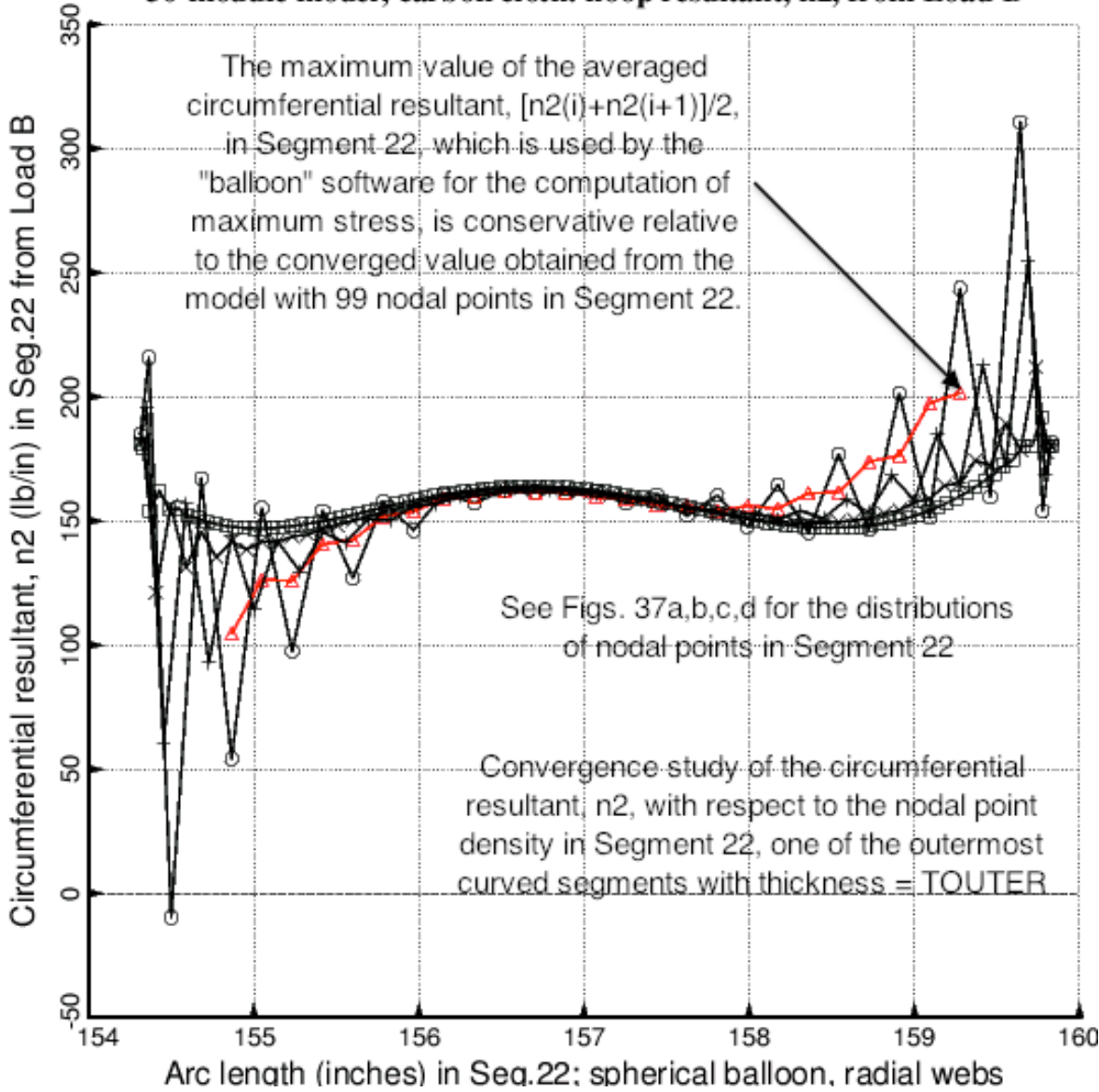


Fig. 39 A convergence study of the circumferential stress resultant, n2, in Segment 22 of the optimized spherical balloon with 50 modules and with radial webs. The material is carbon fiber cloth the properties of which are listed in Table 13. This figure shows the axisymmetric pre-buckling distributions of n2 in Segment 22 caused by Load B (the "fixed", non-eigenvalue loads: PINNER = 0 psi, PMIDDLE = 60 psi, POUTER = 0 psi). Notice that the significant spurious local "zig-zag" component of n2 near both ends of Segment 22 diminishes dramatically with increasing numbers of nodal points in Segment 22. The red curve, which is used by the "balloon" software during optimization cycles, is the same curve as that displayed in the previous figure.

try7..R,Z_LOADSTEP11

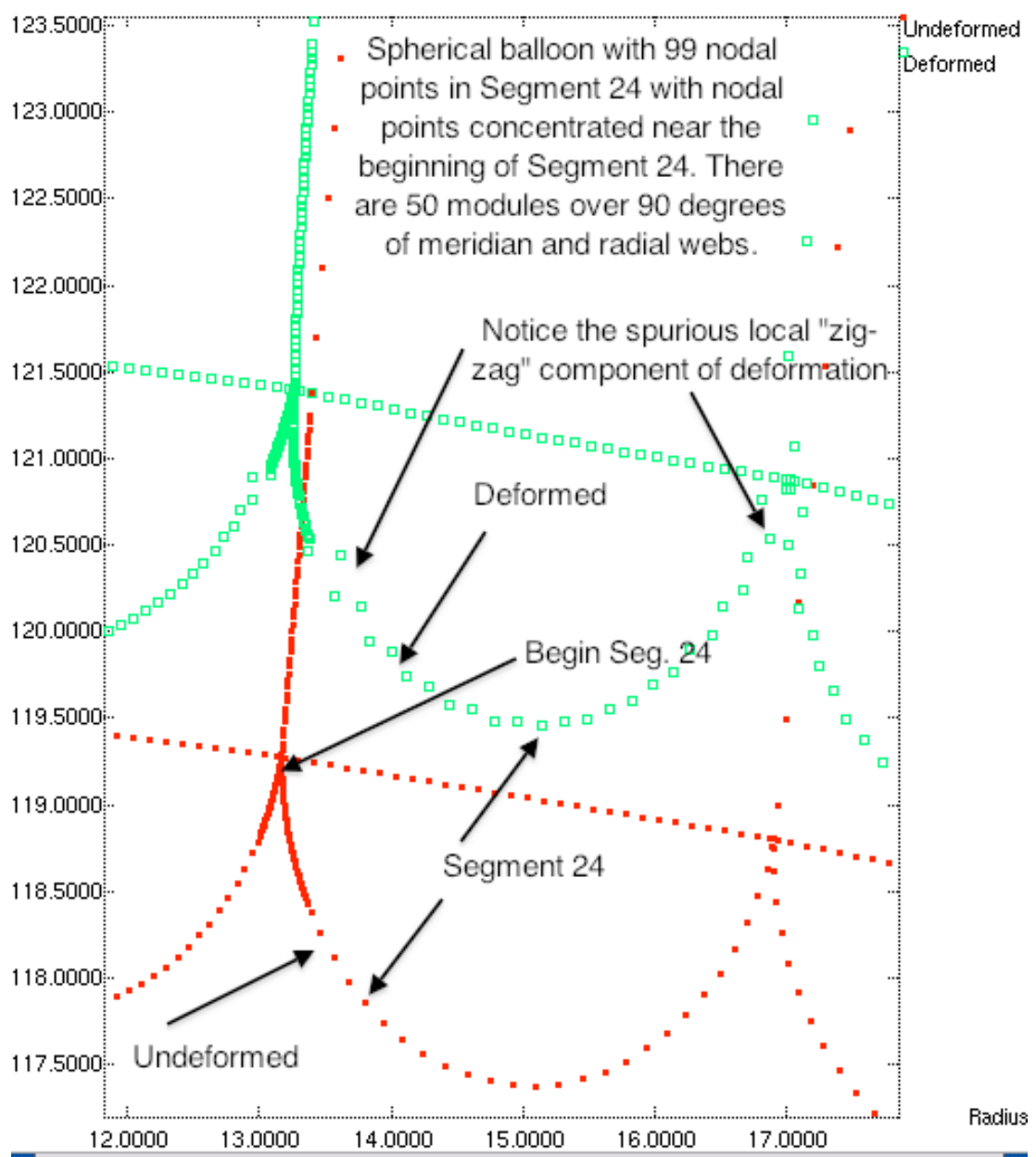


Fig. 40 The nodal point discretization in Segment 24 and in the neighborhood of Segment 24 in the optimized spherical balloon with 50 modules and with radial webs. The material is carbon fiber cloth the properties of which are listed in Table 13. This figure shows the axisymmetric pre-buckling deformation caused by Load B (the “fixed”, non-eigenvalue loads: PINNER = 0 psi, PMIDDLE = 60 psi, POUTER = 0 psi) in this local region of the spherical balloon. The axisymmetric pre-buckling deformation of the entire model of the spherical balloon is analogous to that displayed in Fig. 12. The predictions of extreme fiber meridional stress in Segment 24 displayed in Figs. 42 and 44 are based on the nodal point distribution in Segment 24 shown here.

- Left-most fiber meridional stress in Seg.4, Module 5 of 50; radial webs; PMIDDLE=60 psi, POUTER=0
- Right-most fiber meridional stress in Seg.4, Module 5 of 50; radial webs; PMIDDLE=60 psi, POUTER=0

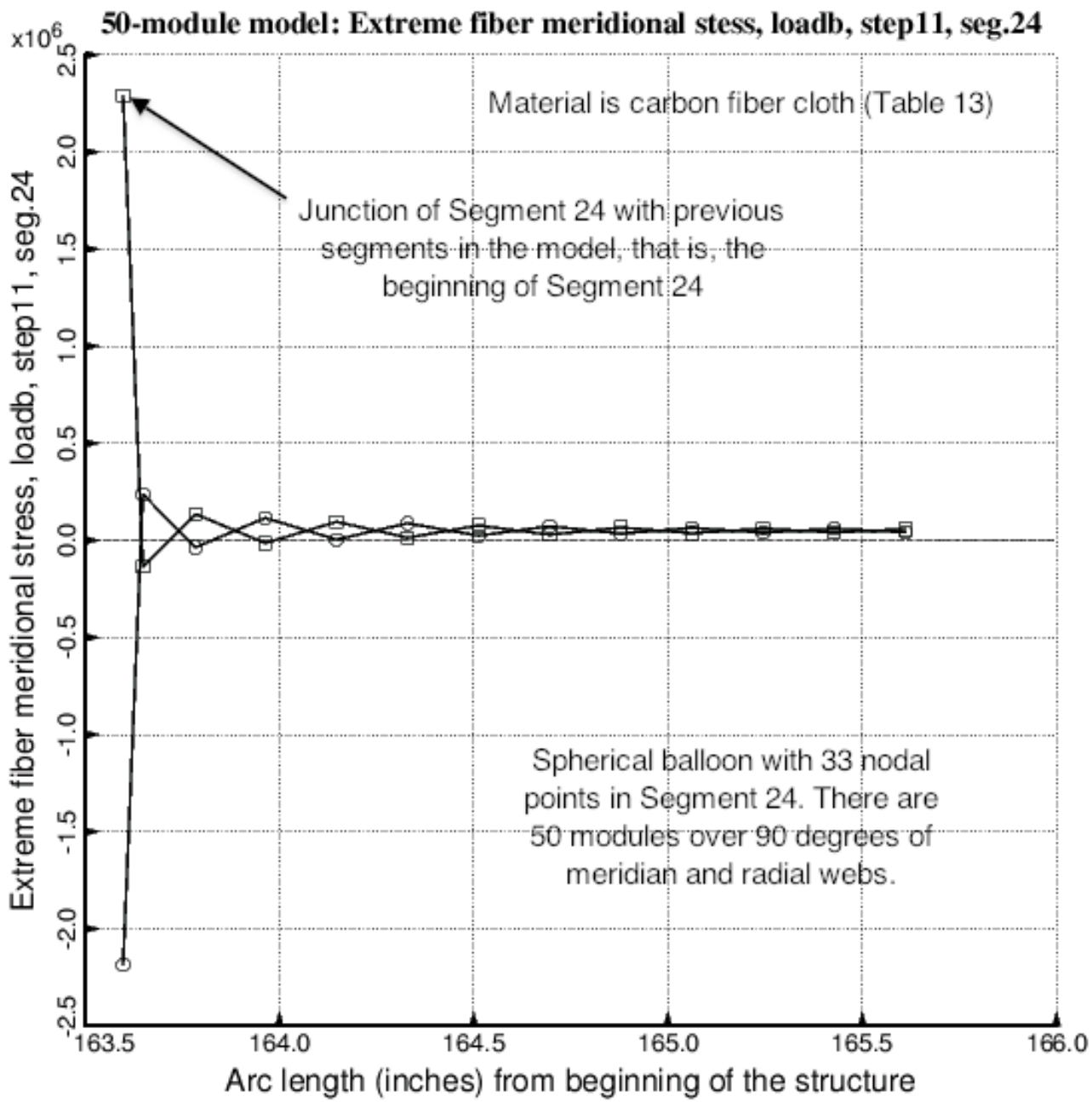


Fig. 41 Extreme fiber meridional stress along the beginning of "shell" Segment No. 24 of the optimized spherical balloon with 50 modules and with radial webs. The pre-buckling axisymmetric stress is generated by Load B, the "fixed", non-eigenvalue loads: PINNER = 0 psi, PMIDDLE = 60 psi, POUTER = 0 psi. The axisymmetric pre-buckling deformation is analogous to those shown in Fig. 12 and in the previous figure. These extreme fiber meridional stresses are derived from the model in which there are 31 nodal points in each segment of the model. This figure is analogous to Fig. 14.

- Left-most fiber meridional stress in Seg.4, Module 5 of 50; radial webs; PMIDDLE=60 psi, POUTER=0
 Right-most fiber meridional stress in Seg.4, Module 5 of 50; radial webs; PMIDDLE=60 psi, POUTER=0

50-module model: Extreme fiber meridional stess, loadb, step11, seg.24

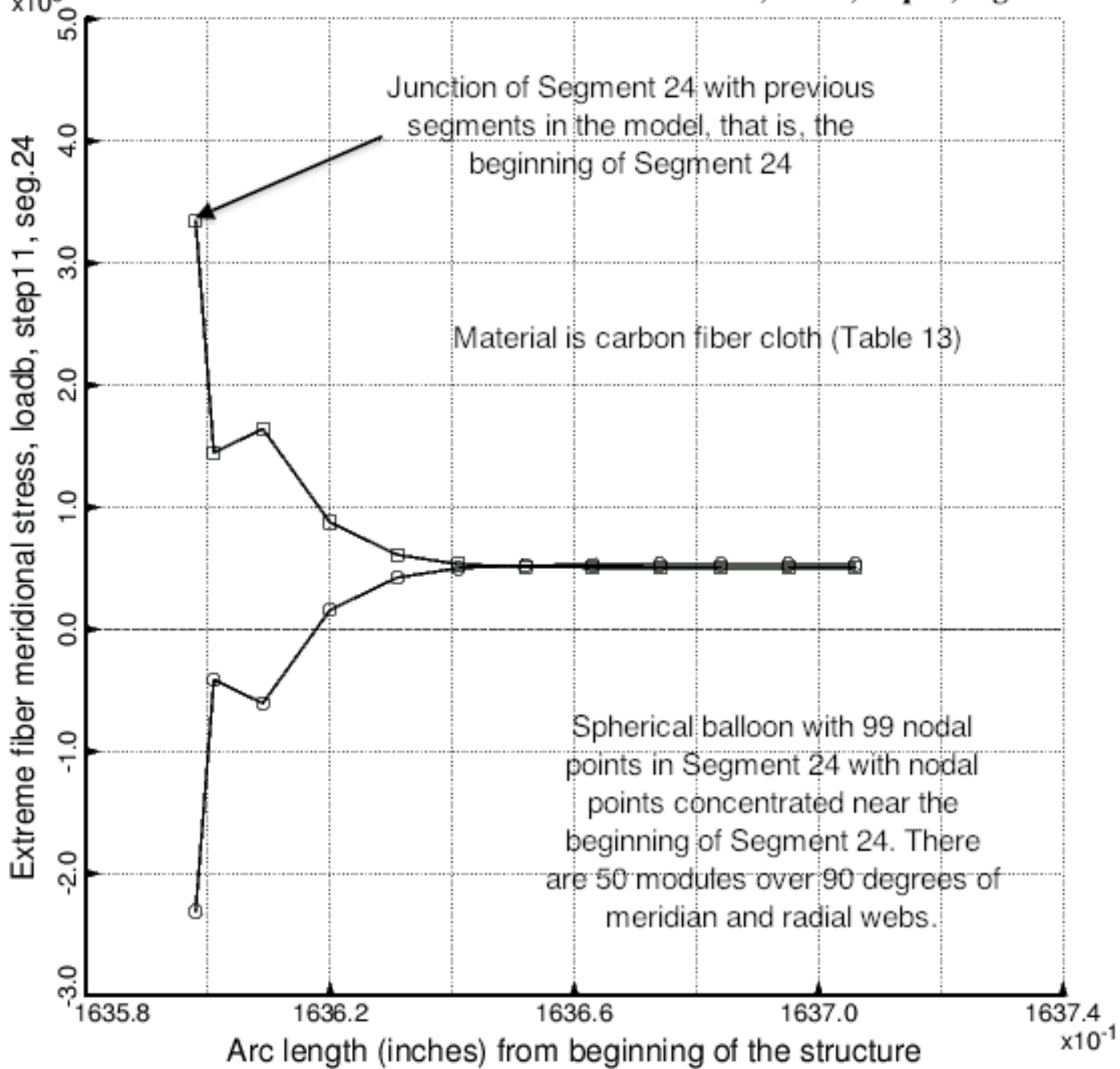


Fig. 42 Extreme fiber meridional stress along the beginning of "shell" Segment No. 24 of the optimized spherical balloon with 50 modules and with radial webs. The pre-buckling axisymmetric stress is generated by Load B, the "fixed", non-eigenvalue loads: PINNER = 0 psi, PMIDDLE = 60 psi, POUTER = 0 psi. The axisymmetric pre-buckling deformation is depicted in Fig. 40. This figure is analogous to Fig. 16.

- Left-most fiber meridional stress in Seg.4, Module 5 of 50; radial webs; PMIDDLE=60 psi, POUTER=0
- Right-most fiber meridional stress in Seg.4, Module 5 of 50; radial webs; PMIDDLE=60 psi, POUTER=0
- Left-most fiber meridional stress in Seg.4, Module 5 of 50; radial webs; refined Seg.24
- Right-most fiber meridional stress in Seg.4, Module 5 of 50; radial webs; refined Seg.24

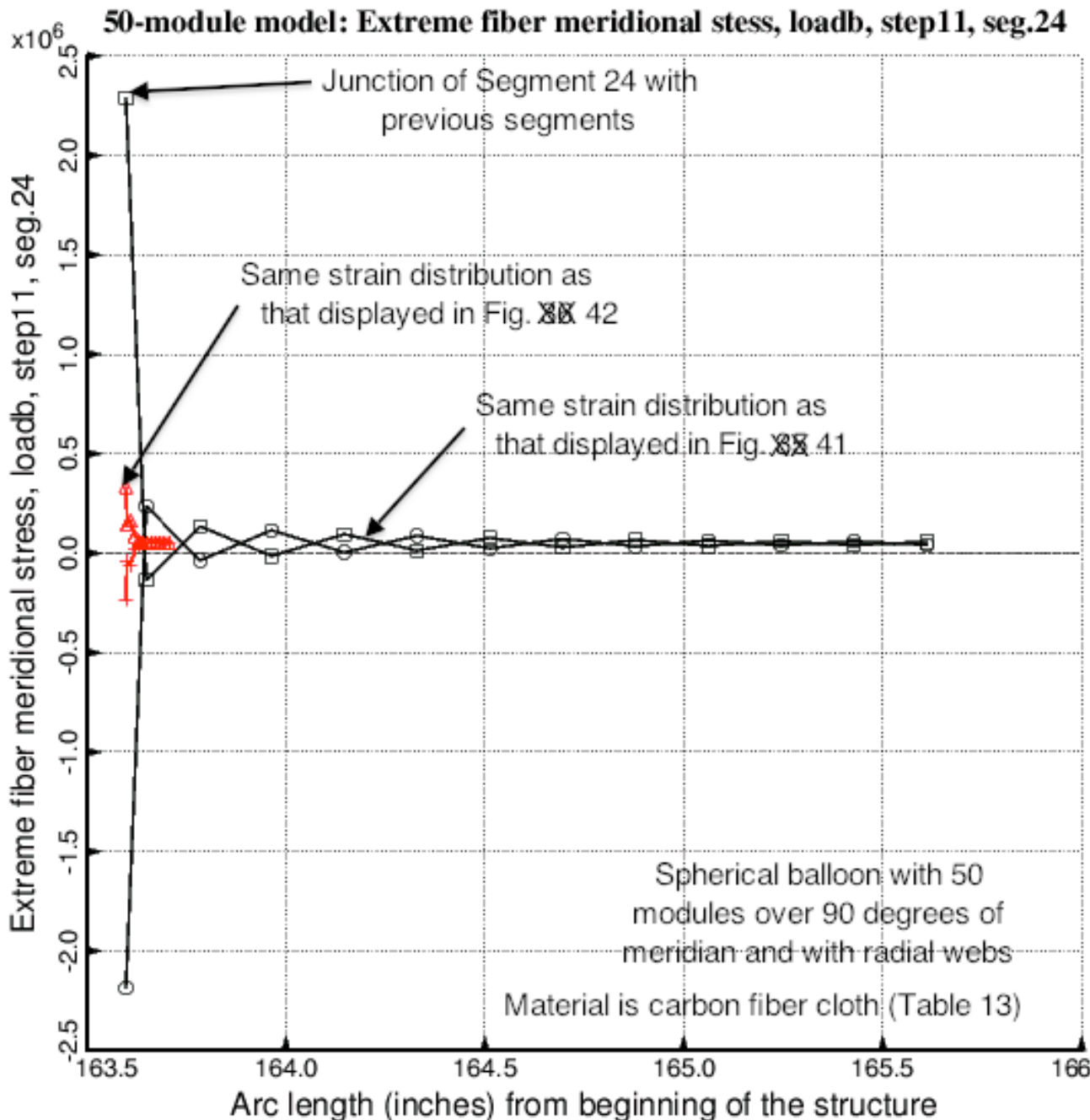


Fig. 43 Axisymmetric pre-buckling extreme fiber meridional stress along the beginning of Segment 24 in the spherical balloon with 50 modules and radial webs. The loading is Load B, the “fixed”, non-eigenvalue loads: PINNER = 0 psi, PMIDDLE = 60 psi, POUTER = 0 psi. The axisymmetric pre-buckling deformation is shown in Fig. 40. This figure is analogous to Fig. 17.

- Left-most fiber meridional stress in Seg.4, Module 5 of 50; radial webs; refined Seg.24
- Right-most fiber meridional stress in Seg.4, Module 5 of 50; radial webs; refined Seg.24
- △ Left-most fiber meridional stress in Seg.4, Module 5 of 50; radial webs; mostrefined Seg.24
- + Right-most fiber meridional stress in Seg.4, Module 5 of 50; radial webs; mostrefined Seg.24

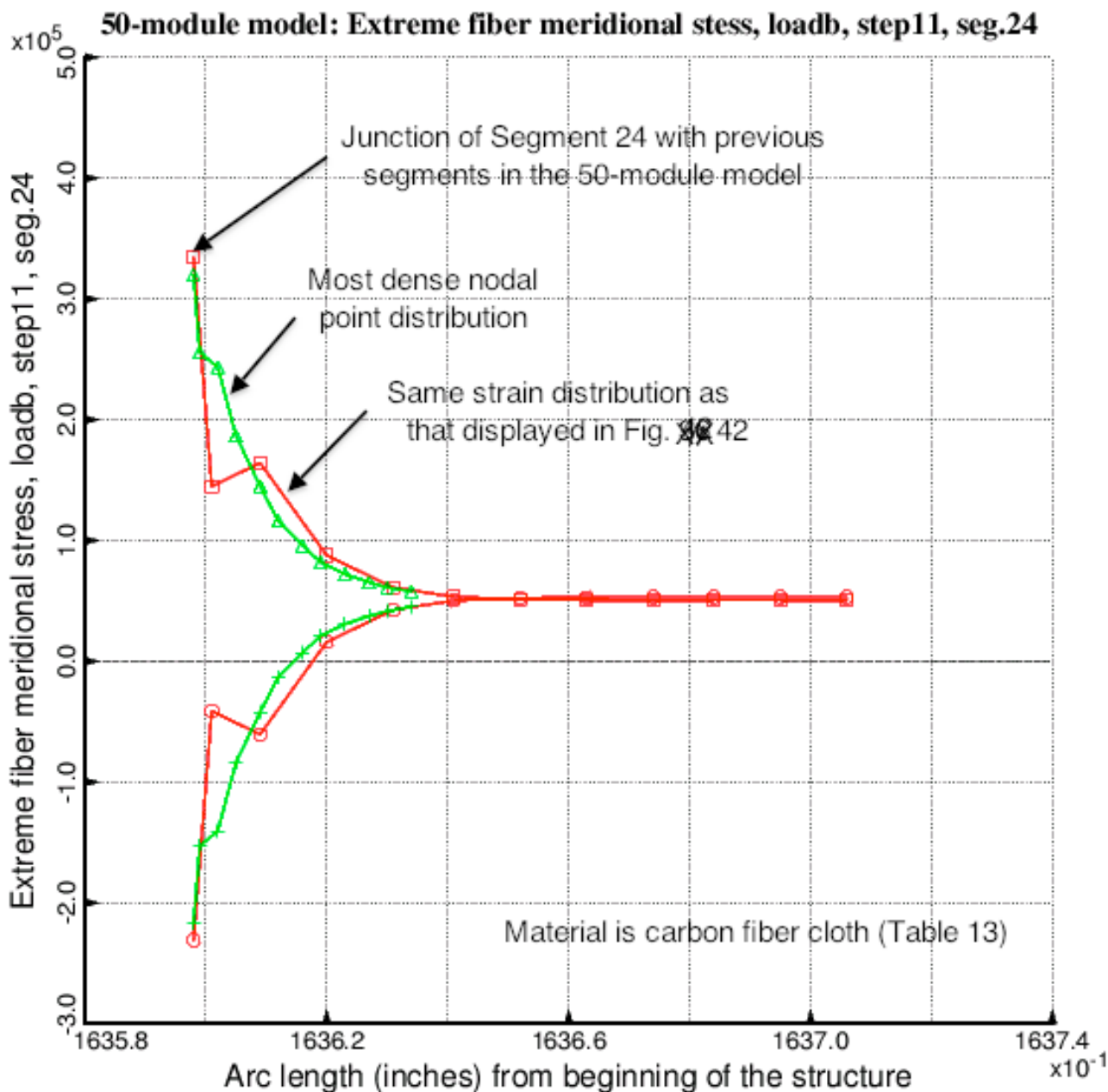
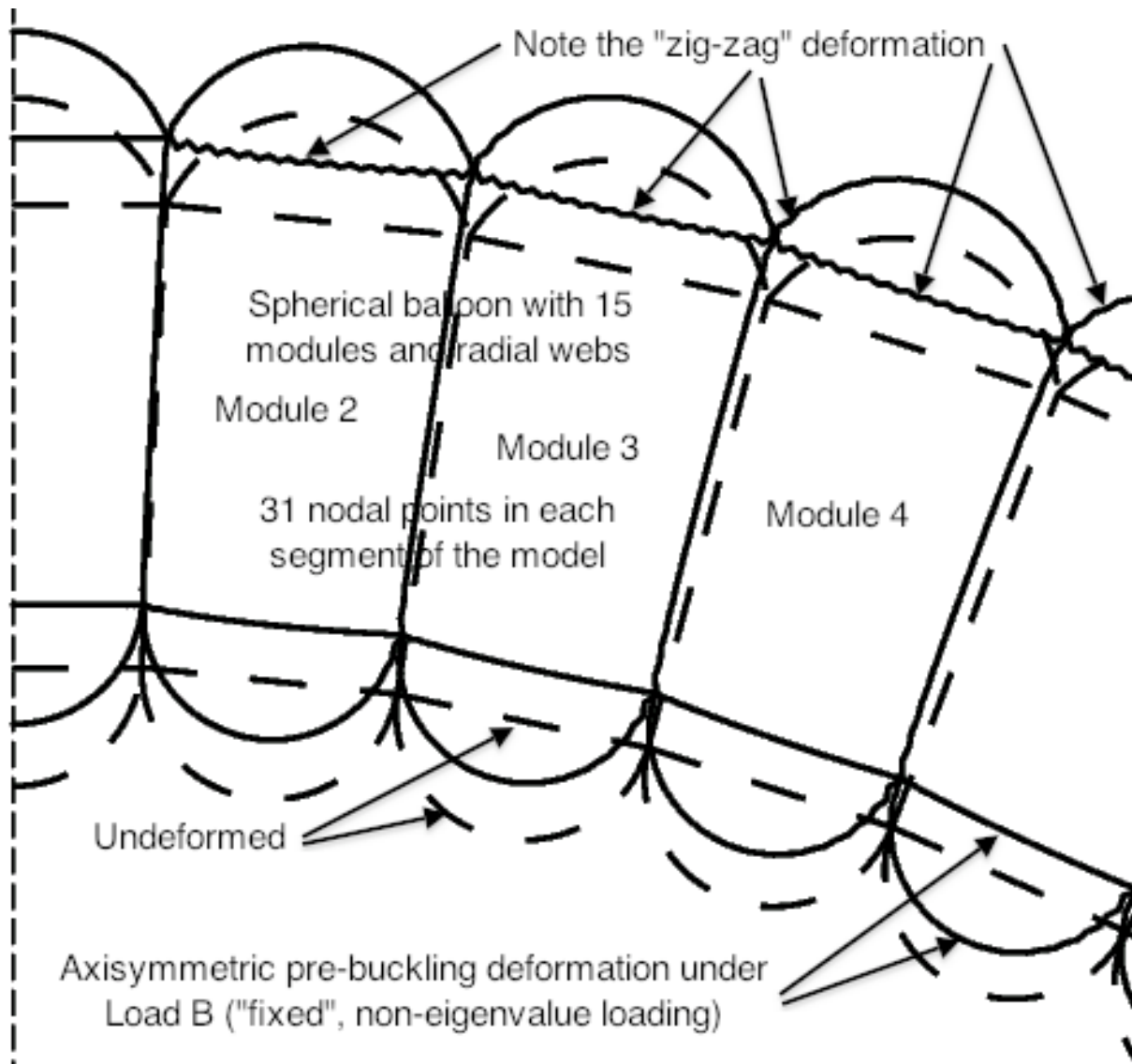


Fig. 44 Axisymmetric pre-buckling extreme fiber meridional stress along the beginning of Segment 24 in the spherical balloon with 50 modules and radial webs. The loading is Load B, the “fixed”, non-eigenvalue loads: PINNER = 0 psi, PMIDDLE = 60 psi, POUTER = 0 psi. The axisymmetric pre-buckling deformation is shown in Fig. 40. The most dense nodal point distribution (green curve) is three times as dense in the immediate neighborhood of the beginning of Segment 24 as the density of the nodal point distribution corresponding to the red curve.



Optimized spherical balloon with 15 modules over 90 degrees of meridian and with radial webs ; carbon fiber cloth

Fig. 45 This figure shows the axisymmetric pre-buckling deformation in the part of the spherical balloon near the pole for the optimized spherical balloon with 15 modules and radial webs. The material is carbon fiber cloth the properties of which are listed in Table 13. The deformation is caused by Load B (the "fixed", non-eigenvalue loads: PINNER = 0 psi, PMIDDLE = 60 psi, POUTER = 0 psi). The axisymmetric pre-buckling deformation of the entire model of the spherical balloon is analogous to that displayed in Fig. 12. There are 31 nodal points in each segment of the balloon. Notice the small spurious local "zig-zag" component of deformation especially in the outer wall with straight segments the thickness of which is TFOUTR. The amplitude of this spurious local "zig-zag" component decreases with increasing numbers of nodal points, as displayed in the next figure.

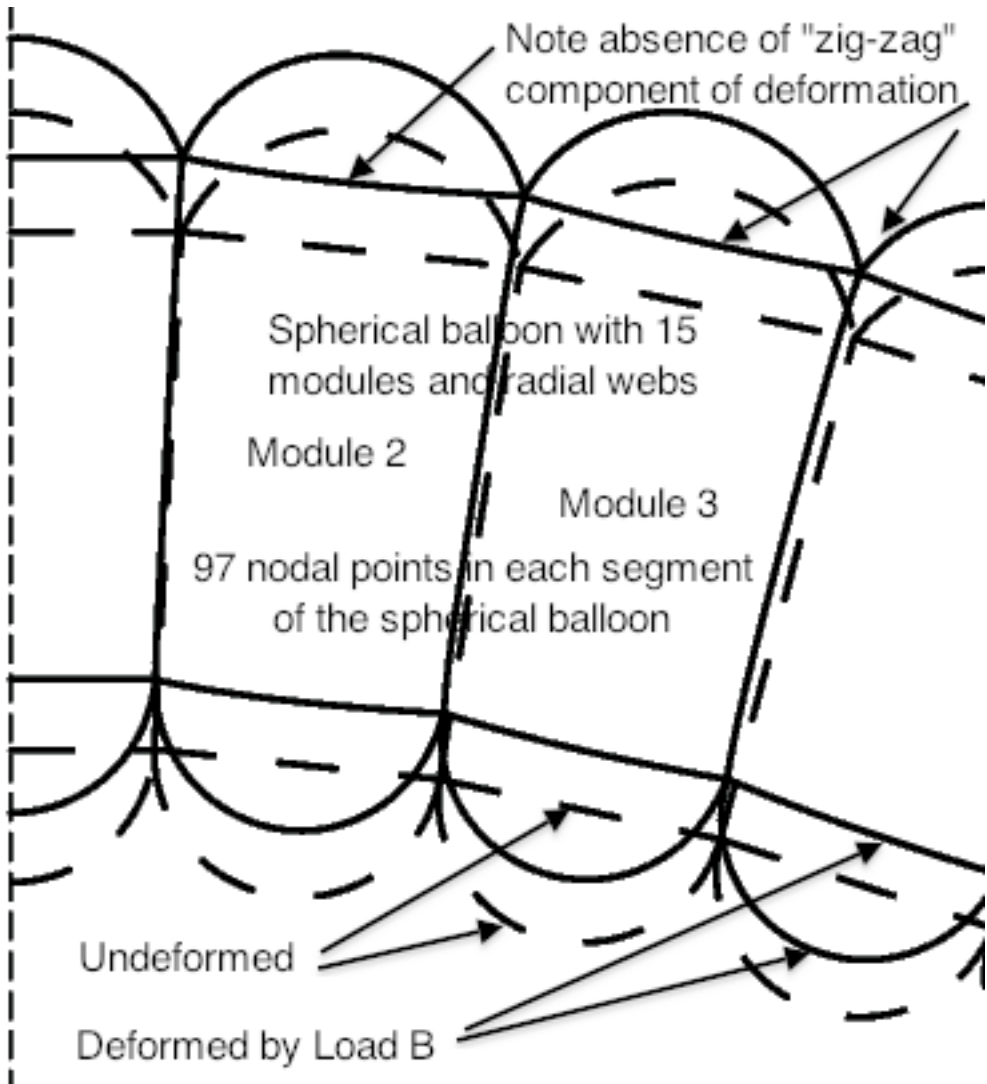


Fig. 46 This figure shows the axisymmetric pre-buckling deformation in the part of the spherical balloon near the pole for the optimized spherical balloon with 15 modules and radial webs. The material is carbon fiber cloth the properties of which are listed in Table 13. The deformation is caused by Load B (the “fixed”, non-eigenvalue loads: PINNER = 0 psi, PMIDDLE = 60 psi, POUTER = 0 psi). The axisymmetric pre-buckling deformation of the entire model of the spherical balloon is analogous to that displayed in Fig. 12. There are 97 nodal points in each segment of the balloon. Notice that the small spurious local “zig-zag” component of deformation visible in the previous figure is absent in this model.

— — Undeformed: optimized balloon with 15 modules over 90 degrees of meridian & 33 nodes/segment
 — Deformed: Eigenvalue No.1 corresponds to local buckling of inner wall with thickness=TFINNR

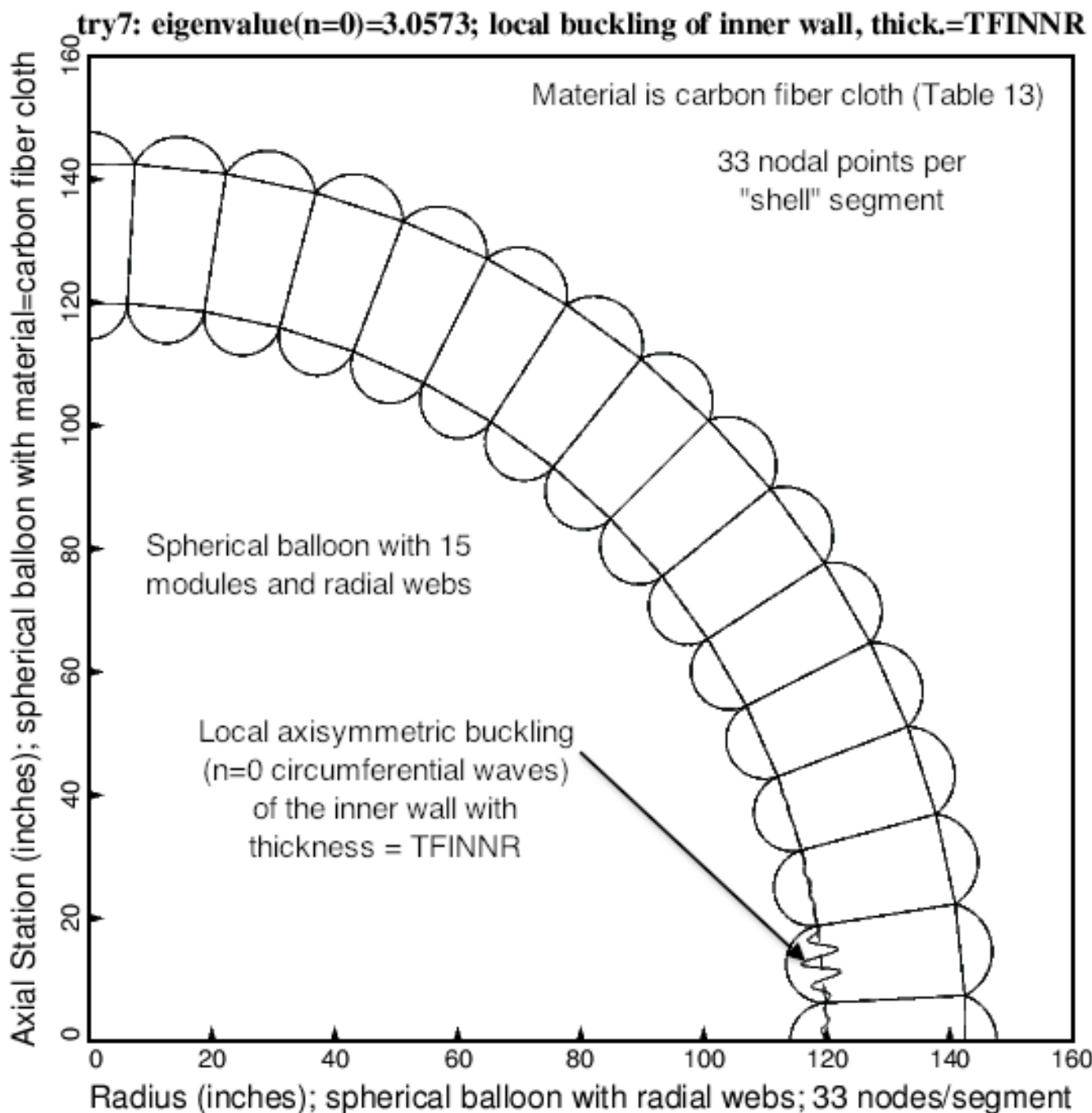


Fig. 47 Axisymmetric ($N = 0$ circumferential waves) bifurcation buckling of the optimized spherical balloon with 15 modules over 90 degrees of meridian and with radial webs. There are 31 nodal points per segment specified in the "balloon" software, SUBROUTINE BOSDEC (NODSEG = 31). (33 nodal points are indicated in the figure because BIGBOSOR4 automatically adds one extra nodal point very near the end of each segment.) Compare with the local buckling mode displayed in the next figure.

— Undeformed: optimized balloon with 15 modules over 90 degrees of meridian & 99 nodes/segment
— Deformed: Eigenvalue No.1 corresponds to local buckling of inner wall with thickness=TFINNR

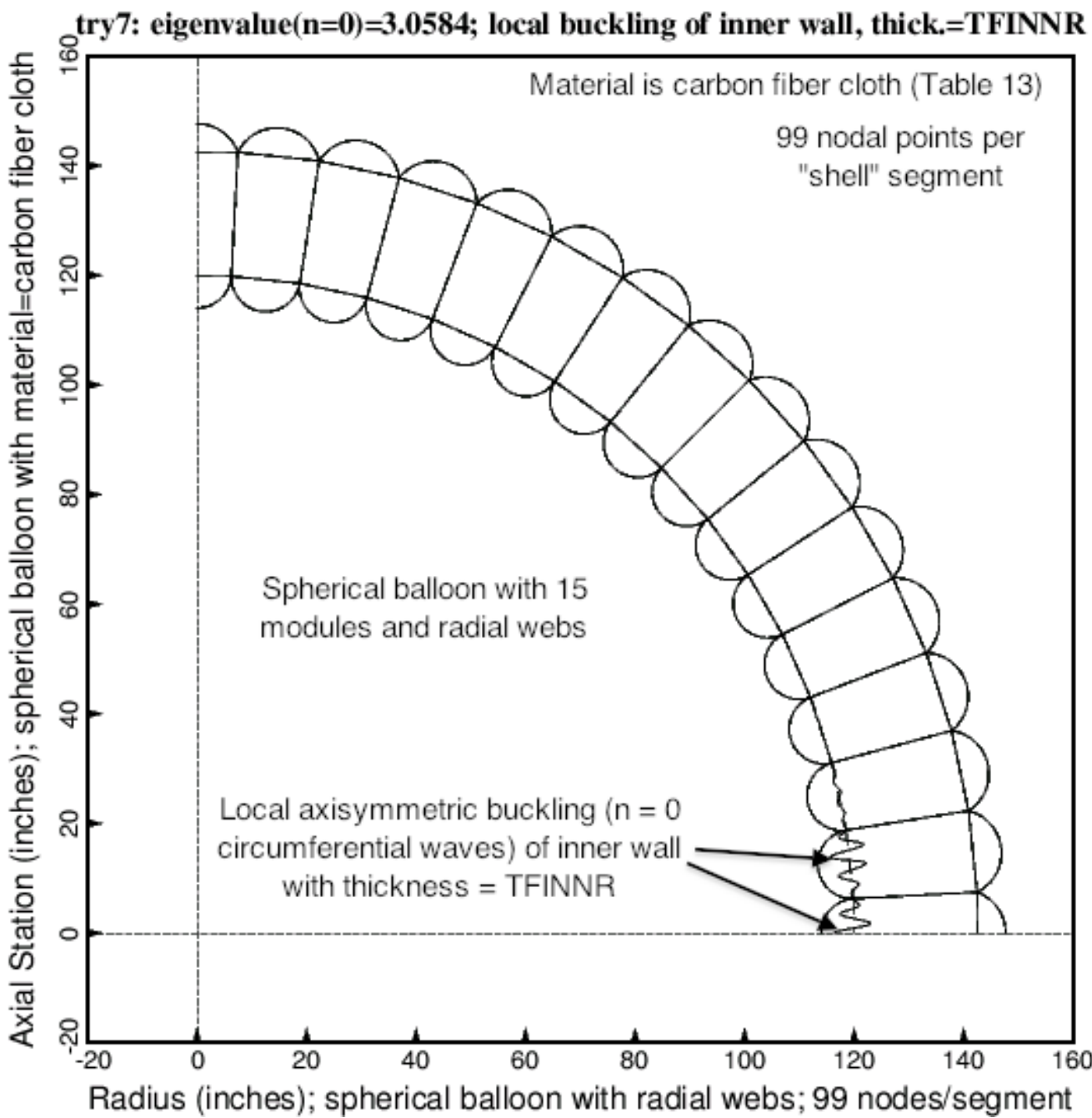


Fig. 48 Axisymmetric ($N = 0$ circumferential waves) bifurcation buckling of the optimized spherical balloon with 15 modules over 90 degrees of meridian and with radial webs. There are 97 nodal points per segment specified in the "balloon" software, SUBROUTINE BOSDEC (NODSEG = 97). (99 nodal points are indicated in the figure because BIGBOSOR4 automatically adds one extra nodal point very near the end of each segment.) Compare with the local buckling mode displayed in the previous figure.

— Undeformed: optimized balloon with 15 modules over 90 degrees of meridian & 33 nodes/segment
 — Deformed: Eigenvalue No.1 corresponds to local buckling of inner wall with thickness=TFINNR

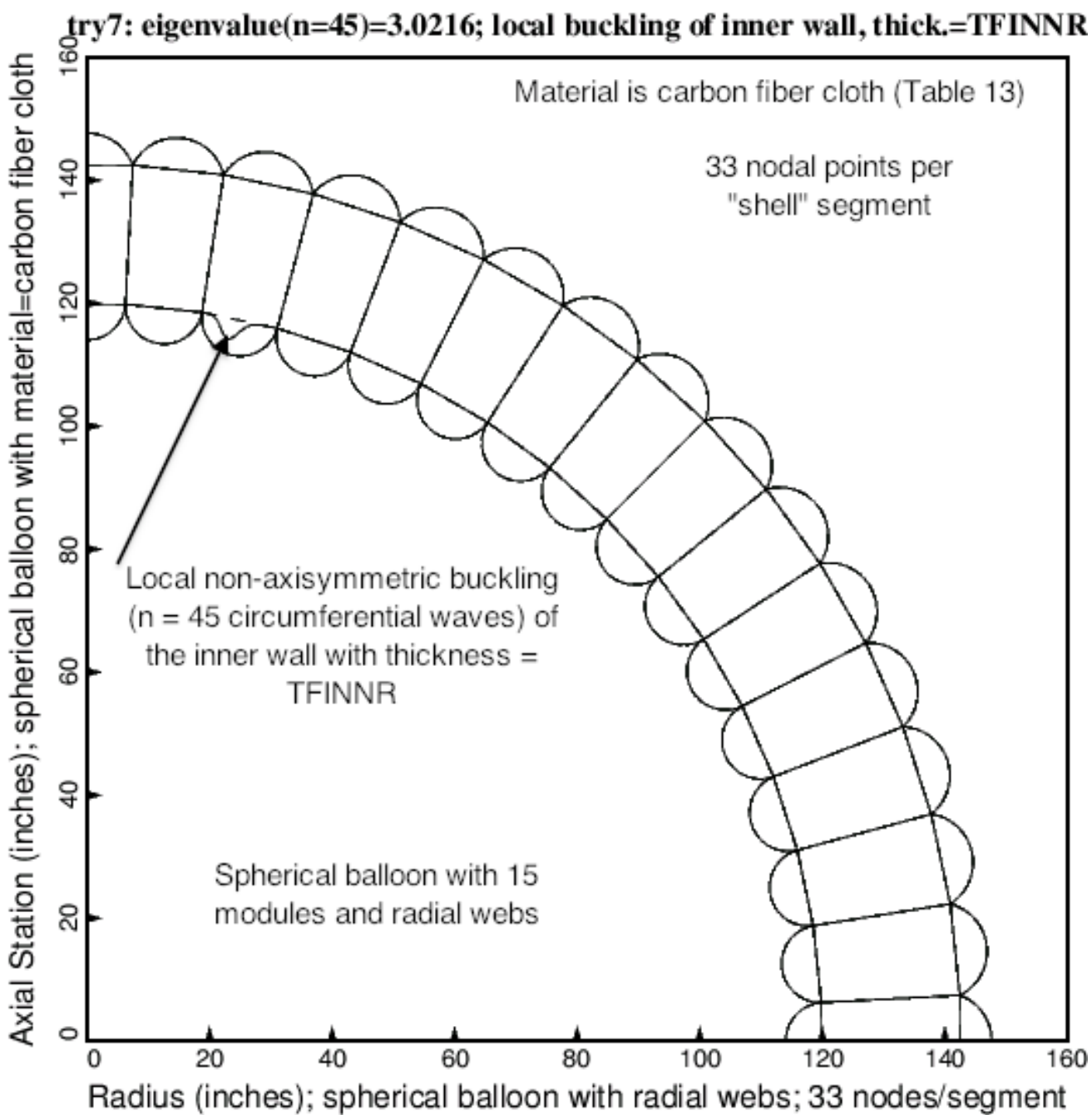


Fig. 49 Non-axisymmetric ($N = 45$ circumferential waves) bifurcation buckling of the optimized spherical balloon with 15 modules over 90 degrees of meridian and with radial webs. There are 31 nodal points per segment specified in the "balloon" software, SUBROUTINE BOSDEC (NODSEG = 31). (33 nodal points are indicated in the figure because BIGBOSOR4 automatically adds one extra nodal point very near the end of each segment.) Compare with the local non-axisymmetric buckling mode displayed in the next figure.

— Undeformed: optimized balloon with 15 modules over 90 degrees of meridian & 99 nodes/segment
 — Deformed: Eigenvalue No.1 corresponds to local buckling of inner wall with thickness=TFINNR

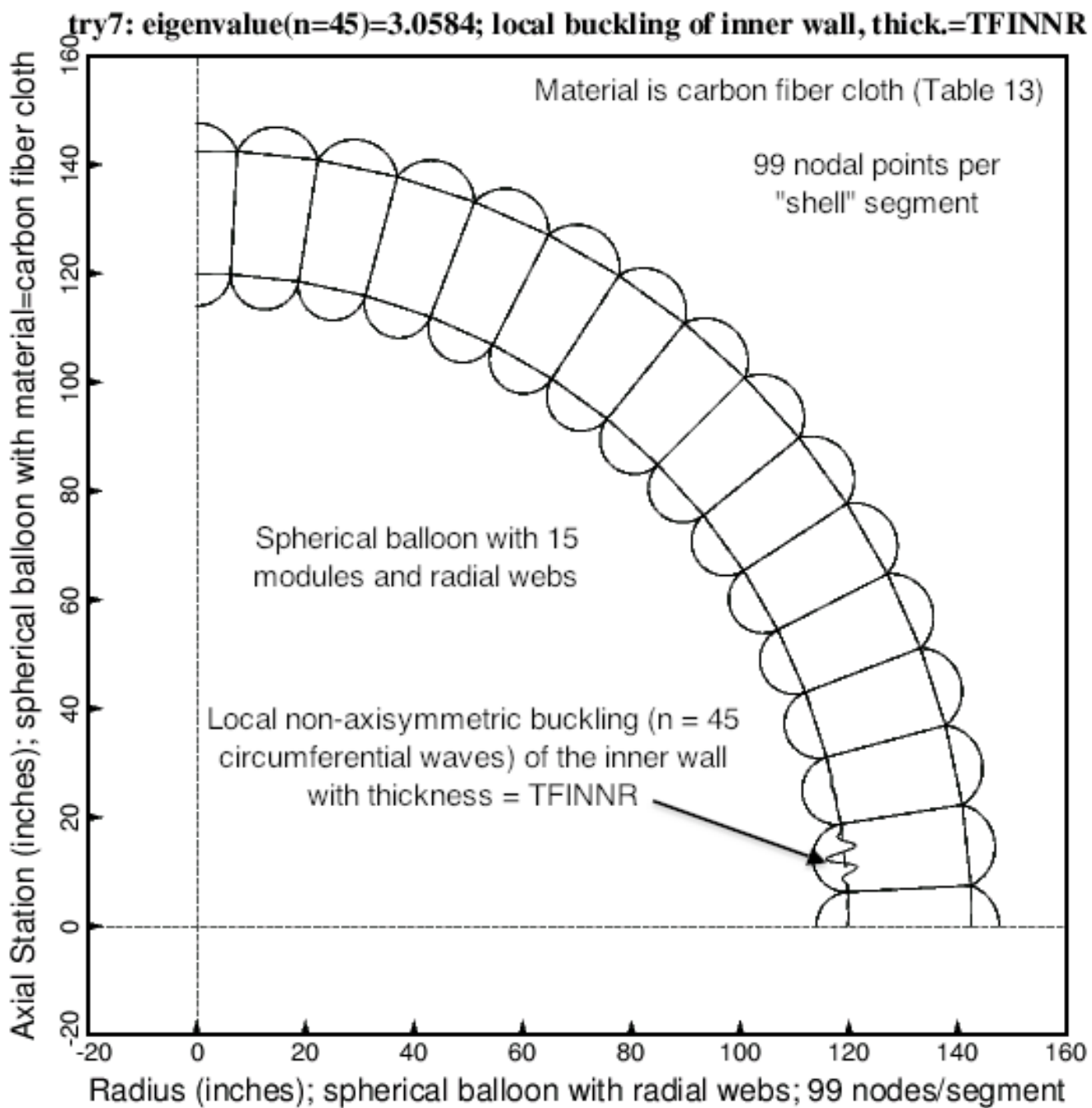


Fig. 50 Non-axisymmetric ($N = 45$ circumferential waves) bifurcation buckling of the optimized spherical balloon with 15 modules over 90 degrees of meridian and with radial webs. There are 97 nodal points per segment specified in the "balloon" software, SUBROUTINE BOSDEC (NODSEG = 97). (99 nodal points are indicated in the figure because BIGBOSOR4 automatically adds one extra nodal point very near the end of each segment.) Compare with the local non-axisymmetric buckling mode displayed in the previous figure.

□ total weight of the spherical balloon with 35 modules over 90 deg.of meridian and truss-like webs

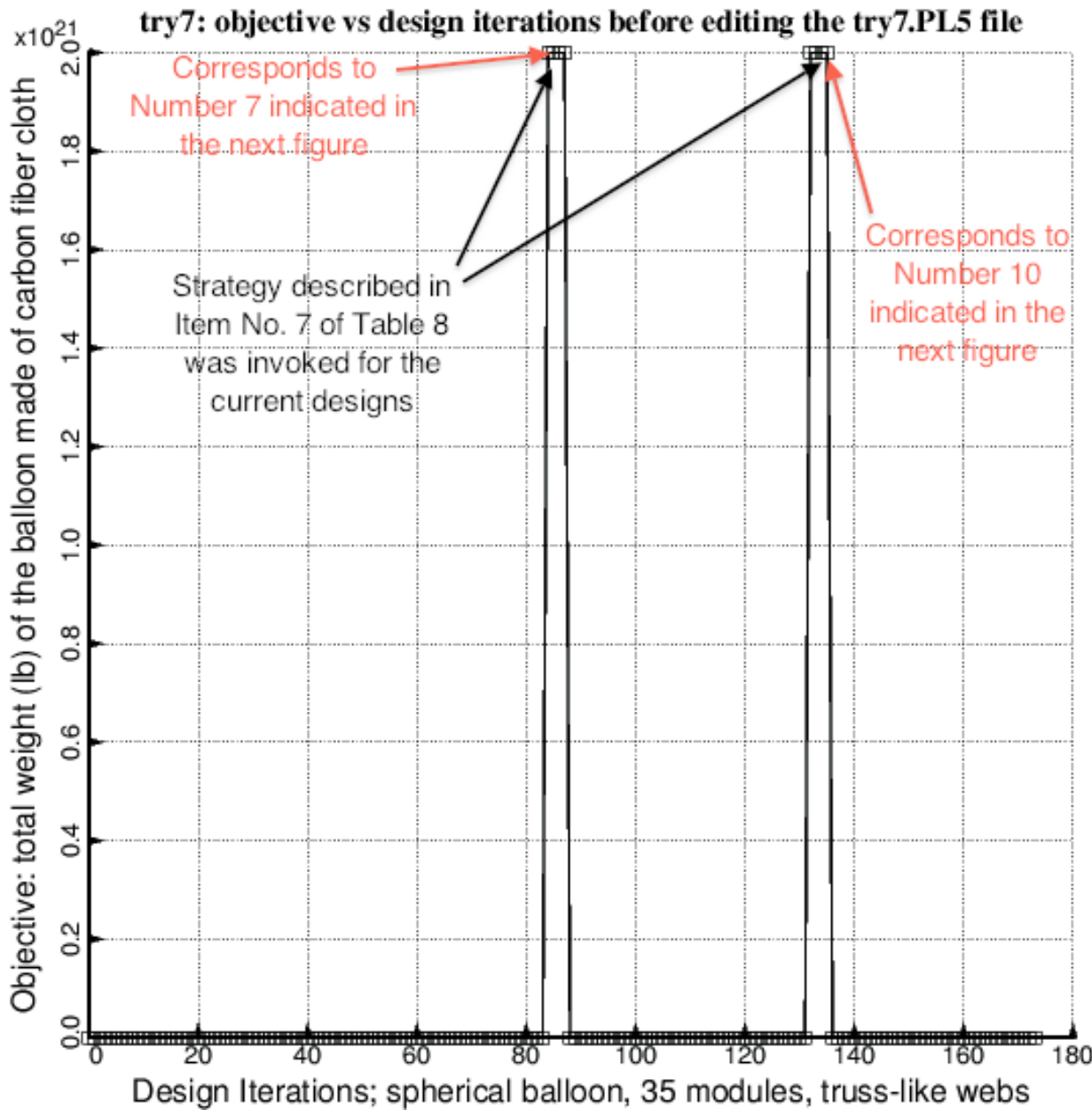


Fig. 51a Optimization of the spherical balloon with 35 modules and truss-like (slanted) webs during a partial execution of SUPEROPT. (SUPEROPT was terminated on purpose at Iteration 175.) This figure is analogous to Fig. 21. The purpose of the strategy described in Item 7d of Table 8 is to prevent lack of convergence of the Newton method for the solution of the nonlinear pre-buckling equilibrium equations from causing the execution of SUPEROPT to terminate prematurely. SUPEROPT “keeps truckin’” in spite of failure of BIGBOSOR4 to obtain the nonlinear pre-buckled state of the spherical balloon. This figure demonstrates that lack of convergence for the **current** design (IMODX = 0) occurred on two occasions during this partial execution of SUPEROPT. The next figure shows the evolution of the objective with the very high values of the objective edited out of the try4.PL5 file.

□ total weight of the spherical balloon with 35 modules over 90 deg.of meridian and truss-like webs

try7: objective vs design iterations after editing the try7.PL5 file

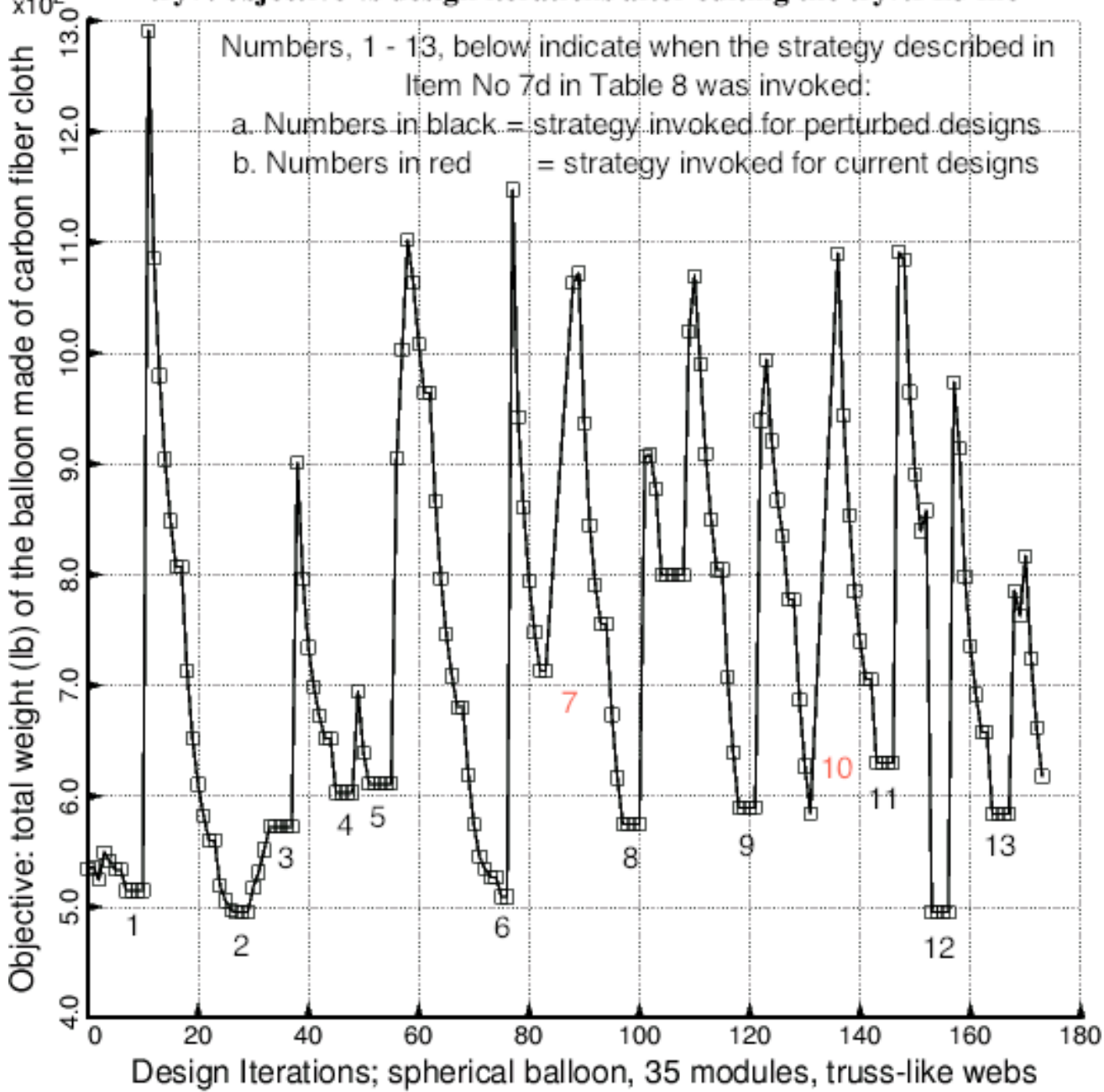


Fig. 51b Optimization of the spherical balloon with 35 modules and truss-like (slanted) webs during a partial execution of SUPEROPT. (SUPEROPT was terminated on purpose at Iteration 175.) This figure is analogous to Fig. 22. This figure is obtained by editing the try4.PL5 file – removing the very high values of WEIGHT shown in the previous figure – and then executing the GENOPT processor called DIPLOT with the edited file, try4.PL5, used as input. Each "spike" in the curve corresponds to a new "starting" design determined randomly by the GENOPT processor called AUTOCHANGE [12].

□ total weight of the spherical balloon with 45 modules over 90 deg.of meridian and truss-like webs

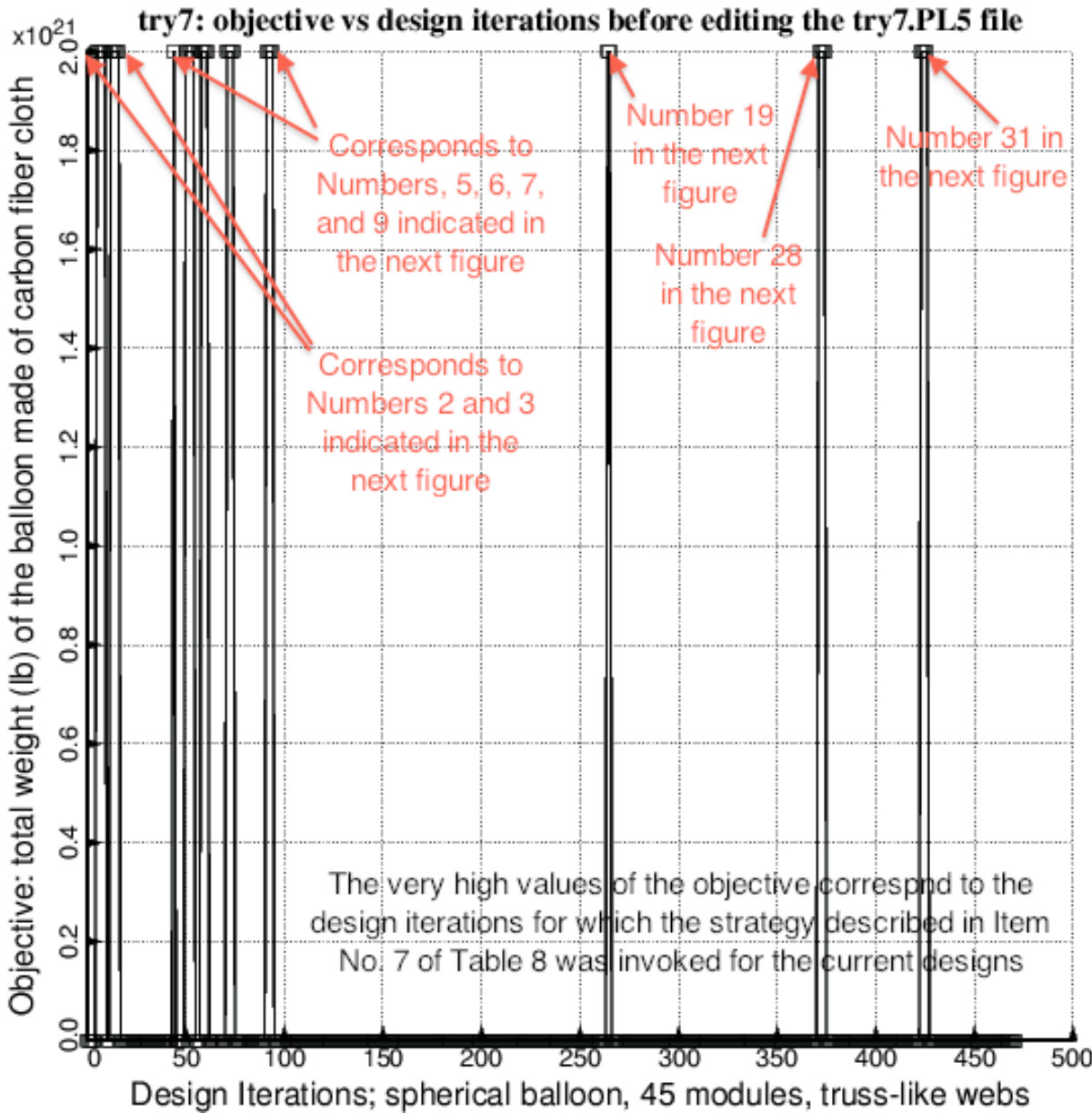


Fig. 52a Optimization of the spherical balloon with 45 modules and truss-like (slanted) webs during a complete execution of SUPEROPT. (SUPEROPT ran successfully for a total of about 470 design iterations.) This figure is analogous to Figs. 21 and 51a. The purpose of the strategy described in Item 7d of Table 8 is to prevent lack of convergence of the Newton method for the solution of the nonlinear pre-buckling equilibrium equations from causing the execution of SUPEROPT to terminate prematurely. SUPEROPT “keeps truckin” in spite of failure of BIGBOSOR4 to obtain the nonlinear pre-buckled state of the spherical balloon. This figure demonstrates that lack of convergence for the **current** design (IMODX = 0) occurred on nine occasions during this complete execution of SUPEROPT. The next figure shows the evolution of the objective with the very high values of the objective edited out of the try4.PL5 file.

□ total weight of the spherical balloon with 45 modules over 90 deg.of meridian and truss-like webs

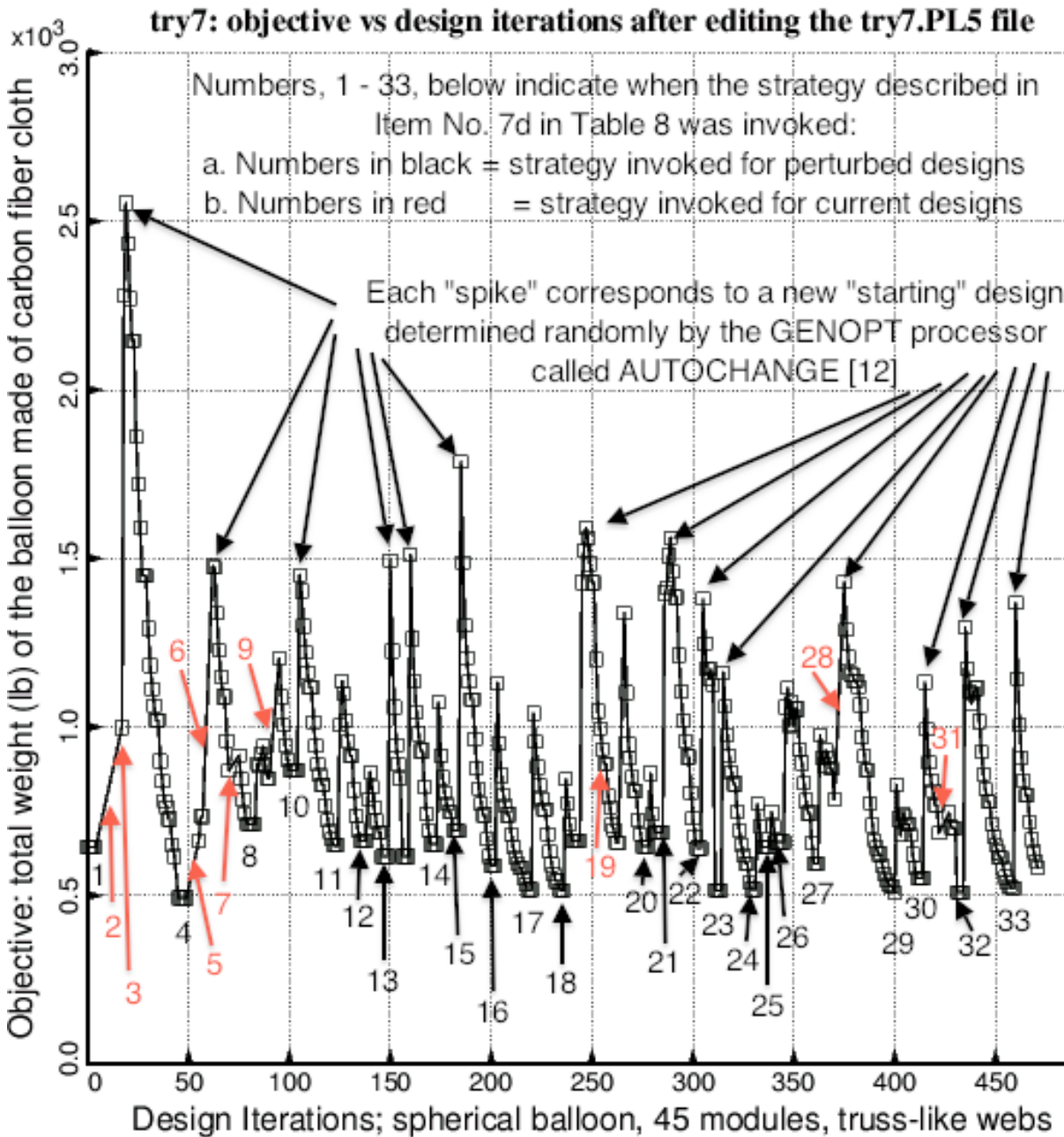


Fig. 52b Optimization of the spherical balloon with 45 modules and truss-like (slanted) webs during a complete execution of SUPEROPT. (SUPEROPT is complete when about 470 design iterations have been processed.) This figure is analogous to Figs. 22 and 51b. This figure is obtained by editing the try4.PL5 file – removing the very high values of WEIGHT shown in the previous figure – and then executing the GENOPT processor called DIPILOT with the edited file, try4.PL5, used as input. The 33 occasions on which there was failure of Newton convergence in BIGBOSOR4's attempt to solve the nonlinear pre-buckling equations significantly diminish the extent of the exploration of design space during the search for a "global" optimum design.

○ 1.- (2.88+0.02*V(1)-1.00*V(3))
 △ (BUCKB4(1)/BUCKB4A(1)) / BUCKB4F(1)-1; F.S.= 3.00
 + (TENLOS(1)/TENLOSA(1)) / TENLOSF(1)-1; F.S.= 3.00
 × (STRM1A(1,1)/STRM1(1,1)) / STRM1F(1,1)-1; F.S.= 1.00
 ◇ (STRM1A(1,3)/STRM1(1,3)) / STRM1F(1,3)-1; F.S.= 1.00
 ▽ (STRM2A(1,1)/STRM2(1,1)) / STRM2F(1,1)-1; F.S.= 1.00
 □ (STRM2A(1,3)/STRM2(1,3)) / STRM2F(1,3)-1; F.S.= 1.00
 × (STRM3A(1,1)/STRM3(1,1)) / STRM3F(1,1)-1; F.S.= 1.00
 ◆ (STRM3A(1,3)/STRM3(1,3)) / STRM3F(1,3)-1; F.S.= 1.00

try7: design margins vs HEIGHT=distance between inner & outer walls

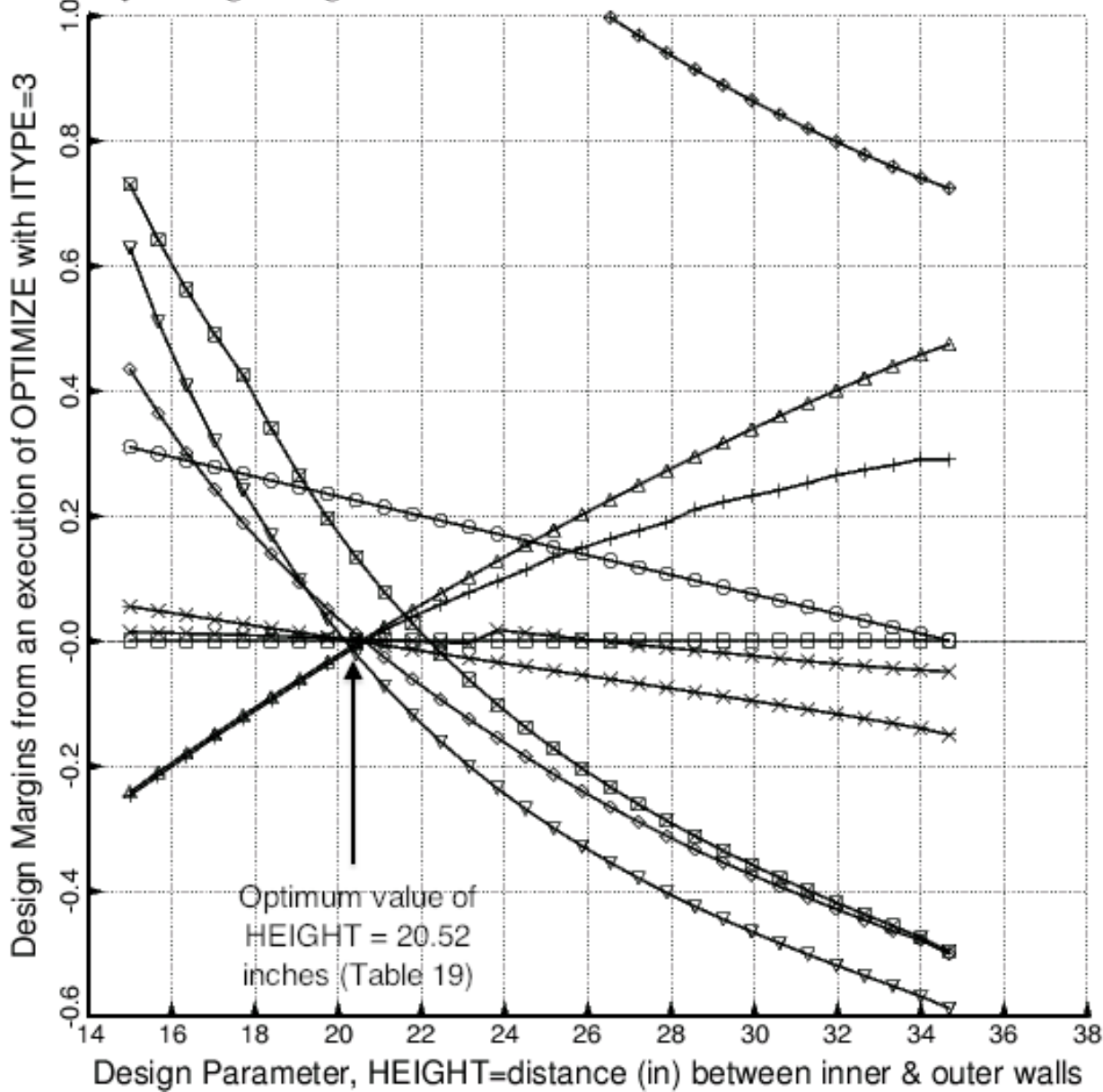


Fig. 53 Design sensitivity of the optimized design listed in Table 19 with respect to the decision variable, HEIGHT, which is defined in Fig. 1. Design sensitivity is explored with ITYPE = 3 in the *.OPT file.

- \square (BUCKB4(1)/BUCKB4A(1)) / BUCKB4F(1)-1; F.S. = 3.00
- \circ (TENLOS(1)/TENLOSA(1)) / TENLOSF(1)-1; F.S. = 3.00
- Δ (STRM1A(1,1)/STRM1(1,1)) / STRM1F(1,1)-1; F.S. = 1.00
- $+$ (STRM1A(1,3)/STRM1(1,3)) / STRM1F(1,3)-1; F.S. = 1.00
- \times (STRM2A(1,1)/STRM2(1,1)) / STRM2F(1,1)-1; F.S. = 1.00
- \diamond (STRM2A(1,3)/STRM2(1,3)) / STRM2F(1,3)-1; F.S. = 1.00
- ∇ (STRM3A(1,1)/STRM3(1,1)) / STRM3F(1,1)-1; F.S. = 1.00

try7: design margins vs RINNER=radius of curvature of innermost wall

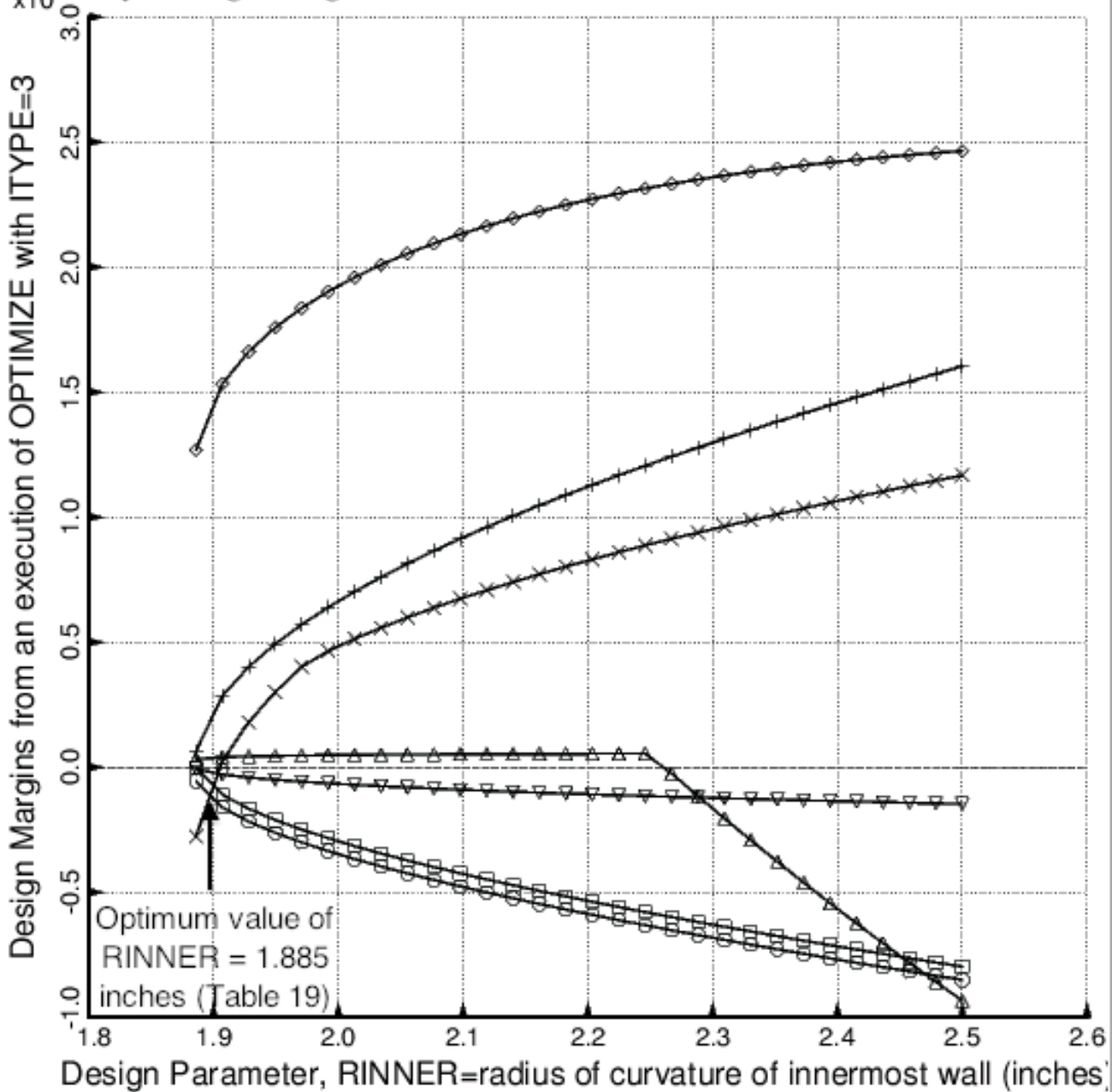


Fig. 54 Design sensitivity of the optimized design listed in Table 19 with respect to the decision variable, $RINNER$, which is defined in Fig. 1. Design sensitivity is explored with ITYPE = 3 in the *.OPT file.

-
- 1.- (2.88-1.00*V(2))
 ○ (BUCKB4(1)/BUCKB4A(1)) / BUCKB4F(1)-1; F.S.= 3.00
 △ (TENLOS(1)/TENLOSA(1)) / TENLOSSF(1)-1; F.S.= 3.00
 + (STRM1A(1,1)/STRM1(1,1)) / STRM1F(1,1)-1; F.S.= 1.00
 × (STRM1A(1,3)/STRM1(1,3)) / STRM1F(1,3)-1; F.S.= 1.00
 ◦ (STRM2A(1,1)/STRM2(1,1)) / STRM2F(1,1)-1; F.S.= 1.00
 ▽ (STRM2A(1,3)/STRM2(1,3)) / STRM2F(1,3)-1; F.S.= 1.00
 ▨ (STRM3A(1,1)/STRM3(1,1)) / STRM3F(1,1)-1; F.S.= 1.00

try7: design margins vs ROUTER=radius of curvature of outermost wall

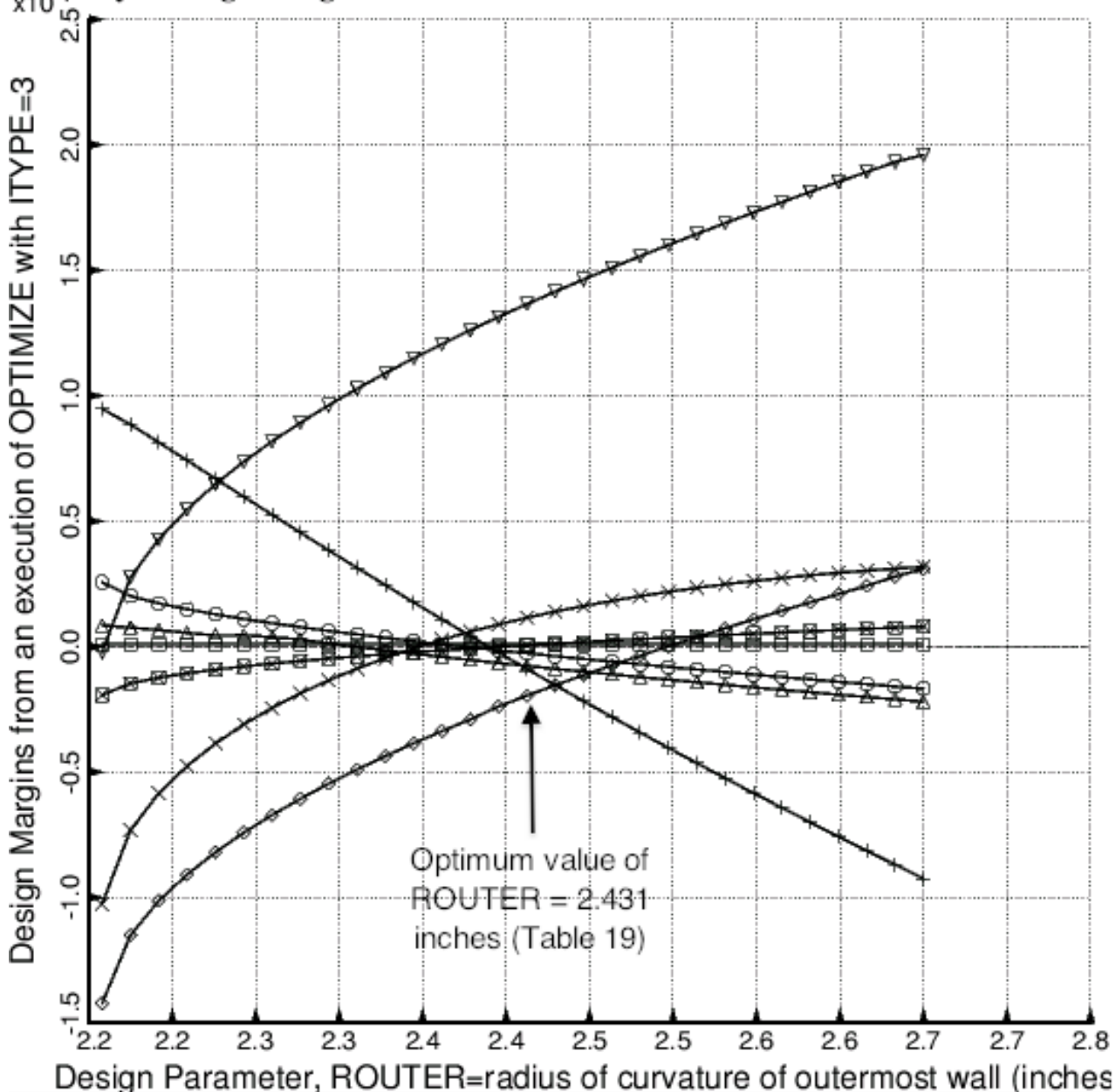


Fig. 55 Design sensitivity of the optimized design listed in Table 19 with respect to the decision variable, ROUTER, which is defined in Fig. 1. Design sensitivity is explored with ITYPE = 3 in the *.OPT file.

- weight/length (lb/in) of the cyl. balloon; truss-like (slanted) webs; "ALMOST FEASIBLE" designs
- weight/length (lb/in) of the cyl. balloon with radial webs; "ALMOST FEASIBLE" designs
- △ weight/length (lb/in) of the cyl. balloon; truss-like (slanted) webs; "FEASIBLE" designs
- + weight/length (lb/in) of the cyl. balloon with radial webs; "FEASIBLE" designs

optimized weight/length of the cylindrical balloon v. no. of modules

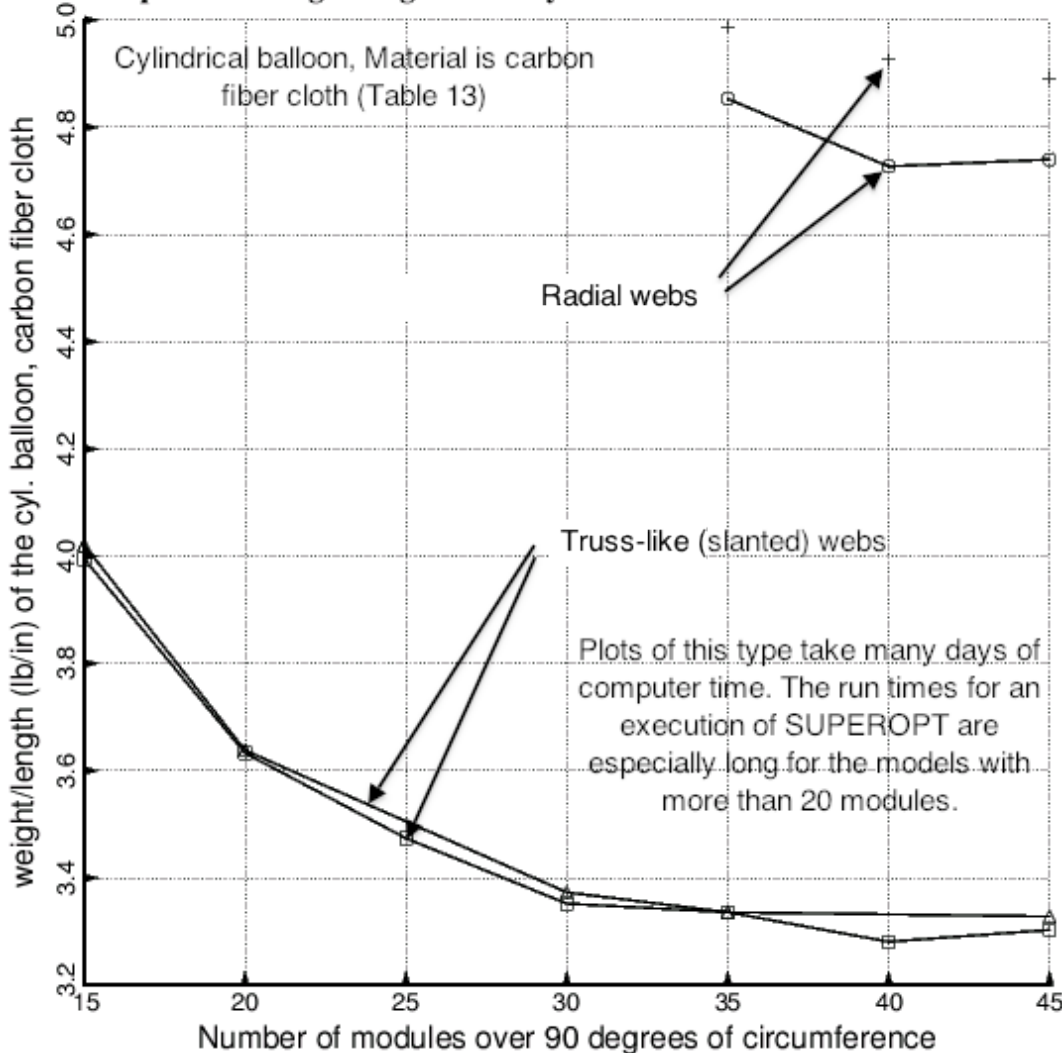


Fig. 56 The weight/length of optimized cylindrical balloons made of carbon fiber cloth as a function of the number of modules over 90 degrees of circumference. All of the results in this figure were obtained with models in which there are 31 nodal points in each segment of the multi-module model. For the models with truss-like webs there are six segments per module plus two additional segments near the circumferential coordinate, 90 degrees (Fig. 4). For models with radial webs there are five segments per module plus four additional segments near 90 degrees (Fig. 3). BIGBOSOR4 can handle up to 45 modules for models with truss-like webs and up to 55 modules for models with radial webs. For models with large numbers of modules the number of nodal points per segment is limited by the total number of degrees of freedom permitted by BIGBOSOR4 for pre-buckling analysis (20000 d.o.f) and for bifurcation buckling analysis (30000 d.o.f.). Compare this figure with Fig. 25 of [1]. The optimized balloons made of carbon fiber cloth are about a factor of 17 lighter than those made of polyethylene terephthalate.

— Undeformed; There are 15 modules over 90 degrees of the circumference of the cylindrical balloon.
 — Deformed; Load set B = PINNER=0 psi, PMIDDLE=60 psi, POUTER=0 psi

try7. Pre-buckled state of cylindrical shell. Only Load Set B is applied.

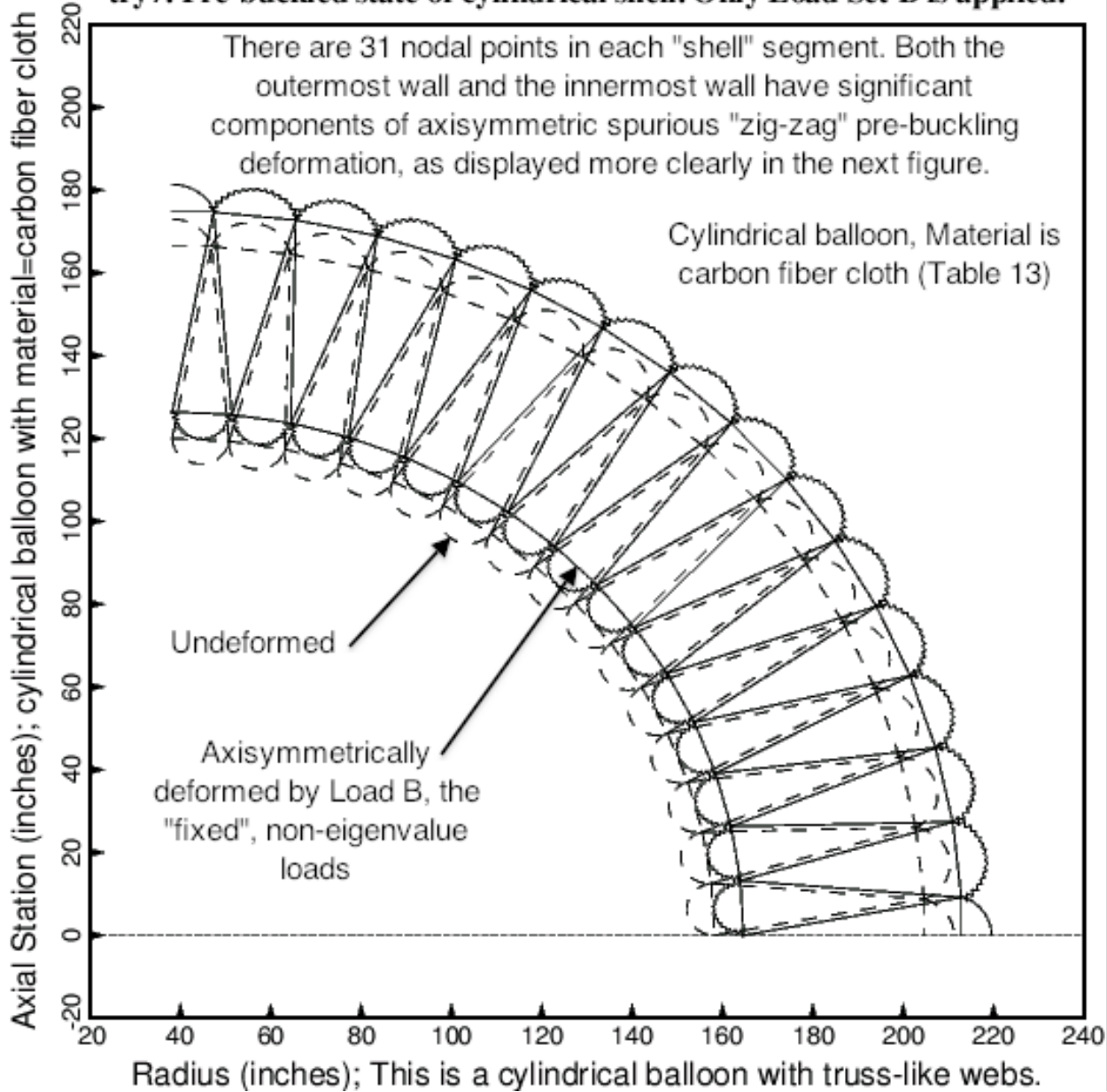


Fig. 57 This figure shows the “axisymmetric” pre-buckling deformation of the optimized cylindrical balloon with 15 modules and truss-like (slanted) webs. The material is carbon fiber cloth the properties of which are listed in Table 13. The deformation is caused by Load B (the “fixed”, non-eigenvalue loads: PINNER = 0 psi, PMIDDLE = 60 psi, POUTER = 0 psi). There are 31 nodal points in each segment of the balloon. Notice the small spurious local “zig-zag” component of deformation especially in the outer wall the thickness of which is TFOUTR. An enlarged view is provided in the next figure. The amplitude of the spurious local “zig-zag” component of displacement decreases with increasing numbers of nodal points, as displayed in Fig. 59.

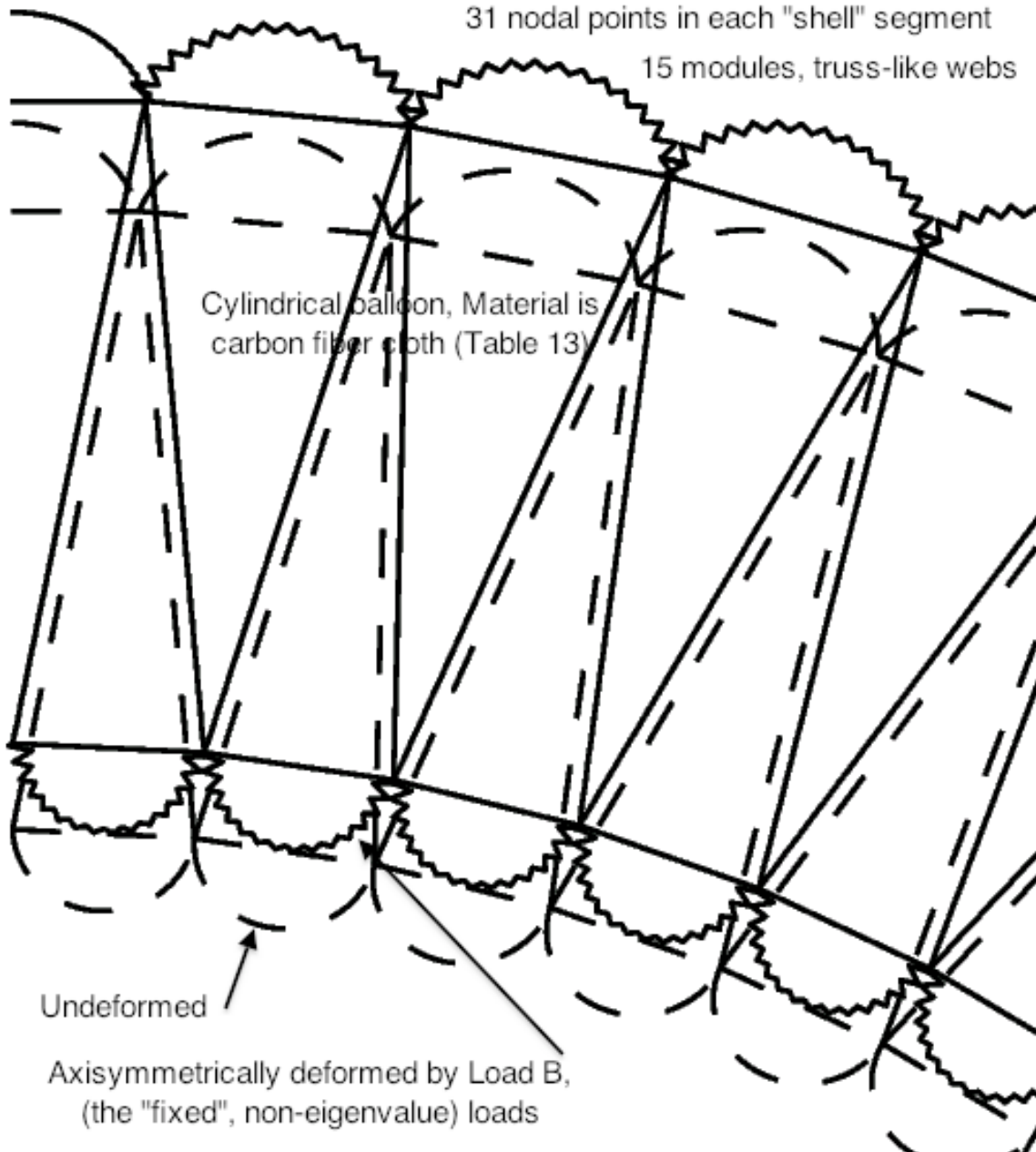


Fig. 58 This figure shows the “axisymmetric” pre-buckling deformation of the part of the optimized cylindrical balloon near 0 degrees of circumference. The cylindrical balloon has 15 modules and truss-like (slanted) webs. The material is carbon fiber cloth the properties of which are listed in Table 13. The deformation is caused by Load B (the “fixed”, non-eigenvalue loads: PINNER = 0 psi, PMIDDLE = 60 psi, POUTER = 0 psi). There are 31 nodal points in each segment of the balloon. Notice the spurious local “zig-zag” component of deformation in both the outermost wall the thickness of which is TFOUTR and in the innermost wall the thickness of which is TFINNR. An overall view of this deformation is provided in the previous figure. The amplitude of the spurious local “zig-zag” component of pre-buckling displacement decreases with increasing numbers of nodal points, as displayed in the next figure.

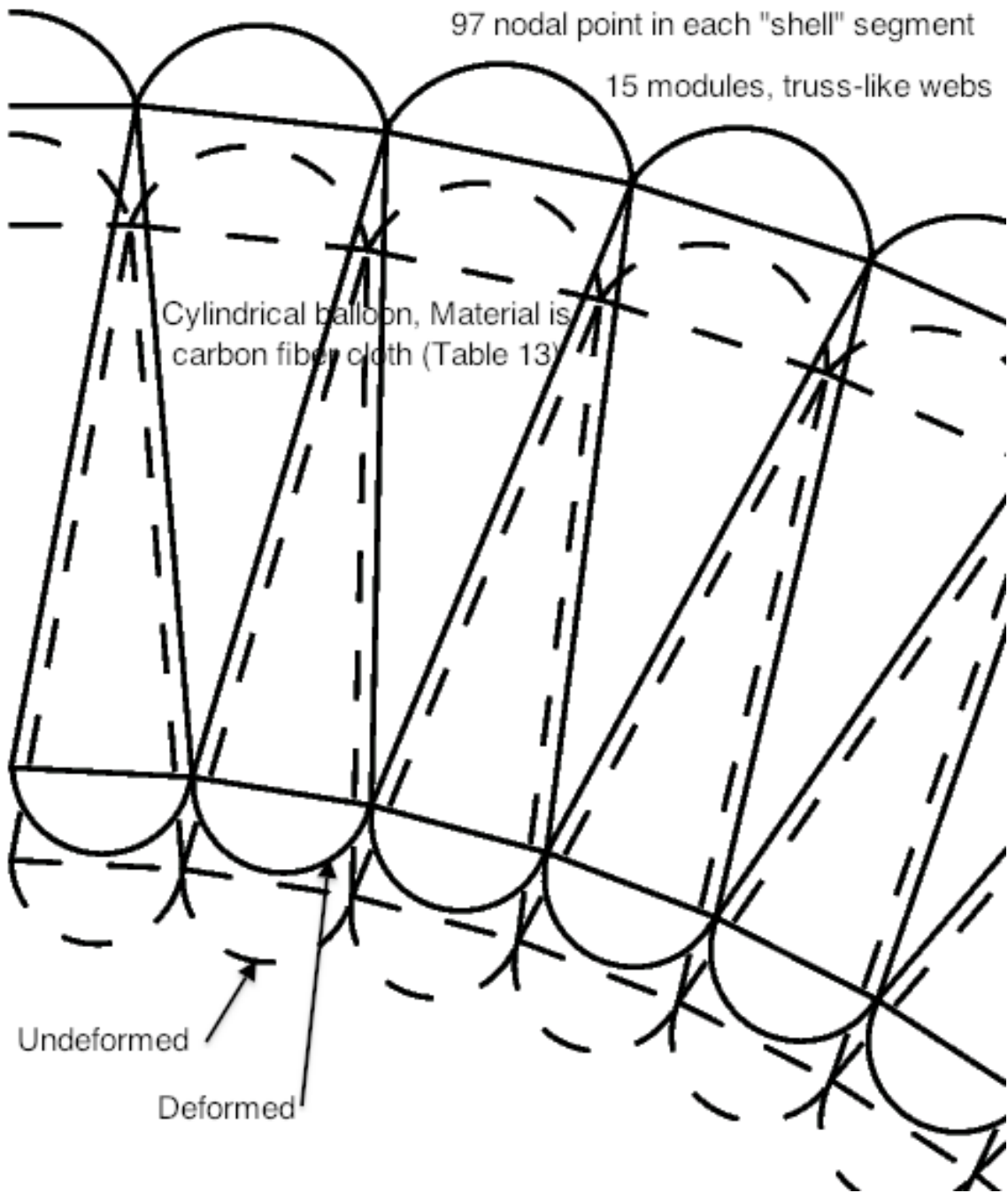


Fig. 59 This figure, which is analogous to the previous figure, shows the axisymmetric pre-buckling deformation of the part of the optimized cylindrical balloon near 0 degrees of circumference. The cylindrical balloon has 15 modules and truss-like (slanted) webs. The material is carbon fiber cloth the properties of which are listed in Table 13. The deformation is caused by Load B (the "fixed", non-eigenvalue loads: PINNER = 0 psi, PMIDDLE = 60 psi, POUTER = 0 psi). There are 97 nodal points in each segment of the balloon. Notice that the spurious local "zig-zag" component of deformation in both the outermost wall and in the innermost wall, so obvious in the previous figure, has disappeared.

— — Undeformed: optimized balloon with 15 modules over 90 degrees of circumference
 — Deformed: Eigenvalue No.1 corresponds to general buckling (ovalization) of the entire balloon

try7: eigenvalue no. 1 = 2.9889 (general buckling, ovalization)

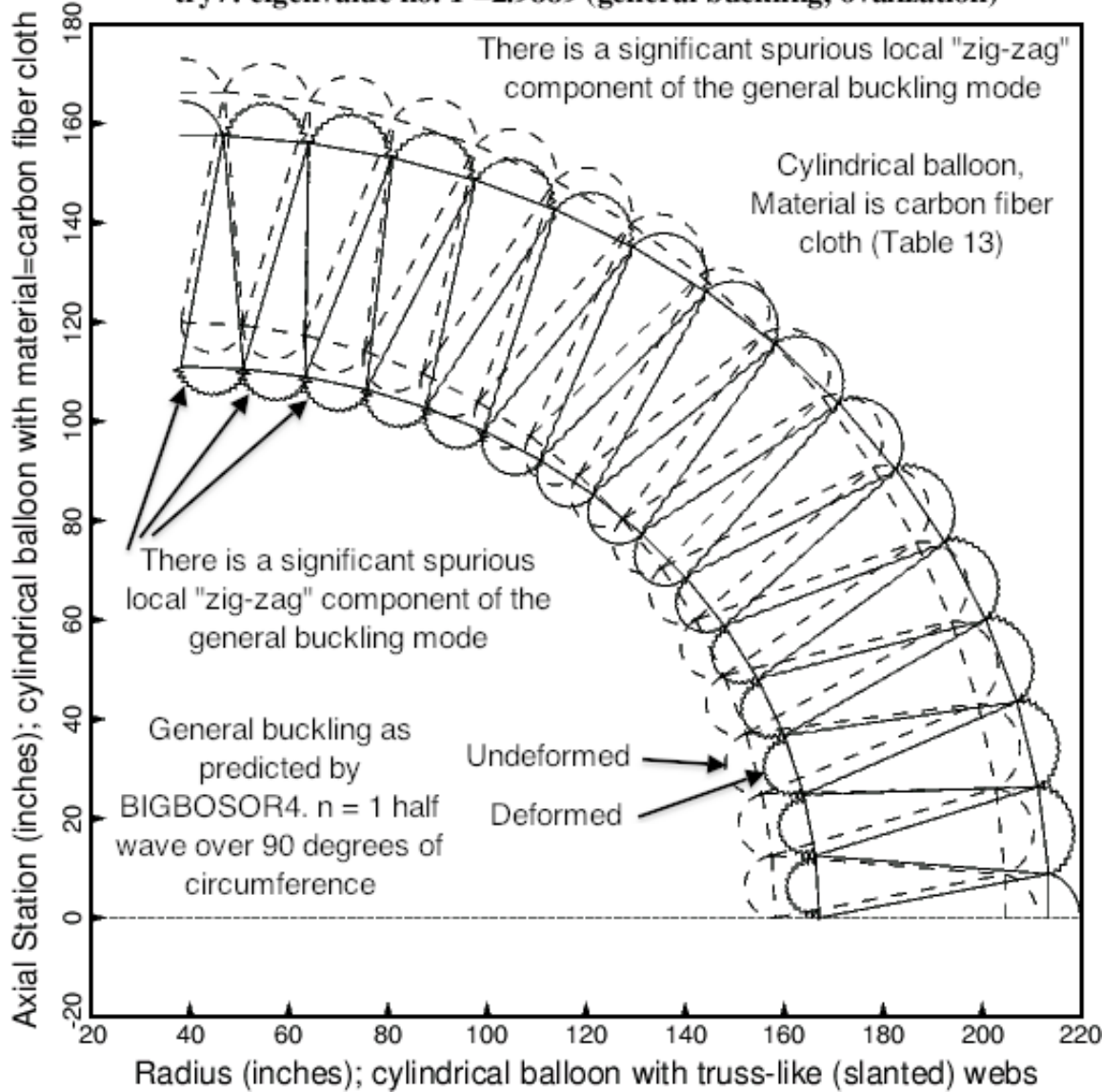


Fig. 60 General buckling of the optimized cylindrical balloon with 15 modules over 90 degrees of circumference and with truss-like webs. There are 31 nodal points in each segment of the model, which is the nodal point density specified in the “balloon” software, SUBROUTINE BOSDEC (NODSEG = 31) for optimization. This figure is analogous to Fig. 11 of [1], which applies to cylindrical balloons made of the much weaker material, polyethelene terephthalate. In the optimized cylindrical balloon made of the much stronger carbon fiber cloth the walls are much thinner than those of the optimized cylindrical balloon shown in Fig. 11 of [1]. For this reason BIGBOSOR4 produces an eigenvector that has a significant component of local spurious “zig-zag” buckling modal displacement. The question is: “Does the presence of the spurious ‘zig-zag’ component of buckling modal displacement significantly affect the critical buckling load factor (eigenvalue) predicted by BIGBOSOR4?” The answer from the predictions listed in Tables 21 and 22 appears to be, “no”.

-- Undeformed: optimized balloon with 15 modules over 90 degrees of circum. & 33 nodes/segment
 — Deformed: Eigenvalue No.2 corresponds to local buckling of inner wall with thickness=TFINNR

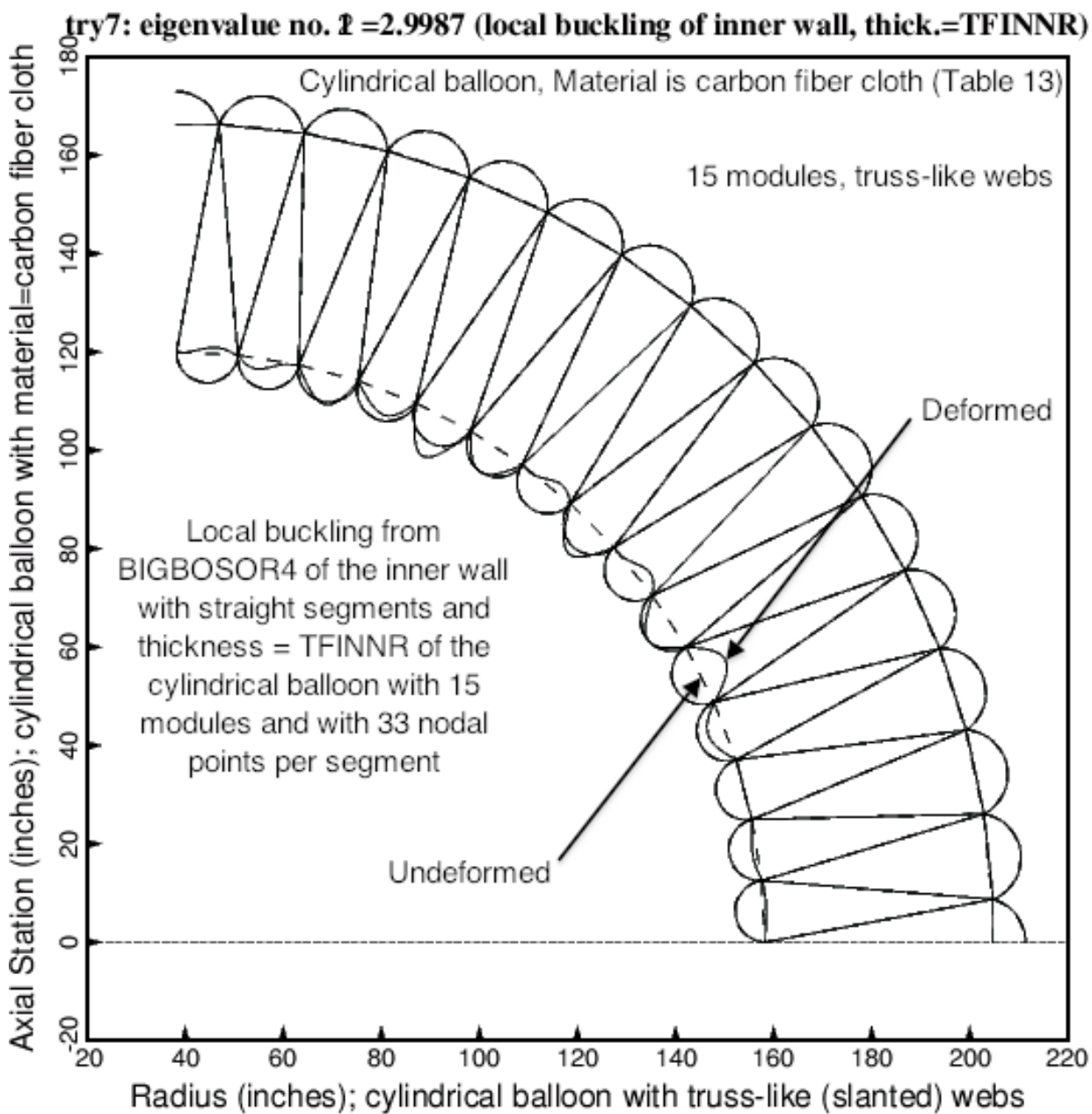


Fig. 61 Local bifurcation buckling from BIGBOSOR4 of the optimized cylindrical balloon with 15 modules and truss-like webs. Local buckling occurs in the inner wall straight segment that has thickness = TFINNR. There are 31 nodal points per segment as specified in the "balloon" software, SUBROUTINE BOSDEC (NODSEG = 31). (33 nodal points are indicated in the figure because BIGBOSOR4 automatically adds one extra nodal point very near the end of each segment.) Notice that this local buckling eigenvector corresponds to eigenvalue no. 2. The eigenvector corresponding to eigenvalue no. 1 is displayed in the previous figure. Compare the local buckling mode shown here with the local buckling mode displayed in the next figure.

— — Undeformed: optimized balloon with 15 modules over 90 degrees of circum. & 99 nodes/segment
 — Deformed: Eigenvalue No.1 corresponds to local buckling of inner wall with thickness=TFINNR

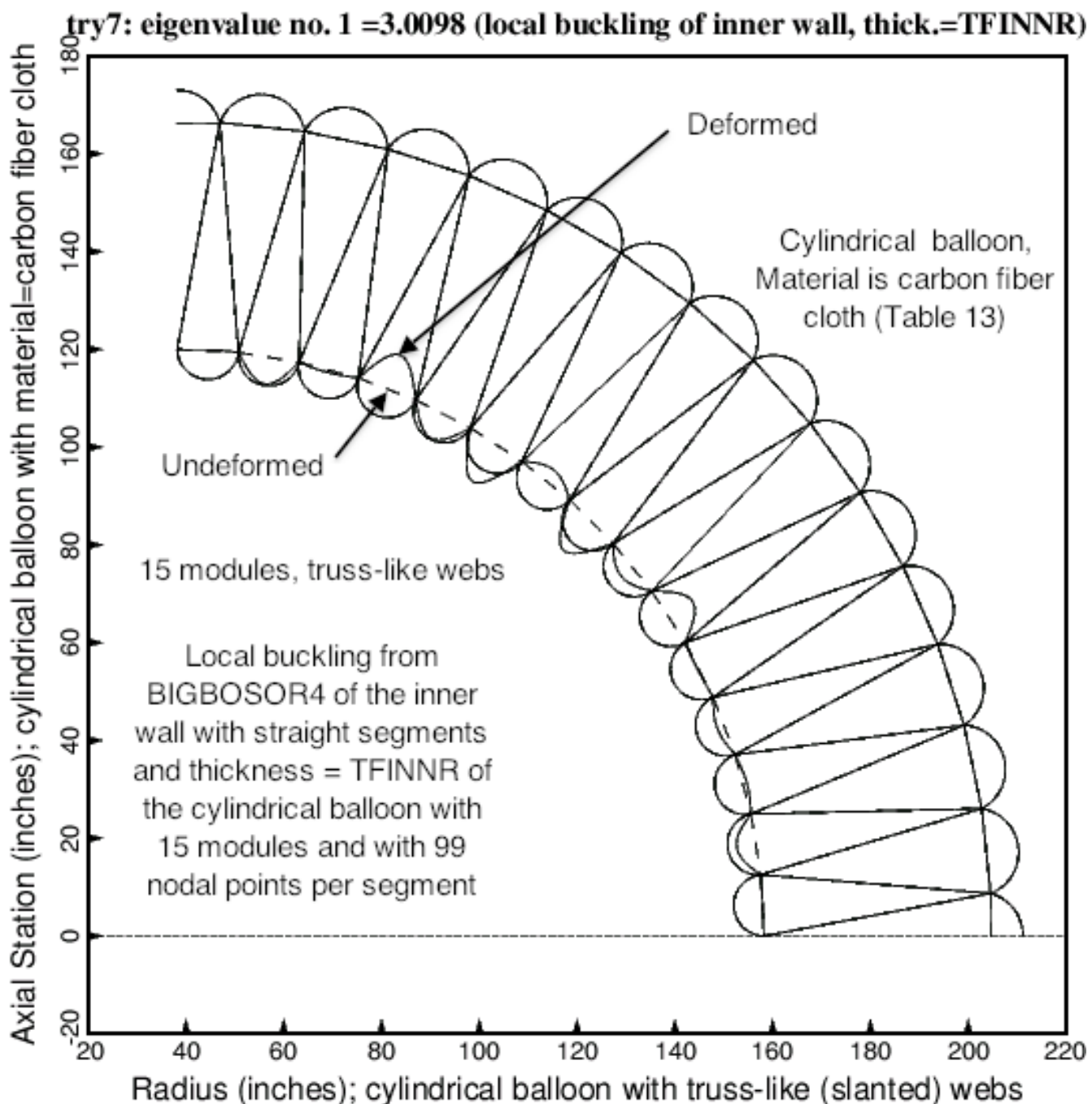


Fig. 62 Local bifurcation buckling from BIGBOSOR4 of the optimized cylindrical balloon with 15 modules and truss-like webs. Local buckling occurs in the inner wall straight segment that has thickness = TFINNR. There are 97 nodal points per segment as specified in the "balloon" software, SUBROUTINE BOSDEC (NODSEG = 97). (99 nodal points are indicated in the figure because BIGBOSOR4 automatically adds one extra nodal point very near the end of each segment.) Compare with the local buckling mode displayed in the previous figure.

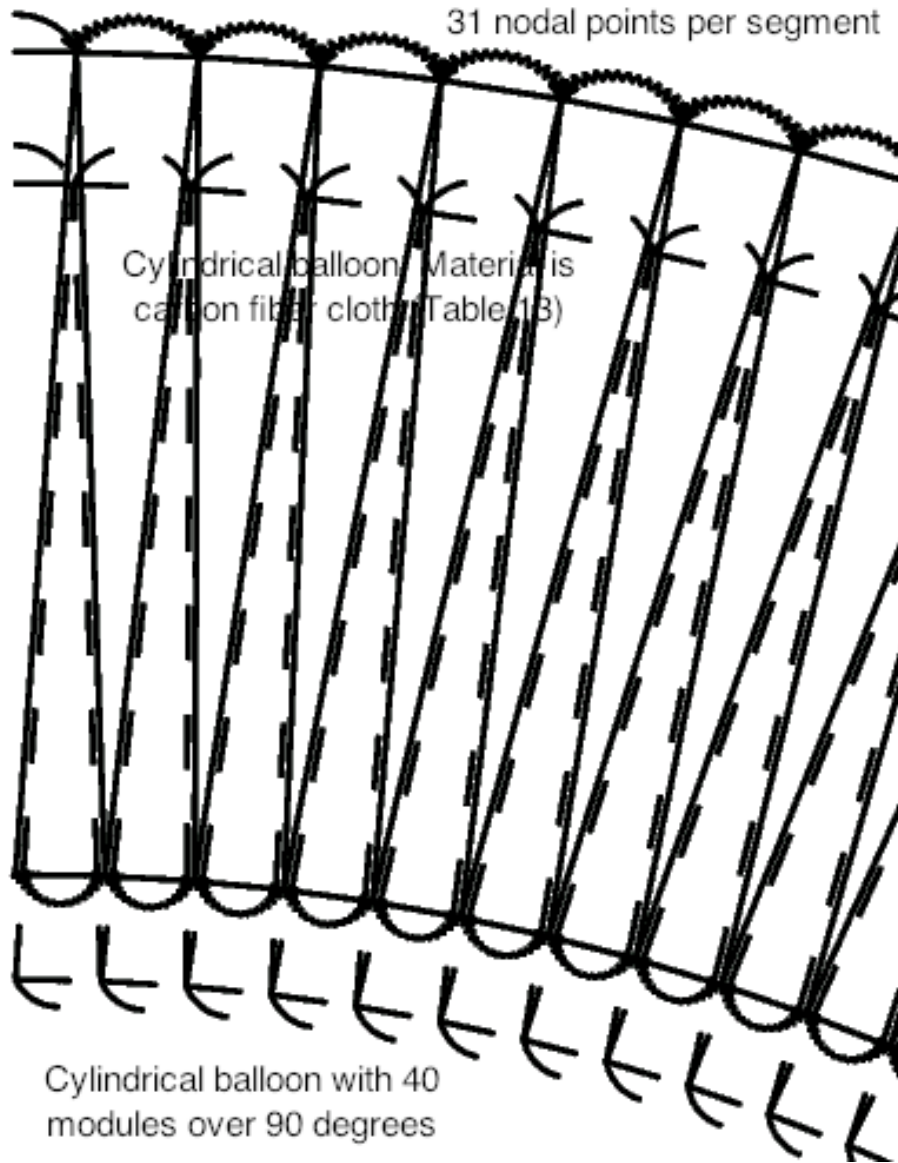


Fig. 63 This figure, which is analogous to Fig. 58, shows the “axisymmetric” pre-buckling deformation of the part of the optimized cylindrical balloon near 0 degrees of circumference. The cylindrical balloon has 40 modules over 90 degrees of circumference and truss-like (slanted) webs. The material is carbon fiber cloth the properties of which are listed in Table 13. The pre-buckling deformation is caused by Load B (the “fixed”, non-eigenvalue loads: PINNER = 0 psi, PMIDDLE = 60 psi, POUTER = 0 psi). There are 31 nodal points in each segment of the balloon, which is specified by the “balloon” software, SUBROUTINE BOSDEC (NODSEG = 31). Notice the spurious local “zig-zag” component of pre-buckling deformation in both the outermost wall the thickness of which is TFOUTR and in the innermost wall the thickness of which is TFINNR. The amplitude of the spurious local “zig-zag” component of pre-buckling displacement would decrease with increasing numbers of nodal points. However, the number of nodal points per segment cannot be increased for models with many modules because BIGBOSOR4 can only solve problems with up to 20000 degrees of freedom for the prediction of pre-buckling states and up to 30000 d.o.f. for the prediction of bifurcation buckling load factors.

— — Undeformed: optimized balloon with 40 modules over 90 degrees of meridian
 ——— Deformed: Eigenvalue No.2 corresponds to local buckling of the inner wall with thickness, TFINNR

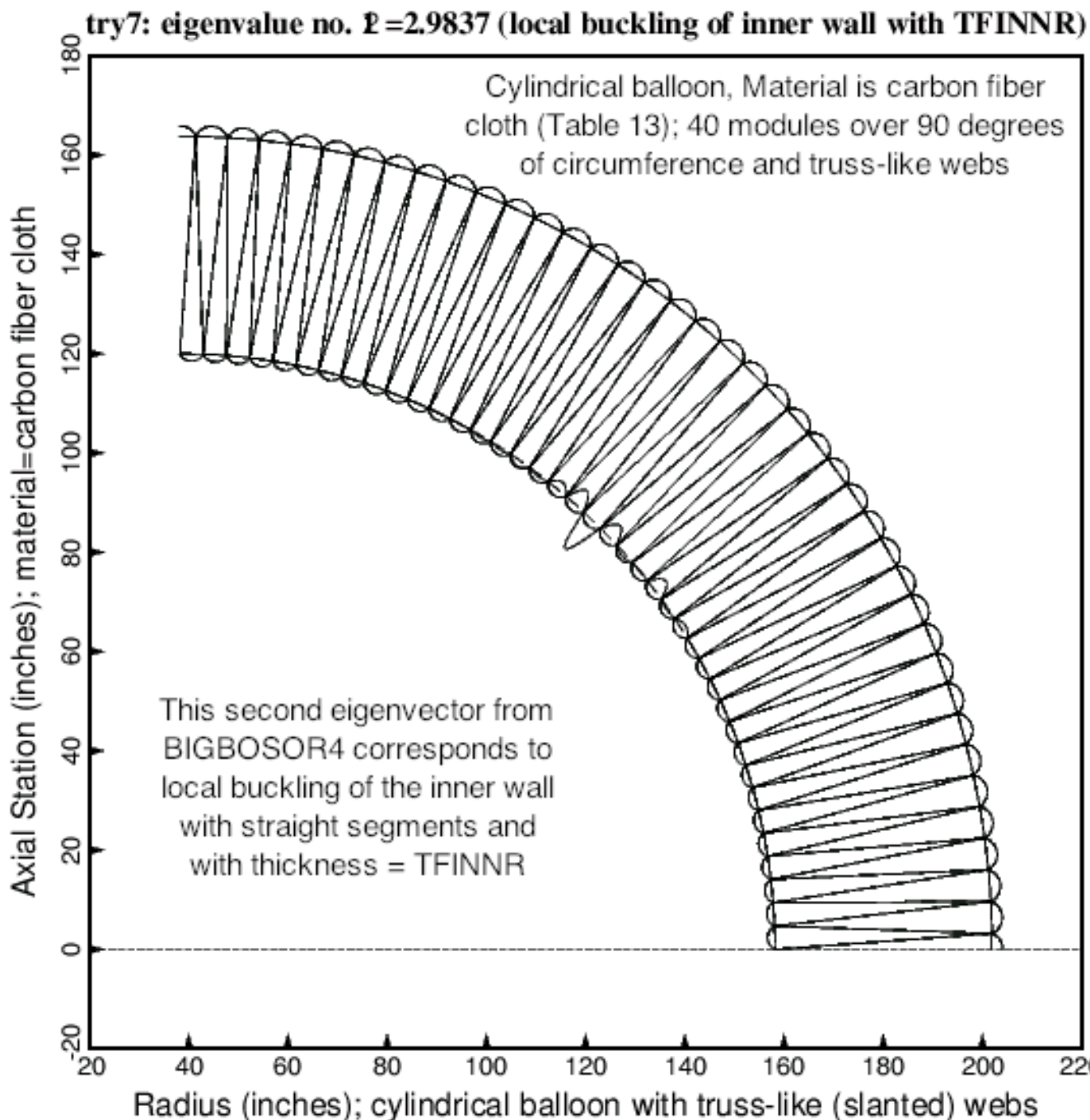


Fig. 64 Local bifurcation buckling from BIGBOSOR4 of the optimized cylindrical balloon with 40 modules over 90 degrees of circumference and truss-like webs. Local buckling occurs in some of the inner wall straight segments that have thickness = TFINNR. There are 31 nodal points per segment as specified in the "balloon" software, SUBROUTINE BOSDEC (NODSEG = 31). Notice that this local buckling eigenvector corresponds to eigenvalue no. 2. The eigenvector corresponding to eigenvalue no. 1 is displayed in the next figure.

— — Undeformed: optimized balloon with 40 modules over 90 degrees
 — Deformed: Eigenvalue No.1 corresponds to general buckling with n=4 circumferential waves

try7: eigenvalue no. 1 = 2.9094 (general buckling, n = 4 circ. waves)

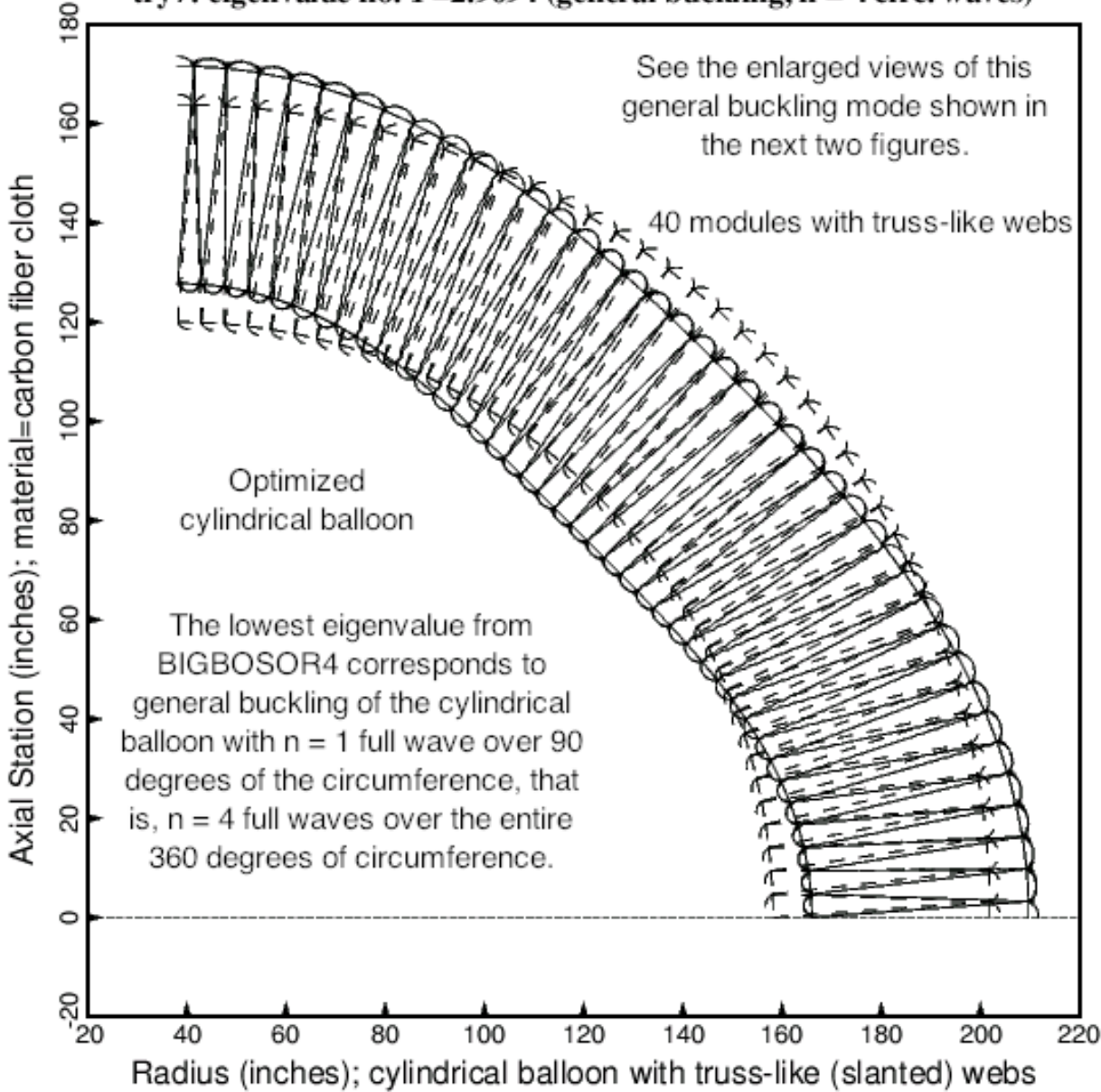


Fig. 65 General buckling of the optimized cylindrical balloon with 40 modules over 90 degrees of circumference and with truss-like webs. There are 31 nodal points in each segment of the model, which is the nodal point density specified in the "balloon" software, SUBROUTINE BOSDEC (NODSEG = 31) for optimization. This figure is analogous to Fig. 60. In this case BIGBOSOR4 produces an eigenvector that has a significant component of local spurious "zig-zag" buckling modal displacement. The question is: "Does the presence of the spurious 'zig-zag' component of buckling modal displacement significantly affect the critical buckling load factor (eigenvalue) predicted by BIGBOSOR4?" The answer from the predictions listed in Tables 21 and 22 appears to be, "no".

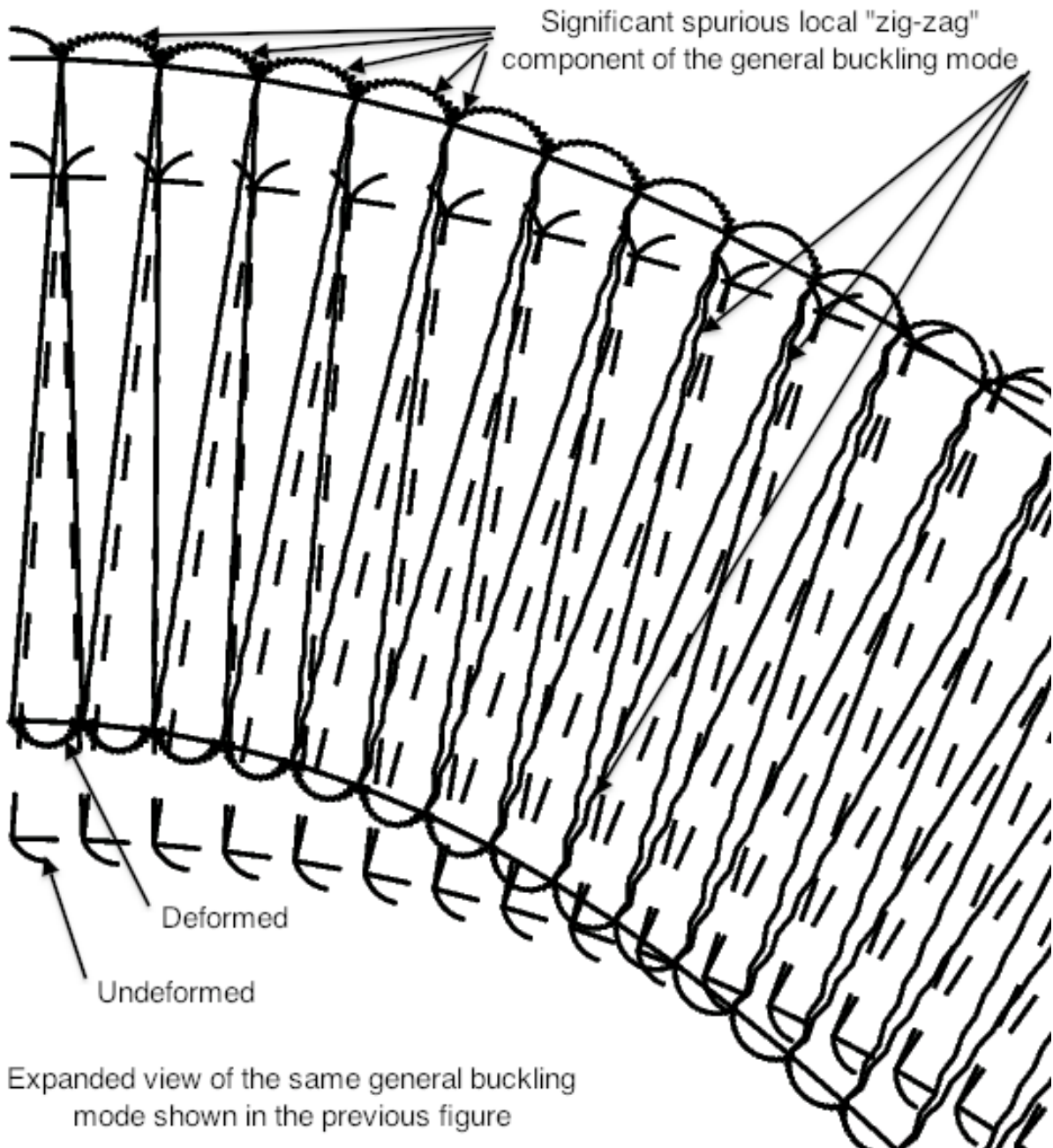


Fig. 66 Detail of general buckling of the optimized cylindrical balloon with 40 modules over 90 degrees of circumference and with truss-like webs. This figure shows an enlarged view of the same buckling mode as that displayed in the previous figure. There are 31 nodal points in each segment of the model, which is the nodal point density specified in the "balloon" software, SUBROUTINE BOSDEC (NODSEG = 31) for optimization. In this case BIGBOSOR4 produces a general buckling eigenvector that has a significant component of local spurious "zig-zag" buckling modal displacement in every segment except those straight segments in the outer wall the thickness of which is TFOUTR and those straight segments in the inner wall the thickness of which is TFINNR.

Close Hdcpy About

Axial Station inches

try7..R,Z_EIGENMODE_1--N_1

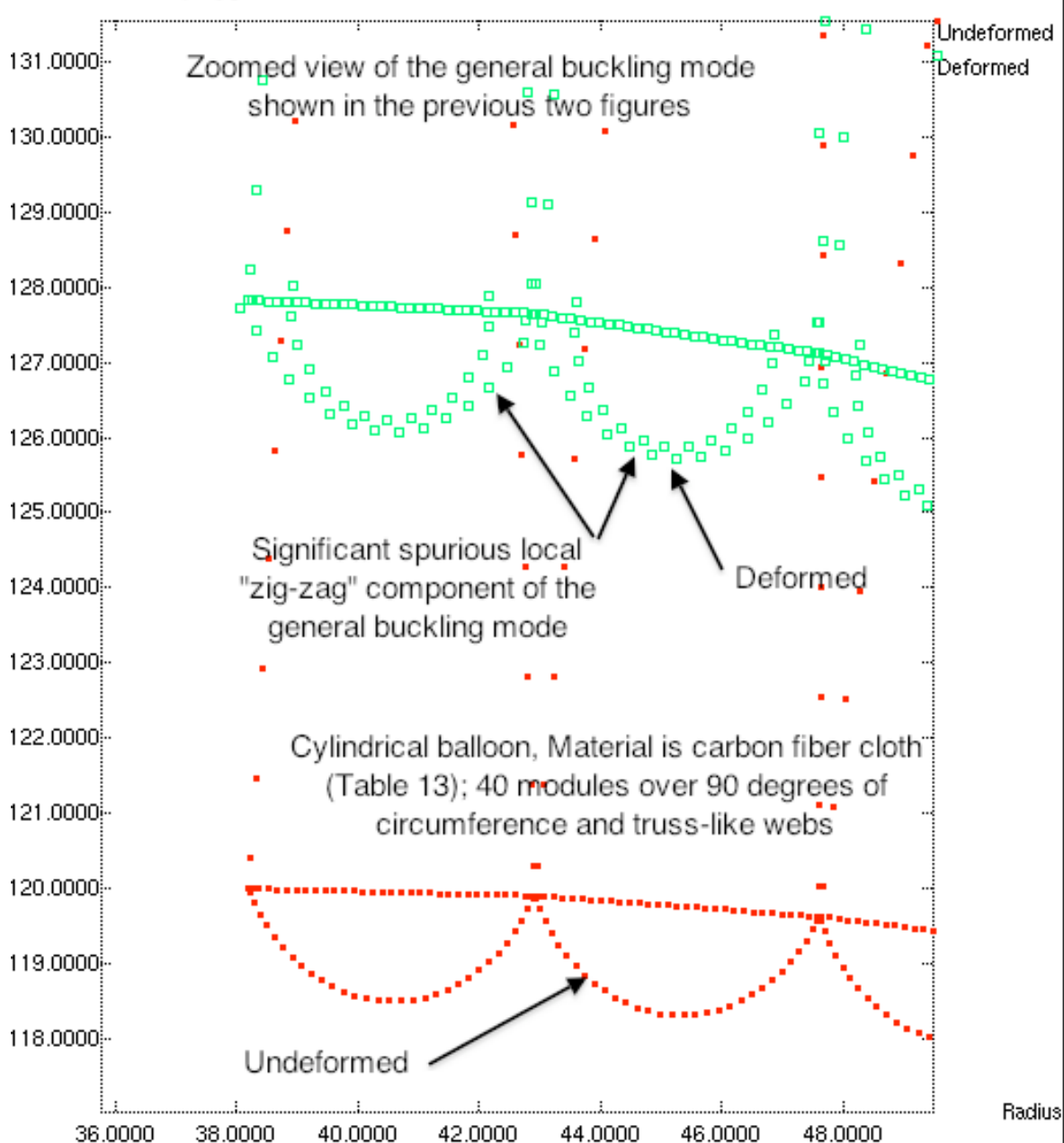


Fig. 67 Detail of general buckling of the optimized cylindrical balloon with 40 modules over 90 degrees of circumference and with truss-like webs. This figure shows an enlarged view of the same buckling mode as that displayed in Fig. 65. There are 31 nodal points in each segment of the model, which is the nodal point density specified in the "balloon" software, SUBROUTINE BOSDEC (NODSEG = 31) for optimization. In this case BIGBOSOR4 produces a general buckling eigenvector that has a significant component of local spurious "zig-zag" buckling modal displacement in every segment except those straight segments in the outer wall the thickness of which is TFOUTR and those straight segments in the inner wall the thickness of which is TFINNR.